Cover Page

Universiteit Leiden

Author: Wijngaarden, Marjolein A.
Title: Metabolic and endocrine adaptations to fasting in lean and obese individuals
Issue Date: 2015-03-26

Metabolic and endocrine adaptations to fasting in lean and obese individuals

Marjolein A. Wijngaarden

Metabolic and endocrine adaptations to fasting in lean and obese individuals

Marjolein A. Wijngaarden

Metabolic and endocrine adaptations to fasting in lean and obese individuals

Proefschrift

ter verkrijging van
de graad van Doctor aan de Universiteit Leiden,
op gezag van Rector Magnificus prof. mr. C.J.J.M. Stolker
volgens besluit van het College voor Promoties
te verdedigen op
donderdag 26 maart 2015
klokke 16.15 uur

door

Marjolein A. Wijngaarden
geboren in 1983
te Amsterdam

Promotiecommissie

Promotores: Prof. dr. H. Pijl
                   Prof. dr. K. Willems van Dijk

Co-promotor: Dr. B. Guigas

Overige leden: Dr. J. van der Grond
                   Prof. dr. E.J.M. Feskens, Universiteit Wageningen
                   Prof. dr. W.H.M. Saris, Universiteit Maastricht

Contents

List of abbreviations

ACC	acetyl-coA carboxylase
ACOX1	peroxisomal acyl-coenzyme A oxidase 1
ADA	American Diabetes Association
ALT	alanine aminotransferase
AMPK	adenosine monophosphate-activated kinase
AMPKKs	AMPK kinases
AST	aspartate aminotransferase
AS160	akt substrate of 160kDa
BMI	body mass index
BOLD	blood-oxygen level dependent
CAMKKβ	Ca^{2+}/calmodulin-dependent protein kinase kinase β
CPT1B	carnitine-palmitoyl transferase 1B
CR	calorie restriction
CREB	cAMP response element-binding protein
CRP	C-reactive protein
CS	citrate synthase
DEGs	differentially expressed genes
4EBP1	eukaryotic initiation factor 4E binding protein;
ECG	electrocardiogram
EF2	eukaryotic elongation factor 2
EGP	endogenous glucose production
ELISA	enzyme-linked immunosorbent assay
ERK	extracellular signal□regulated kinase;
FAT/CD35	fatty acid transporter CD36
FA/FFA	free fatty acid
FFM	fat-free mass
fMRI	functional magnetic resonance imaging
FM	fat mass
FOXO	forkhead box protein O
FPG	fasting plasma glucose
FSH	follicle-stimulating hormone
FT4	free thyroxine

GLM	general linear model
GLUT4	glucose transporter isoform 4
GO	gene ontology
GS	glycogen synthase
GSK3	glycogen synthase kinase 3
G6Pase	glucose-6-phosphatase catalytic subunit
HADHA	hydroxyacyl-CoA dehydrogenase/3-ketoacyl-CoA thiolase/enoyl-CoA hydratase, alpha subunit
Hb	hemoglobin
HDAC	histone deacetylase
HDL	high-density lipoprotein
HRV	heart rate variability
MRS	magnetic resonance spectroscopy
HOMA-IR	homeostatic model assessment of insulin resistance
HPLC	high-performance liquid chromatography
hsCRP	high sensitive c-reactive protein
IGF-1	insulin-like growth factor 1
IGT	impaired glucose tolerant
IL	interleukin
IFNγ	interferon gamma
IR	insulin receptor
IRβ	insulin receptor β
IRS	insulin receptor substrate
LBM	lean body mass
LC-CoA	long chain fatty accid-CoA
LDL	low density lipoprotein
LH	luteinizing hormone
LKB1	liver kinase B1
LPL	lipoprotein lipase
LUMC	leiden unviversity medical center
MRI	magnetic resonance imaging
mtDNA	mitochondrial DNA
mTOR	mammalian target of rapamycin
mTORC1	mammalian target of rapamycin complex 1
OGTT	oral glucose tolerance test

PI3K	phosphatidylinositol 3-kinase
PDK	phosphatidyolinositol dependent protein kinase
PGC-1α	peroxisome proliferator-activated receptor gamma coactivator 1-alpha
PKB(Akt)	protein kinase B (also known as Akt)
PKC	protein kinase C
PPAR-δ	peroxisome proliferator-activated receptor delta
ppm	parts per million
PRAS40	proline rich Akt substrate of 40 kDa
REE	resting energy expenditure
RQ	respiratory quotient
S6	ribosomal protein S6
S6K	ribosomal protein S6 kinase
SHBG	sex-hormone binding globulin
SIRT1	sirtuin 1
SEM	standard error of the mean
Ser	serine
T3	triiodothyronine
TC	total cholesterol
TE	echo time
TG	triglyceride
Thr	threonine
TR	repetition time
TRH	thyrotropin releasing hormone
TSC2	tuberous sclerosis protein 2
TSH	thyroid-stimulating hormone
Tyr	tyrosine
T2DM	type 2 diabetes mellitus
VLCD	very low calorie diet
VLDL	very low density lipoprotein
WHO	world health organization

Chapter 1

1

Introduction

1

Fasting and energy-sensing

A prolonged fast has tremendous effects on metabolism. Mainly insulin, but also glucose levels quickly decline over the course of a couple of days. During the fed state energy is mainly derived from carbohydrate oxidation. This switches during fasting towards lipid oxidation. The amount of carbohydrate and lipid oxidation can be estimated by indirect calorimetry. This method uses the CO_2 and O_2 in the exhaled air to calculate substrate oxidation [1]. During a fast, the increase in lipid oxidation leads to the production of ketone bodies (beta-hydroxybutyrate and acetoacetae) in the liver, which can be used as fuel by the brain when glucose levels drop [2]. After 2-3 days of fasting, liver glucose stores (glycogen) are depleted. At this point, glucose is synthesized in the kidney and also in the liver from lactate, pyruvate, glycerol and amino acids such as alanine (gluconeogenesis) [3].

While fasting, the activity of hormonal axes such as the thyroid-axis – important for metabolism – and the reproductive axis are downregulated. With respect to the thyroid-hormone axis this is characterized by decreased thyroid-stimulating hormone (TSH) and triiodothyronine (T3) levels whereas T4 levels remain stable which is due to an altered deiodinase activity during fasting and leptin might be involved as well [4;5]. Likely, the reduction in T3 levels saves energy during fasting. The pituitary-gonadal axis is downregulated during fasting as well; plasma levels of follicle-stimulating hormone (FSH), luteinizing hormone (LH) and testosterone decrease during fasting whereas sex-hormone binding globulin (SHBG) levels increase [6]. Most likely, this is an evolutionary mechanism to prevent reproduction when food is sparse.

On a molecular level, so-called energy-sensing pathways are affected during fasting. The adenosine monophosphate-activated kinase (AMP-activated kinase, AMPK) is of special interest. This enzyme is phosphorylated by liver kinase B1 (LKB1), in response to energy depletion and the coinciding increase in AMP/ATP ratio. Generally speaking, the actions of AMPK aim to restore energy balance; AMPK inhibits anabolic processes and stimulates catabolic processes. AMPK is also involved in the metabolic shift towards lipid oxidation during fasting; AMPK phosphorylates and thereby deactivates acetyl-CoA carboxylase 1 (ACC). This results in an increased fatty acid oxidation and reduced lipid storage [7]. The most important effects of AMPK on glucose metabolism are that it increases glucose uptake [8;9] and inhibits the hepatic glucose production [10-12]. Besides AMPK, there are many upstream and downstream (in)direct targets that play a role during fasting with respect to either energy-sensing or the

1

metabolic shift such as the sirtuins (SIRT, from silent information regulators), histone deacetylase 4 (HDAC4), mammalian target of rapamycin (mTOR), Forkhead box O (FOXO), protein kinase B (PKB/Akt), pyruvate dehydrogenase kinase isozyme 4 (PDK4), glucose transporter type 4 (GLUT4), cluster of differentiation 36 (CD36) and ACC.

Obesity

The body mass index (BMI) is used to define obesity; the BMI is calculated by dividing body weight (in kilograms) by the square of height (in meters).The World Health Organization defines obesity as a BMI ≥ 30 kg/m^2 and overweight as a BMI between 25 and 30 kg/m^2. The prevalence of obesity has doubled since 1980. In 2008 there were 1.5 billion overweight and 500 million obese adults (>20 years) [13]. Obesity is a risk factor for cardiovascular diseases, diabetes, musculoskeletal disorders and many forms of cancer (e.g. endometrial, breast and colon cancer). Since it became clear that AMPK is important for sensing and repairing energy balance disturbances, and obesity is clearly a result from disrupted energy balance, the role of AMPK in type 2 diabetes mellitus and obesity has been investigated. Skeletal muscle is very flexible with respect to the metabolic shift from glucose towards fatty acid oxidation. Since the *musculus vastus lateralis* is easily accessible, energy-sensing pathways are often studied in human biopsy materials of this muscle. With respect to AMPK, thus far only few alterations in obesity and type 2 diabetes mellitus (T2DM) have been found. One study has shown that AMPK activity is reduced in muscle from obese subjects [14]. In contrast, other studies showed that skeletal muscle AMPK activity is similar between lean and obese individuals or obese subjects and T2DM patients [15;16].

Brain

The hypothalamus is probably the most important area of the brain involved in the homeostasis of metabolism, food intake and energy expenditure [17]. The hypothalamus is located in the ventral part of the diencephalon, below the thalamus. The hypothalamus has important hormonal effects, since it secretes factors and hormones that stimulate the pituitary to secrete hormones (with neuro-endocrine feedback). The hypothalamic arcuate nucleus receives information about the peripheral blood through the median eminence, where the blood-brain barrier is absent [18]. Claude

Bernard was the first to suggest a role for the hypothalamus in glucose homeostasis in 1855 [19]. It is now known that different hypothalamic areas have different roles in weight maintenance. Animal studies show that damaging the lateral hypothalamus induces weight loss whereas damaging the ventromedial part (VMH) of the hypothalamus induces obesity (3-6). On a neuronal level, food intake is regulated by hypothalamic neurons that either stimulate (orexigenic) or inhibit (anorexigenic) food intake. The orexigenic neurons contain NPY (neuropeptide Y) and AGRP (agouti-related protein), neurotransmitters that stimulate food intake [23-25]. Anorexigenic neurons contain CART (cocaine- and amphetamine-regulated transcript) and POMC (proopiomelanocortin), neurotransmitters that inhibit food intake [26-28].

Functional Magnetic Resonance Imaging

When a human body is placed in a magnetic resonance imaging (MRI) scanner its hydrogen nuclei get excited by radiofrequency pulses in two directions; longitudinal and transversal. Contrasts on MR images are based on the relaxation of these excitated nuclei; longitudinal relaxation (T1) and transverse relaxation (T2). Functional MRI (fMRI) uses blood-oxygen-level dependent (BOLD) signals as a measure of brain activity. The basics behind this mechanism were described at first by Linus Pauling in 1936 which was later implemented by Seiji Ogawa [29;30]. Oxygenated hemoglobin (Hb) is diamagnetic, whereas deoxygenated Hb is paramagnetic. Brain activity in a certain brain region increases the blood flow to this region. This alters the ratio of oxygenated Hb versus deoxygenated Hb in favor of the oxygenated hemoglobin in the blood stream itself and in the surrounding tissues. Paramagnetic molecules reduce signal intensity (T2 value) and result in a dark image. When the amount of paramagnetic molecules in the blood decreases (during increased brain activity) the opposite occurs; the signal intensity increases. Since this was discovered, a lot of research has been performed in the neuropsychological field to correlate brain function with specific brain regions.

Within the brain, the hypothalamus is involved in the regulation of food intake and energy expenditure [17] whereas the rewarding effects of food are mainly regulated in the amygdala [31]. As reviewed, the brain – mainly the hypothalamus again - also plays a role in glucose homeostasis [32]. To date, however, there are not many functional MRI studies that looked at the effect of fasting on neuronal activity. A positron emission tomography (PET) study showed that a 36 hour fast ("hunger"), compared to the

1

satiated state, increased regional cerebral bloodflow (rCBF) in the hypothalamus, insula, (para)limbic areas (such as the ACC), thalamus, cadaute, precuneus, putamen and cerebellum [33]. Two other PET studies looked at the response to respectively the taste or ingestion of a meal after a 36 hour fast in lean and obese individuals. rCBF increased in the midbrain and insula and decreased in the PCC, temporal cortex and OFC in obese compared to lean participants in response to tasting a meal after the fast [34]. Meal ingestion, after a 36 hour fast, led to a higher increase in rCBF the prefrontal cortex in obese compared to lean individuals [35]. Besides, a larger rCBF decrease was seen in the (para)limbic areas in obese compared to lean individuals. Decreases in the hypothalamus, ACC and thalamus upon satiation were smaller in obese than lean participants [35].

Heart Rate Variability

During a short-term fast in humans, the activity of the sympathetic nervous system (SNS) increases [36;37]. A derivative of SNS activity, heart rate variability (HRV), can easily be measured in humans by electrocardiography. Indeed, heart rate is under control of the autonomic nervous system (as reviewed [38]). The autonomic nervous system consists of the sympathetic nervous system that increases heart rate and the parasympathetic nervous system that decreases heart rate. The balance between these autonomic branches is extremely dynamic and quickly adapts to environmental cues, such as fasting. The sympathetic nervous system mobilizes energy whereas the parasympathetic nervous system is important for the digestion of food and energy storage. Disbalances of the autonomic nervous system mostly result in hyperactivity of the sympathetic nervous system and a decrease in parasympathetic nervous system activity. In obesity, an increased SNS activity has been previously described [39].

Outline Thesis

The general aim of this thesis was to study the physiological adaptations to a prolonged-fast in different populations on several parameters. In these studies, we were mainly interested in the response of energy-sensing pathways in skeletal muscle. First, we hoped to contribute to the understanding of normal fasting physiology. Besides, a better understanding of the response of these energy-sensing pathways to a prolonged-fast - and the possible differences in this response between lean and

obese subjects - may lead to the identification of factors that are involved in the patho-physiology of obesity. A bit far stretched, baseline differences between lean and obese subjects in the functioning of their energy-sensing systems might give cues for therapeutic targets.

In the current thesis, we hypothesized that the response to fasting would be different between lean and obese subjects. Next to the energy-sensing pathways, we also studied the neuronal response with functional MRI scanning and we assessed the response of the autonomic nervous system by heart rate variability measurements. These studies are described in the "middle" chapters of this thesis. The thesis starts with a chapter that is dedicated to the time-course of energy-sensing adaptations during a 24 hour fast in healthy young men. At the very end of this thesis, we describe the result of a study in which we hypothesized that the adaptations to a 60 hour fast would be altered by the presence of food related odours during fasting.

In **chapter two**, we hypothesized that the response to a prolonged fast of 48 hours would be different between lean and obese individuals. We compared this response on several levels in 14 obese and 12 lean individuals: we made fMRI scans, took blood samples, performed an indirect calorimetry, an electrocardiogram to measure HRV and took muscle biopsies. All measurements were performed both before and after the 48 hour fast (the indirect calorimetry and blood sampling were also per-formed after 24 hours of fasting). The results of the HRV measurements, used to study the effect of fasting on SNS activity in lean and obese individuals, are described in **chapter three**. In **chapter four** we describe the differential effect of fasting on the hypothalamus, amygdala and posterior cingulate cortex functional connectivity net-works (fMRI) in lean and obese individuals. In **chapter five**, we investigated the time course of metabolic adaptations in response to a 24 hour fast. We investigated this time course by taking blood samples, by performing an indirect calorimetry (to meas-ure lipid and carbohydrate oxidation) and by taking muscle biopsies in a group of 12 healthy young male volunteers at 3 time points during a 24 hour fast (different in that respect compared to chapter two). In the muscle biopsies we were mainly interested in the so-called "energy-sensing" pathways. In **chapter six** we evaluated the hypoth-esis that the response to fasting would be influenced by the presence or absence of visual and odorous food cues, based on a study in *Drosophila Melanogaster* [40]. Twelve lean men fasted twice during 60 hours; once in the presence and once in the absence of food cues. We studied the effects of the presence and absence of the

1

food cues on blood parameters, lipid and glucose oxidation (measured by indirect calorimetry) and the hypothalamic BOLD signal (measured by fMRI). In **chapter seven** we discuss all chapters described above.

1

References

1. Simonson DC, DeFronzo RA. Indirect calorimetry: methodological and interpretative problems. *Am J Physiol* 1990; 258(3 Pt 1): E399-E412.

2. Owen OE, Morgan AP, Kemp HG, Sullivan JM, Herrera MG, Cahill GF, Jr. Brain metabolism during fasting. *J Clin Invest* 1967; 46(10): 1589-1595.

3. Cahill GF, Jr. Fuel metabolism in starvation. *Annu Rev Nutr* 2006; 26:1-22.: 1-22.

4. Heemstra KA, Soeters MR, Fliers E, Serlie MJ, Burggraaf J, van Doorn MB, van der Klaauw AA, Romijn JA, Smit JW, Corssmit EP, Visser TJ. Type 2 iodothyronine deiodinase in skeletal muscle: effects of hypothyroidism and fasting. *J Clin Endocrinol Metab* 2009; 94(6): 2144-2150.

5. Boelen A, Wiersinga WM, Fliers E. Fasting-induced changes in the hypothalamus-pituitary-thyroid axis. *Thyroid* 2008; 18(2): 123-129.

6. Bergendahl M, Aloi JA, Iranmanesh A, Mulligan TM, Veldhuis JD. Fasting suppresses pulsatile luteinizing hormone (LH) secretion and enhances orderliness of LH release in young but not older men. *J Clin Endocrinol Metab* 1998; 83(6): 1967-1975.

7. Davies SP, Sim AT, Hardie DG. Location and function of three sites phosphorylated on rat acetyl-CoA carboxylase by the AMP-activated protein kinase. *Eur J Biochem* 1990; 187(1): 183-190.

8. Nakano M, Hamada T, Hayashi T, Yonemitsu S, Miyamoto L, Toyoda T, Tanaka S, Masuzaki H, Ebihara K, Ogawa Y, Hosoda K, Inoue G, Yoshimasa Y, Otaka A, Fushiki T et al. alpha2 Isoform-specific activation of 5'adenosine monophosphate-activated protein kinase by 5-aminoimidazole-4-carboxamide-1-beta-d-ribonucleoside at a physiological level activates glucose transport and increases glucose transporter 4 in mouse skeletal muscle. *Metabolism* 2006; 55(3): 300-308.

9. Kurth-Kraczek EJ, Hirshman MF, Goodyear LJ, Winder WW. 5' AMP-activated protein kinase activation causes GLUT4 translocation in skeletal muscle. *Diabetes* 1999; 48(8): 1667-1671.

10. Andreelli F, Foretz M, Knauf C, Cani PD, Perrin C, Iglesias MA, Pillot B, Bado A, Tronche F, Mithieux G, Vaulont S, Burcelin R, Viollet B. Liver adenosine monophosphate-activated kinase-alpha2 catalytic subunit is a key target for the control of hepatic glucose production by adiponectin and leptin but not insulin. *Endocrinology* 2006; 147(5): 2432-2441.

1

11. Shaw RJ, Lamia KA, Vasquez D, Koo SH, Bardeesy N, Depinho RA, Montminy M, Cantley LC. The kinase LKB1 mediates glucose homeostasis in liver and therapeutic effects of metformin. *Science* 2005; 310(5754): 1642-1646.

12. Koo SH, Flechner L, Qi L, Zhang X, Screaton RA, Jeffries S, Hedrick S, Xu W, Boussouar F, Brindle P, Takemori H, Montminy M. The CREB coactivator TORC2 is a key regulator of fasting glucose metabolism. *Nature* 2005; %20;437(7062): 1109-1111.

13. World Health Organization. Obesity and Overweight, Fact Sheet No 311. 2011. 14. Bandyopadhyay GK, Yu JG, Ofrecio J, Olefsky JM. Increased malonyl-CoA levels in muscle from obese and type 2 diabetic subjects lead to decreased fatty acid oxidation and increased lipogenesis; thiazolidinedione treatment reverses these defects. *Diabetes* 2006; 55(8): 2277-2285.

15. Steinberg GR, Smith AC, van Denderen BJ, Chen Z, Murthy S, Campbell DJ, Heigenhauser GJ, Dyck DJ, Kemp BE. AMP-activated protein kinase is not down-regulated in human skeletal muscle of obese females. *J Clin Endocrinol Metab* 2004; 89(9): 4575-4580.

16. Hojlund K, Mustard KJ, Staehr P, Hardie DG, Beck-Nielsen H, Richter EA, Wojtaszewski JF. AMPK activity and isoform protein expression are similar in muscle of obese subjects with and without type 2 diabetes. *Am J Physiol Endocrinol Metab* 2004; 286(2): E239-E244.

17. Schwartz MW, Woods SC, Porte D, Jr., Seeley RJ, Baskin DG. Central nervous system control of food intake. *Nature* 2000; 404(6778): 661-671.

18. Broadwell RD, Brightman MW. Entry of peroxidase into neurons of the central and peripheral nervous systems from extracerebral and cerebral blood. *J Comp Neurol* 1976; 166(3): 257-283.

19. Bernard C. *Lecons de Physiologie Experimentale Appliqué a la Medicine Faites au College de France*. Bailere et Fils: Paris, France, 1855.

20. Marshall NB, Barrnett RJ, Mayer J. Hypothalamic lesions in goldthioglucose injected mice. *Proc Soc Exp Biol Med* 1955; 90(1): 240-244.

21. Brecher G, Waxler SH. Obesity in albino mice due to single injections of goldthioglucose. *Proc Soc Exp Biol Med* 1949; 70(3): 498-501.

22. Nagamachi Y. Effect of satiety center damage on food intake, blood glucose and gastric secretion in dogs. *Am J Dig Dis* 1972; 17(2): 139-148.

23. Kalra SP, Dube MG, Sahu A, Phelps CP, Kalra PS. Neuropeptide Y secretion increases in the paraventricular nucleus in association with increased appetite for

food. *Proc Natl Acad Sci U S A* 1991; 88(23): 10931-10935.

24. Stanley BG, Kyrkouli SE, Lampert S, Leibowitz SF. Neuropeptide Y chronically injected into the hypothalamus: a powerful neurochemical inducer of hyperphagia and obesity. *Peptides* 1986; 7(6): 1189-1192.

25. Zarjevski N, Cusin I, Vettor R, Rohner-Jeanrenaud F, Jeanrenaud B. Chronic intracerebroventricular neuropeptide-Y administration to normal rats mimics hormonal and metabolic changes of obesity. *Endocrinology* 1993; 133(4): 1753-1758.

26. Fan W, Boston BA, Kesterson RA, Hruby VJ, Cone RD. Role of melanocortinergic neurons in feeding and the agouti obesity syndrome. *Nature* 1997; 385(6612): 165-168.

27. Hagan MM, Rushing PA, Pritchard LM, Schwartz MW, Strack AM, Van Der Ploeg LH, Woods SC, Seeley RJ. Long-term orexigenic effects of AgRP-(83—-132) involve mechanisms other than melanocortin receptor blockade. *Am J Physiol Regul Integr Comp Physiol* 2000; 279(1): R47-R52.

28. Rossi M, Kim MS, Morgan DG, Small CJ, Edwards CM, Sunter D, Abusnana S, Goldstone AP, Russell SH, Stanley SA, Smith DM, Yagaloff K, Ghatei MA, Bloom SR. A C-terminal fragment of Agouti-related protein increases feeding and antagonizes the effect of alpha-melanocyte stimulating hormone in vivo. *Endocrinology* 1998; 139(10): 4428-4431.

29. Pauling L, Coryell CD. The Magnetic Properties and Structure of Hemoglobin, Oxyhemoglobin and Carbonmonoxyhemoglobin. *Proc Natl Acad Sci U S A* 1936; 22(4): 210-216.

30. Ogawa S, Lee TM, Kay AR, Tank DW. Brain magnetic resonance imaging with contrast dependent on blood oxygenation. *Proc Natl Acad Sci U S A* 1990; 87(24): 9868-9872.

31. Baxter MG, Murray EA. The amygdala and reward. *Nat Rev Neurosci* 2002; 3(7): 563-573.

32. Lam CK, Chari M, Lam TK. CNS regulation of glucose homeostasis. *Physiology (Bethesda)* 2009; 24:159-70.: 159-170.

33. Tataranni PA, Gautier JF, Chen K, Uecker A, Bandy D, Salbe AD, Pratley RE, Lawson M, Reiman EM, Ravussin E. Neuroanatomical correlates of hunger and satiation in humans using positron emission tomography. *Proc Natl Acad Sci U S A* 1999; 96(8): 4569-4574.

1

34. DelParigi A, Chen K, Salbe AD, Reiman EM, Tataranni PA. Sensory experience of food and obesity: a positron emission tomography study of the brain regions affected by tasting a liquid meal after a prolonged fast. *Neuroimage* 2005; 24(2): 436-443.

35. Gautier JF, Chen K, Salbe AD, Bandy D, Pratley RE, Heiman M, Ravussin E, Reiman EM, Tataranni PA. Differential brain responses to satiation in obese and lean men. *Diabetes* 2000; 49(5): 838-846.

36. Chan JL, Mietus JE, Raciti PM, Goldberger AL, Mantzoros CS. Short-term fasting-induced autonomic activation and changes in catecholamine levels are not mediated by changes in leptin levels in healthy humans. *Clin Endocrinol (Oxf)* 2007; 66(1): 49-57.

37. Webber J, Macdonald IA. The cardiovascular, metabolic and hormonal changes accompanying acute starvation in men and women. *Br J Nutr* 1994; 71(3): 437-447.

38. Dampney RA. Functional organization of central pathways regulating the cardiovascular system. *Physiol Rev* 1994; 74(2): 323-364.

39. Muscelli E, Emdin M, Natali A, Pratali L, Camastra S, Gastaldelli A, Baldi S, Carpeggiani C, Ferrannini E. Autonomic and hemodynamic responses to insulin in lean and obese humans. *J Clin Endocrinol Metab* 1998; 83(6): 2084-2090.

40. Libert S, Zwiener J, Chu X, Vanvoorhies W, Roman G, Pletcher SD. Regulation of Drosophila life span by olfaction and food-derived odors. *Science* 2007; 315(5815): 1133-1137.

Chapter 2

2

Effects of prolonged fasting on AMPK signaling, gene expression and mitochondrial respiratory-chain content in skeletal muscle from lean and obese individuals

Marjolein A. Wijngaarden[1], Gerard C. van der Zon[2], Ko Willems van Dijk[1,3], Hanno Pijl[1], Bruno Guigas[2,4]

[1] Department of Endocrinology and Metabolism, Leiden University Medical Center, Leiden, The Netherlands
[2] Department of Molecular Cell Biology, Leiden University Medical Center, Leiden, The Netherlands
[3] Department of Human Genetics, Leiden University Medical Center, Leiden, The Netherlands
[4] Department of Parasitology, Leiden University Medical Center, Leiden, The Netherlands

2

Abstract

Obesity in humans is often associated with metabolic inflexibility but the underlying molecular mechanisms remain incompletely understood. The aim of the present study was to investigate how adaptation to prolonged fasting affects energy/nutrient-sensing pathways and metabolic gene expression in skeletal muscle from lean and obese individuals. Twelve lean and 14 non-diabetic obese subjects were fasted for 48 hours. Whole-body glucose/lipid oxidation rates were determined by indirect calorimetry and blood and skeletal muscle biopsies were collected and analyzed. In response to fasting, body weight loss was similar in both groups but the decrease in plasma insulin and leptin, and the concomitant increase in growth hormone were significantly attenuated in obese subjects. The fasting-induced shift from glucose toward lipid oxidation was also severely blunted. At molecular level, the expression of insulin receptor ß (IRβ) was lower in skeletal muscle from obese subjects at baseline, whereas the fasting-induced reductions in insulin signaling were similar in both groups. The protein expression of mitochondrial respiratory-chain components, although not modified by fasting, was significantly reduced in obese subjects. Some minor differences in metabolic gene expression were observed at baseline and in response to fasting. Surprisingly, fasting reduced AMP-activated protein kinase (AMPK) activity in lean but not in obese subjects, whereas the expression of AMPK subunits was not affected. We conclude that whole-body metabolic inflexibility in response to prolonged fasting in obese humans is associated with lower skeletal muscle IRβ and mitochondrial respiratory-chain content as well as a blunted decline of AMPK activity.

Introduction

Obesity is an endemic metabolic disorder affecting almost half a billion people worldwide. Human beings, as all living organisms, have to constantly adjust their metabolism in response to changes in environmental nutrient availability. Metabolic inflexibility, which reflects the inability to adapt tissue-specific substrate oxidation to whole-body fuel availability, was suggested to be implicated in the development of obesity, insulin resistance and type 2 diabetes [1-4]. Thus, the shift from carbohydrate toward lipid oxidation during the transition from postprandial to fasting state is impaired in obese subjects [4]. Taken together, metabolic inflexibility is manifest in a range of metabolic pathways and tissues, notably in skeletal muscle[5], but little is known about the underlying molecular mechanism(s) [6;7].

To ensure efficient metabolic adaptations to nutritional or environmental changes, various energy/nutrient-sensing pathways are mobilized in peripheral tissues [8]. Among them, the AMP-activated protein kinase (AMPK), a serine/threonine protein kinase, which acts as a cellular energy and nutrient sensor, is believed to play a crucial role in the regulation of tissue-specific substrate metabolism [9-11]. AMPK consists of a heterotrimeric complex containing a catalytic subunit α and two regulatory β and γ subunits. Each subunit has several isoforms encoded by distinct genes, giving multiple heterotrimer combinations with different tissue distribution and cellular localization [9-11]. The α subunit contains a threonine residue (Thr172) whose phosphorylation by upstream AMPK kinases, such as the liver kinase B (LKB1) or calmodulin-dependent protein kinase kinase β (CAMKKβ), is required for AMPK activation. The β subunit acts as a scaffold to which the two other subunits are bound, and contains a carbohydrate binding site which allows AMPK to sense energy reserves in the form of glycogen [9-11]. Binding of AMP and/or ADP to the γ subunit activates AMPK via a complex mechanism involving direct allosteric activation, phosphorylation on Thr172 by AMPKK, and inhibition of dephosphorylation by protein phosphatase(s) that remain to be identified [9-11]. Thus, any change in cellular energy status activates AMPK, leading to concomitant inhibition of energy-consuming processes and stimulation of ATP-generating pathways in order to restore energy balance [9-11]. As a result, glycogen and protein synthesis, as well as cell growth and differentiation, are inhibited, whereas fatty acid (FA) oxidation and glucose uptake are stimulated [9-11]. This regulation involves phosphorylation by AMPK of key metabolic enzymes and transcription factors involved in gene expression [9;11].

The purpose of the present study was to investigate whether metabolic adaptations to prolonged fasting differ in lean and obese individuals and whether this is associated with changes in skeletal muscle AMPK signaling pathway, as previously reported in rodents [12;13].

2

Materials and Methods

Ethical approval

The present study (Clinical Trial Registration Number: NTR2401) was approved by the Medical Ethical Committee of the Leiden University Medical Centre and performed in accordance with the principles of the revised Declaration of Helsinki. All volunteers gave written informed consent before participation.

Subjects

Twenty-six volunteers, 12 lean (2 males, 10 females, body mass index (BMI) 23.3 ± 0.5 kg/m^2) and 14 obese (2 males, 12 females, BMI 35.2 ± 1.2 kg/m^2) subjects were included. All of them were healthy weight-stable non-smoking Caucasians with a fasting plasma glucose ≤5.6 mmol/l and without family history of diabetes. Height, weight, body mass index (BMI), hip and waist circumference were recorded according to World Health Organization recommendations.

Study design

All participants were admitted to our research center after an overnight fast. The intervention study started after a standardized breakfast (t=0, two slices of brown bread with cheese), followed by 48 hours of fasting. Water and caffeine-free tea were allowed *ad libitum*. To ensure complete adherence to the study, the subjects were kept under supervision in our research center during the whole experimental period. Blood samples were taken after breakfast (t=90 min) and after 24 and 48 hours of fasting by venapuncture in the elbow. Muscle biopsies (~50-75 mg) from *musculus vastus lateralis* were collected after breakfast (t=135 min) and after 48 hours of fasting, as previously described [14].

Indirect calorimetry

Subjects were placed under the ventilated hood after 45 min, 24 hours and 48 hours of fasting (OxyconPro, Mijnhardt Jaegher, The Netherlands). Substrate oxidation was calculated from CO_2 and O_2 concentrations in the exhaled air, as previously described [15].

Laboratory analysis

Serum glucose, total cholesterol, high density lipoprotein (HDL) cholesterol, triglyc-

erides (TG) and c-reactive protein (CRP) were measured on a Modular Analytics P-800 system (Roche Diagnostics, Germany). Low density lipoprotein (LDL) cholesterol was calculated according to the Friedewald equation [16]. Serum insulin and insulin-like growth factor 1 (IGF-1) were measured by immunoluminometric assay on an Immulite 2500 automated system (Siemens Healthcare Diagnostics, The Netherlands). Cortisol, free T4 (FT4) and thyroid stimulating hormone (TSH) were measured by electrochemoluminescence immunoassay on a Modular Analytics E-170 system (Roche Diagnostics, Germany). Triiodothyronine (T3) was measured with by fluorescence polarization immunoassay on an AxSym system (Abbott, US). Growth hormone (GH) was measured by immunofluorometric assay (Wallac, Finland). Serum active ghrelin, leptin and adiponectin were determined by radioimmunoassay (Millipore, USA).

Western Blot

Skeletal muscle biopsies (~30-45 mg) were homogenized by Ultra-Turrax (22 000 rpm; 2x5 sec) in a 6:1 (v/w) ratio of ice-cold buffer containing: 50 mM HEPES (pH 7.6), 50 mM NaF, 50 mM KCl, 5 mM NaPPi, 1 mM EDTA, 1 mM EGTA, 5 mM β-GP, 1 mM Na3VO4, 1 mM DTT, 1% NP40 and protease inhibitors cocktail (Complete, Roche, The Netherlands). Western blots were performed using phospho-specific (Ser473-PKB, phospho-Akt substrate and Thr172-AMPKα from Cell Signaling; Thr246-PRAS40 from Biosource; Tyr612-IRS1 from Invitrogen) or total primary antibodies (Tubulin and AMPKβ1+2 from Cell Signaling; AMPKα1 and AMPKα2 from Kinasource; AMPKγ1, PGC-1α and MitoProfile OXPHOS from AbCam; AMPKγ3, IRβ and LKB1 from Santa Cruz; CAMKKα/β from BD Biosciences; AMPKα2 truncated is a kind gift of Pr. DG Hardie), as previously described[17].

AMPK activity

AMPK heterotrimeric complexes were immunoprecipitated from 500 µg of muscle lysate using protein A-agarose beads (GE Healthcare, The Netherlands) and a pan α-specific AMPK antibody (Santa Cruz) incubated together at 4°C overnight on a rotating wheel. After incubation, the immunoprecipitate was washed twice in ice-cold lysis buffer without NP40 and once in ice-cold assay buffer containing: 50 mM HEPES (pH 7.2), 80 mM KCl, 1 mM EDTA, 5 mM MgCl2, 1 mM DTT, 1% glycerol and 1 mg/ml FFA-free BSA. The reaction was initiated at 30°C by addition of a mixture of 200 µM AMP, 200 µM SAMS-peptide (kind gift from Dr. L. Bertrand, Brussels, Belgium), 100 µM Mg-ATP, and 2 µCi of [γ-32P]ATP (PerkinElmer, The Netherlands). After 15 min,

2

the beads were briefly spun down and 20 µl of supernatant was spotted onto P81 filter paper (Whatman, GE Healthcare, The Netherlands). After extensive washing in 1% phosphoric acid, the filter paper was dried and analyzed for radioactivity using a Tri-Carb Liquid Scintillation Counter (Packard, The Netherlands). The non-specific activity (without SAMS-peptide) was subtracted from the specific kinase activity, which was expressed in mU/mg protein.

RNA isolation and real-time RT-PCR
Total RNA was isolated from skeletal muscle biopsies (~25-30 mg) using the phenol-chloroform extraction method (Tripure RNA Isolation reagent, Roche, Germany) and quantified by NanoDrop. First-strand cDNA were synthesized from 1 µg total RNA using a Superscript first strand synthesis kit (Invitrogen, The Netherlands). Real-time PCR assays were performed using specific primers sets (sequences provided on request) and SYBR Green on a StepOne Plus Real-time PCR system (Applied Biosystems, US). mRNA expression was normalized to ribosomal protein S18 (*Rps18*) and expressed as arbitrary units.

Statistical analysis
All data are presented as mean ± standard error of the mean (SEM). For metabolic parameters and indirect calorimetry, a mixed model was used to determine the effects of fasting in between groups. For Western blot and RT-qPCR, the data were analyzed with unpaired or paired t-tests for determining the baseline differences and within group effects, respectively. All the statistical analysis were performed using SPSS for Windows version 18.0 (SPSS Inc., US).

Results

Effects of fasting on body weight, body composition and metabolic parameters in lean and obese subjects
The anthropometric and metabolic characteristics of the subjects were determined at baseline (post-meal), *i.e.* ~90 min after a standardized breakfast (300 Kcal), and after 24 or 48h of fasting (Table 1). At baseline, body weight, BMI and waist-to-hip ratio were significantly higher in obese than in lean subjects. Plasma glucose, insulin, leptin and triglycerides levels were also elevated in the obese group (+11%, +148%, +204% and +40%, respectively; p<0.05), reflecting whole-body insulin/leptin resist-

Table 1. Anthropometric and metabolic parameters at baseline and during fasting in lean and obese subjects

	Lean			Obese			Interaction p-value
	Post-meal	24h fast	48h fast	Post-meal	24h fast	48h fast	
Age (years)	27 ± 3			30 ± 3			
Length (cm)	175 ± 3			174 ± 2			
Weight (kg)	72 ± 3	nd	69 ± 3*	107 ± 4#	nd	104 ± 4*	0.20
Body mass index (kg/m^2)	23.3 ± 0.5	nd	22.5 ± 0.5*	35.2 ± 1.2#	nd	34.4 ± 1.2*	0.94
Waist-Hip ratio	0.80 ± 0.02	nd	nd	0.87 ± 0.01#	nd	nd	
Glucose (mmol/l)	4.5 ± 0.2	4.2 ± 0.2	3.5 ± 0.1*	5.0 ± 0.2#	4.7 ± 0.1	4.0 ± 0.2*	0.92/0.94
Insulin (mU/l)	7.9 ± 2.0	1.0 ± 0.1*	1.2 ± 0.2*	19.6 ± 2.1#	4.7 ± 1.4*	3.2 ± 0.8*	0.00/0.00
Growth Hormone (mU/l)	0.9 ± 0.3	nd	9.0 ± 2.0*	0.7 ± 0.4	nd	3.1 ± 0.6*	0.01
IGF-1 (nmol/l)	20.1 ± 2.1	nd	20.2 ± 1.8	17.4 ± 2.0	nd	19.5 ± 2.2	0.35
Leptin (µg/l)	11.9 ± 1.8	6.6 ± 1.2*	4.1 ± 0.4*	36.2 ± 3.6#	28.2 ± 3.5*	20.6 ± 3.2*	0.37/0.01
Adiponectin (µg/l)	11.1 ± 1.2	nd	10.5 ± 1.2	7.6 ± 1.0#	nd	7.4 ± 0.9	0.61
Ghrelin (pg/ml)	168 ± 27	nd	198 ± 34	184 ± 45	nd	228 ± 53	0.87
Cholesterol (mmol/l)	4.7 ± 0.3	nd	5.0 ± 0.3*	5.0 ± 0.2	nd	5.3 ± 0.3*	0.86
Triglycerides (mmol/l)	1.0 ± 0.1	nd	1.0 ± 0.1	1.4 ± 0.1#	nd	1.4 ± 0.1	0.63
HDL (mmol/l)	1.5 ± 0.1	nd	1.6 ± 0.1	1.4 ± 0.1	nd	1.4 ± 0.1	0.41
LDL (mmol/l)	2.7 ± 0.2	nd	3.0 ± 0.2*	3.0 ± 0.1	nd	3.4 ± 0.2*	0.43
TSH (mU/l)	1.6 ± 0.2	1.2 ± 0.1*	1.0 ± 0.1*	2.0 ± 0.1	1.4 ± 0.2*	1.7 ± 0.3	0.75/0.10
T3 (nmol/l)	1.8 ± 0.1	1.6 ± 0.1*	1.3 ± 0.1*	2.1 ± 0.1	1.9 ± 0.1*	1.7 ± 0.1*	0.82/0.11
FT4 (pmol/l)	15.4 ± 0.5	nd	16.0 ± 0.7	14.5 ± 0.5	nd	15.0 ± 0.6	0.96
CRP (mg/l)	1.3 ± 0.3	nd	5.0 ± 1.1*	5.1 ± 1.0	nd	9.9 ± 2.4*	0.55
Cortisol (µmol/l)	0.38 ± 0.07	nd	0.61 ± 0.08*	0.37 ± 0.06	nd	0.49 ± 0.08*	0.18

Data are shown as mean ± SEM, n=12-14. *, $p<0.05$ vs basal ; #, $p<0.05$ vs lean subjects; nd, not determined. Interaction p-value between post-meal and 24 hours/post-meal and 48 hour

2

ance and glucose intolerance. In response to fasting, body weight was decreased to the same extent in obese and lean subjects (-2.8% *vs* -3.5%, respectively; p<0.05). As expected, fasting induced a significant decrease in plasma glucose, insulin, leptin, T3 and TSH levels, whereas circulating total cholesterol, LDL, growth hormone, CRP and cortisol increased in both groups (Table 1). However, the fasting-induced changes in plasma insulin (at 24 and 48h: -76% and -84% *vs* -87% and -85% in obese and lean, respectively; p<0.01), growth hormone (at 48h: +343% *vs* +900% for obese and lean, respectively; p<0.01) and leptin (at 24 and 48h: -22% and -43% *vs* -45% and -66% in obese and lean, respectively; p<0.01) levels were significantly attenuated in obese subjects (Table 1).

Effects of fasting on whole-body glucose and lipid oxidation rates in lean and obese subjects

The substrate oxidation rates were determined by indirect calorimetry at baseline and after 24 and 48 hours of fasting (Table 2). At baseline, the absolute resting energy expenditure (REE, in Kcal/day) was significantly higher in obese than in lean subjects (+24%; p<0.05), an effect that however disappeared when the data are corrected for lean body mass (Kcal/day/Kg FFM). This metabolic feature is associated with higher lipid (+62%) and lower glucose (-22%; p<0.05) oxidation rates. Fasting led to significant decrease in respiratory quotient (RQ), indicating a shift in substrate metabolism from glucose toward lipid oxidation in both groups (Table 2). However, these fasting-induced changes were significantly attenuated in the obese subjects, with a lower reduction in glucose oxidation (at 24 and 48h: -38% and -60% vs -53% and -70% in obese and lean, respectively; p<0.01) and a lesser increase in lipid oxidation (at 24 and 48h: +41% and +76% vs +133% and +214% in obese and lean, respectively; p<0.01). In addition, the REE was also differently affected in response to fasting between groups, with a significant decrease only evidenced in the obese group (at 48h: -7% vs +3% in obese and lean, respectively; p<0.01) (Table 2).

Effect of fasting on insulin signaling pathways in human skeletal muscle from lean and obese subjects

The protein expression and phosphorylation state of key molecules involved in the insulin signaling pathway were determined in skeletal muscle biopsies at baseline and after 48h of fasting (Figure 1). Tubulin expression, used as a housekeeping protein, was similar between lean and obese subjects at baseline and was not affected

Table 2. Substrate oxidation rates at baseline and during fasting in lean and obese subjects

	Lean			Obese			Interaction p-value
	Post-meal	24h fast	48h fast	Post-meal	24h fast	48h fast	
Resting energy expenditure (kcal/day)	1502 ± 68	1444 ± 70	1546 ± 83	1856 ± 63#	1734 ± 59*	1719 ± 55*	0.24/0.00
Resting energy expenditure (kcal/kgFFM/day)	29.7 ± 1.6	28.6 ± 1.4	30.7 ± 1.2	30.4 ± 0.8	28.6 ± 0.9*	28.6 ± 0.9*	0.46/0.01
Respiratory quotient	0.94 ± 0.03	0.82 ± 0.02*	0.77 ± 0.02*	0.87 ± 0.01#	0.82 ± 0.02*	0.78 ± 0.01*	0.03/0.01
Lipid oxidation (µmol/kgFFM/min)	2.1 ± 0.6	4.9 ± 0.6*	6.6 ± 0.7*	3.4 ± 0.4	4.8 ± 0.6*	5.9 ± 0.5*	0.09/0.02
Glucose oxidation (µmol/kgFFM/min)	23.6 ± 2.8	11.0 ± 1.4*	7.1 ± 1.6*	18.3 ± 1.6#	11.4 ± 1.6*	7.4 ± 1.4*	0.07/0.08

Data are shown as mean ± SEM, n=12-14. *, $p<0.05$ vs basal ; #, $p<0.05$ vs lean subjects; kgFFM, kilogram fat free mass. Interaction p-value between post-meal and 24 hours/post-meal and 48 hours.

by fasting (Figure 1A). By contrast, the insulin receptor β (IRβ) expression was significantly lower in obese when compared to lean subjects at baseline (Figure 1B, -18%; p=0.02), but its increase in response to fasting was similar in both groups (+17% and +18% in lean and obese, respectively; p<0.05). Downstream IRβ, the phosphorylation of insulin-receptor substrate (IRS) 1, protein kinase B (PKB, also called Akt) and of PKB downstream targets Proline-Rich Akt Substrate of 40kDa (PRAS40) and Akt Substrate of 160 kDa (AS160) on key regulating residues were similar between lean and obese subjects at baseline (Figure 1C-F). In line with the decrease in plasma insulin levels, the phosphorylation states of these proteins were similarly reduced after 48h fast in both groups. Of note, protein expression of IRS1, PKB, PRAS40 and AS160 were not affected whatever the conditions (data not shown).

Effect of fasting on AMPK expression and signaling in human skeletal muscle from lean and obese subjects

We next assessed whether prolonged fasting affects the protein expression and phosphorylation state of AMPKα on its activating Thr172 residue. AMPKα expression was similar in lean and obese subjects whatever the condition (Figure 2A). Surprisingly, AMPK-Thr172 phosphorylation, which was not different between groups at baseline, was reduced by fasting in lean (-19%, p=0.08) but not in obese (-1%, p=0.90) individuals (Figure 2B-
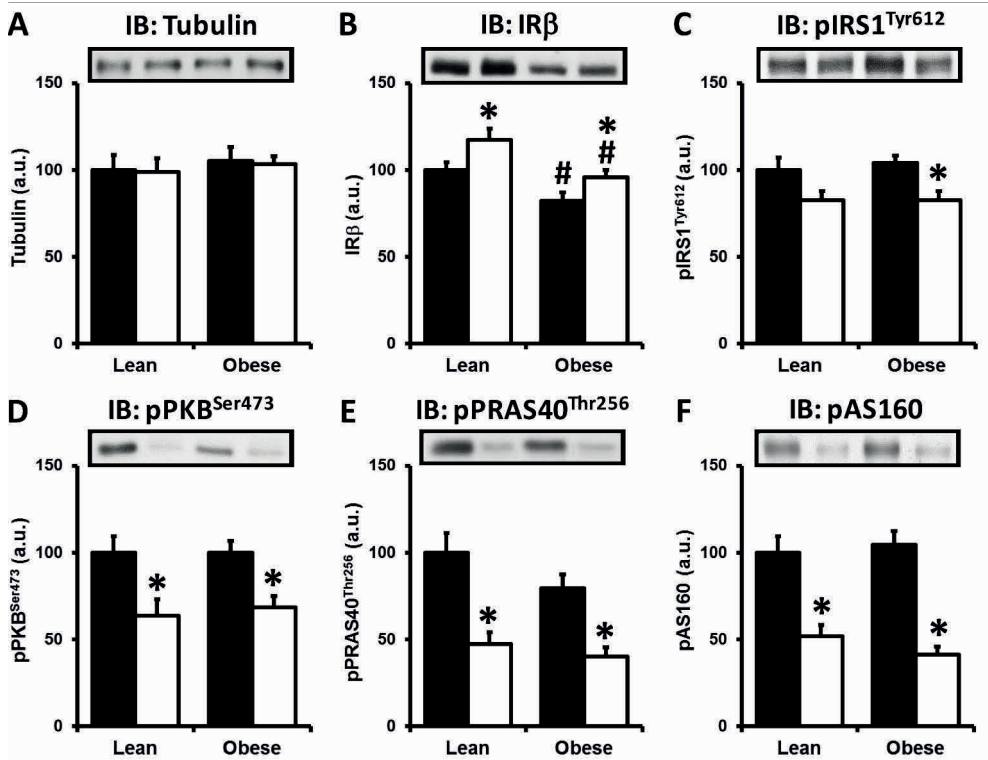
Figure 1. Effect of fasting on insulin signaling pathways in skeletal muscle from lean and obese subjects.

The expression of tubulin (A), insulin receptor β (B) and the phosphorylation states of Tyr612-IRS1 (C), Ser473-PKB (D), Thr256-PRAS40 (E) and phospho-AS160 (F) were assessed by Western Blot in skeletal muscle from lean and obese subjects before (black bars) and after 48h of fasting (open bars). Representative blots for one subject per group are shown. Results are normalized to lean subjects and expressed as mean ± SEM; n=12-14; *p<0.05 compared with baseline, #p<0.05 compared with lean subjects.

C). This borderline significant trend was confirmed by determination of AMPK activity using a kinase assay (Figure 2D). Furthermore, the fasting-induced change in the phosphorylation state of acetyl-CoA carboxylase (ACC) at Ser221, one of the main AMPK downstream target, followed the same pattern although not reaching a significant threshold (-18% in lean vs +4% in obese, p=0.07 and p=0.72, respectively). Although some differences were observed at the mRNA levels (Table 3), the protein expression of the different isoforms of AMPK catalytic α and regulatory β and γ subunits were similar at baseline, except for the AMPKγ2 short isoform that was significantly lower in obese when compared to lean subjects (Figure 3). The expression of all these AMPK subunits was not affected by fasting in either group, suggesting that the difference in AMPK response between lean and obese is unlikely due to changes
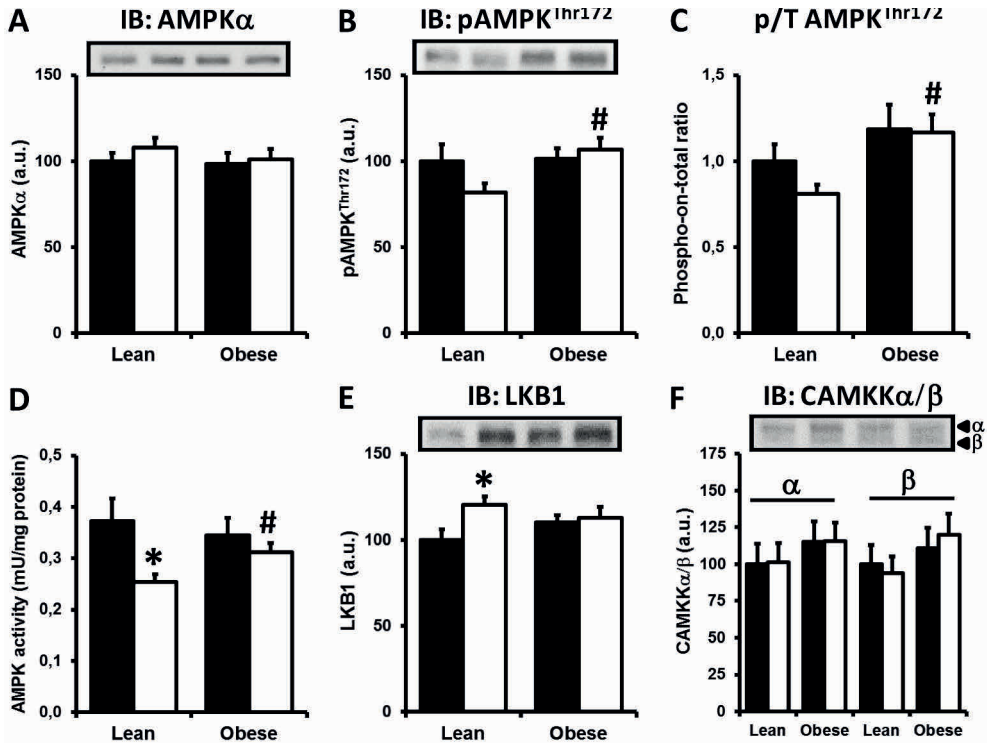
Figure 2. Effect of fasting on AMPK signaling in skeletal muscle from lean and obese subjects.
The phosphorylation state of AMPKα on Thr172 (B) and the expression of AMPK(pan)α (A), LKB1 (E) and CAMKKα/β (F) were assessed by Western Blot in skeletal muscle from lean and obese subjects before (black bars) and after 48h of fasting (open bars). The phospho-on-total ratio for AMPKα-Thr172 was calculated (C). AMPK activity was determined by kinase assay following immunoprecipitation of the AMPK heterotrimer using a pan α antibody (D). Representative blots for one subject per group are shown. Results are normalized to lean subjects and expressed as mean ± SEM; n=12-14; *p<0.05 compared with baseline, #p<0.05 compared with lean subjects.

in heterotrimer composition. Of note, the protein expression of the AMPK upstream kinase LKB1, but not of CAMKKα/β, was significantly increased by fasting only in lean subjects (Figure 2E-F).

Effect of fasting on metabolic genes expression in human skeletal muscle from lean and obese subjects

The mRNA expression of key genes involved in glucose and lipid metabolism were determined in skeletal muscle from lean and obese subjects. At baseline, transcript levels of HK1, PKM2, PPARA, CD36, ACACA, ATP2A1, ACADM, ACOX3 and PDK4 were significantly higher in obese when compared to lean individuals, whereas LPL mRNA expression was found to be significantly lower (Table 4). Prolonged fasting in-

2

Table 3. Effects of fasting on mRNA expression of AMPK kinases and AMPK subunits in skeletal muscle from lean and obese subjects

Gene name	Gene symbol	Entrez gene	Lean		Obese		Interaction p-value
			Post-meal	48h fast	Post-meal	48h fast	
Liver Kinase B1 (LKB1)	STK11	6794	1.0 ± 0.1	1.3 ± 0.2	1.2 ± 0.2	1.4 ± 0.3	0.33
Calcium/calmodulin-dependent protein kinase kinase a (CAMKK a)	CAMKK1	10645	1.0 ± 0.2	1.8 ± 0.6	1.0 ± 0.6	2.0 ± 2.0	0.92
Calcium/calmodulin-dependent protein kinase kinase b (CAMKK b)	CAMKK2	84254	1.0 ± 0.1	1.2 ± 0.2	1.1 ± 0.3	1.1 ± 0.5	0.41
AMP-activated protein kinase α1	PRKAA1	5562	1.0 ± 0.1	1.1 ± 0.1	1.1 ± 0.1	1.2 ± 0.1	0.68
AMP-activated protein kinase α2	PRKAA2	5563	1.0 ± 0.1	1.1 ± 0.1	1.0 ± 0.1	1.2 ± 0.2*	0.27
AMP-activated protein kinase β1	PRKAB1	5564	1.0 ± 0.1	1.3 ± 0.2*	1.0 ± 0.1	1.2 ± 0.1*	0.82
AMP-activated protein kinase β2	PRKAB2	5565	1.0 ± 0.1	1.0 ± 0.2	1.2 ± 0.2	1.2 ± 0.2	0.76
AMP-activated protein kinase γ1	PRKAG1	5571	1.0 ± 0.1	2.0 ± 0.4*	1.7 ± 0.2#	1.6 ± 0.3	0.06
AMP-activated protein kinase γ2^{ALL}	PRKAG2	51422	1.0 ± 0.2	0.7 ± 0.2*	1.1 ± 0.1	0.7 ± 0.0*	0.70
AMP-activated protein kinase γ2^{LONG}	PRKAG2	51422	1.0 ± 0.1	1.6 ± 0.4*	1.0 ± 0.1	1.5 ± 0.3*	0.68
AMP-activated protein kinase γ3	PRKAG3	53632	1.0 ± 0.2	0.8 ± 0.2	1.8 ± 0.7	1.0 ± 0.4*	0.00

Data are shown as mean ± SEM, n=8-6. *, $p < 0.05$ vs post-meal; #, $p < 0.05$ vs lean subjects
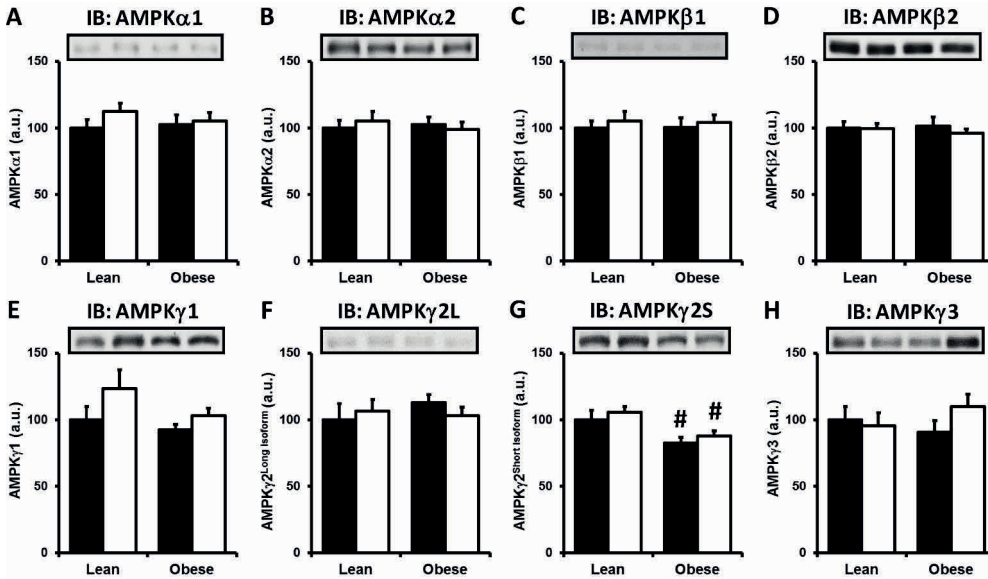
Figure 3: Effect of fasting on protein expression of AMPK regulatory subunits in skeletal muscle from lean and obese subjects.
The expression of AMPKα1 (A), AMPKα2 (B), AMPKβ1 (C), AMPKβ2 (D), AMPKγ1 (E), AMPKγ2 (long isoform, F), AMPKγ2 (short isoform, G), and AMPKγ3 (H) were assessed by Western Blot in skeletal muscle from lean and obese subjects before (black bars) and after 48h of fasting (open bars). Representative blots for one subject per group are shown. Results are normalized to lean subjects and expressed as mean ± SEM; n=12-14; *p<0.05 compared with baseline, #p<0.05 compared with lean subjects.

duces significant upregulation of INSR, PDK4, PFKFB3 and UCP3, and downregulation of HK2 and PPARGC1A mRNA expression in lean subjects (Table 4), in line with previous studies [18-21]. Furthermore, we also report that SLC2A4, PKM2, CD36, ACSL1, NDUFB8 and ACAT2 were significantly reduced in response to fasting. However, among these key metabolic transcription factors and genes only ACAT2, SLC2A1 and NRF1, were shown to be differentially affected by fasting in lean and obese individuals (Table 4).

Effect of fasting on PGC-1α and mitochondrial respiratory-chain components expression in human skeletal muscle from lean and obese subjects
Finally, the protein expression of PGC-1α, a key transcription factor involved in mitochondrial biogenesis, and of several mitochondrial respiratory-chain complex subunits were measured in skeletal muscle from lean and obese subjects (Figure 4). At baseline, we found that although PGC-1α expression was similar in both groups, all the respiratory-chain subunits were significantly lower in the obese when compared to
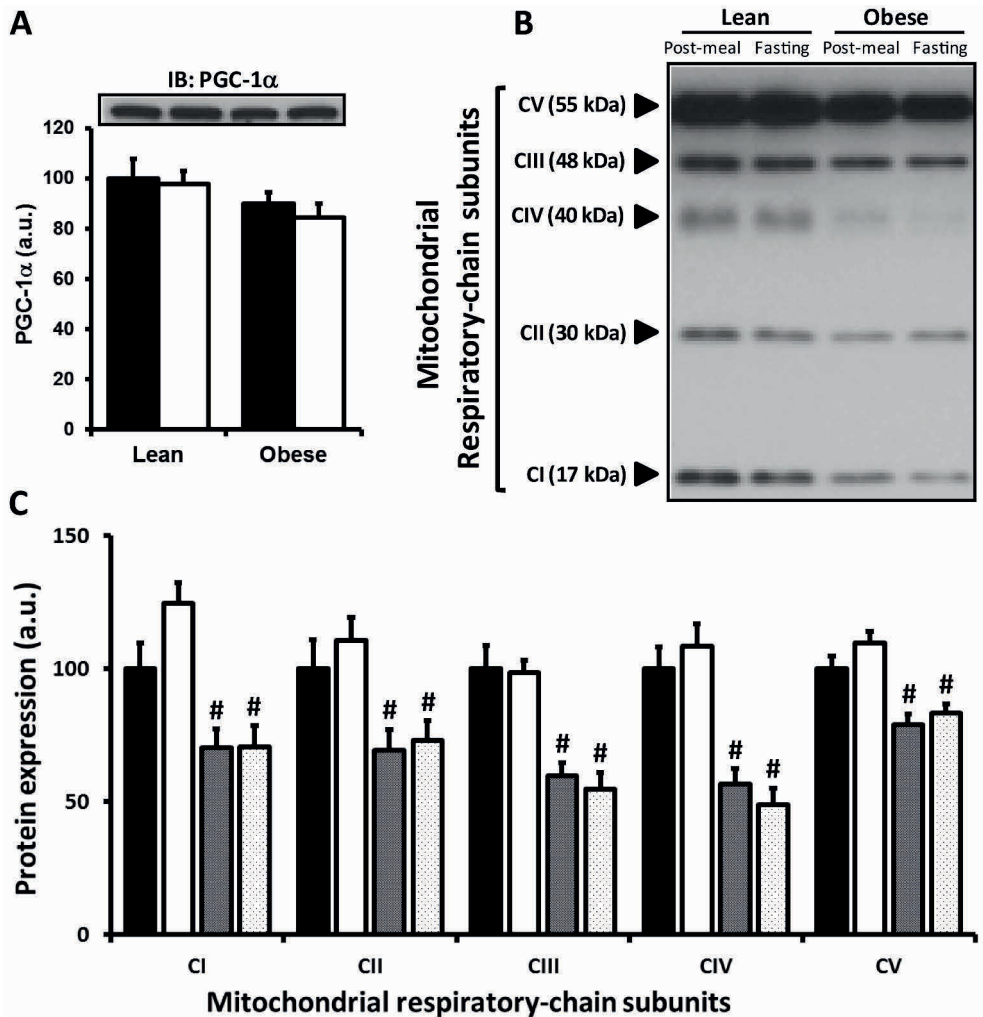
Figure 4: Effect of fasting on mitochondrial respiratory-chain subunits expression in skeletal muscle from lean and obese subjects.

The expression of PGC-1α (A) and various mitochondrial respiratory-chain subunits (CI: NDUFB8; CII: SDHB; CIII: UQCRC2; CIV: MTCO1; CV:ATP5A) were assessed by Western Blot in skeletal muscle before (closed bars) and after 48h of fasting (open bars) in lean and obese subjects (black and grey bars, respectively). Representative blots are shown. Results are normalized to lean subjects and expressed as mean ± SEM; n=12-14; *p<0.05 compared with baseline, #p<0.05 compared with lean subjects.

lean subjects (-30%, -30%, -40%, -43% and -21% for CI to V, respectively; $p<0.05$). The expression of PGC-1α and mitochondrial proteins were not significantly affected by fasting in both groups, although a trend for a specific increase in the respiratory-chain complex 1 subunit (+25%; $p=0.06$) was observed in skeletal muscle from lean subjects (Figure 4).

2

2

Table 4. Effects of fasting on metabolic gene expression in skeletal muscle from lean and obese subjects

Gene name	Gene symbol	Entrez gene	Lean		Obese		Interaction p-value
			Post-meal	48h fast	Post-meal	48h fast	
Glucose metabolism							
Transcription factors							
Carbohydrate-responsive element-binding protein (ChREBP)	*MLXIPL*	51085	1.0 ± 0.1	0.9 ± 0.3	1.0 ± 0.2	0.8 ± 0.1	0.91
Glucose transport and phosphorylation							
Insulin receptor	*INSR*	3643	1.0 ± 0.1	1.6 ± 0.3	1.0 ± 0.1	1.6 ± 0.2*	0.84
Akt substrate of 160 kDa (AS160)	*TBC1D4*	9882	1.0 ± 0.1	1.2 ± 0.2	1.2 ± 0.1#	1.6 ± 0.2*	0.91
TBC1D1	*TBC1D1*	23216	1.0 ± 0.2	1.0 ± 0.2	1.4 ± 0.2#	1.4 ± 0.4	0.88
Solute carrier family 2, member 1 (GLUT-1)	*SLC2A1*	6513	1.0 ± 0.2	1.1 ± 0.3	1.0 ± 0.3	2.2 ± 0.6*	0.05
Solute carrier family 2, member 4 (GLUT-4)	*SLC2A4*	6517	1.0 ± 0.1	0.7 ± 0.2*	1.0 ± 0.1	0.7 ± 0.1*	0.64
Hexokinase 1	*HK1*	3098	1.0 ± 0.1	1.3 ±0.2	1.4 ± 0.2#	1.5 ± 0.2	0.44
Hexokinase 2	*HK2*	3099	1.0 ± 0.2	0.4 ± 0.2*	0.9 ± 0.2	0.3 ± 0.1*	0.86
Glycolysis							
Phosphofructokinase	*PFKM*	5213	1.0 ± 0.1	1.0 ± 0.2	1.1 ± 0.1	0.9 ± 0.1	0.76
6-phosphofructo-2-kinase/fructose-2,6-biphosphatase 3	*PFKFB3*	5209	1.0 ± 0.2	7.2 ± 2.6*	2.0 ± 0.8	9.7 ± 5.3*	0.44
Pyruvate kinase	*PKM2*	5315	1.0 ± 0.1	0.7 ± 0.2*	1.5 ± 0.3#	0.8 ± 0.1*	0.31
Glycogen metabolism							
Glycogen synthase 1	*GYS1*	2997	1.0 ± 0.3	1.0 ± 0.3	1.3 ± 0.6	0.7 ± 0.5	0.17
Glycogen phosphorylase	*PYGM*	5837	1.0 ± 0.1	0.9 ± 0.1	1.0 ± 0.1	0.8 ± 0.1	0.61
Fatty acid metabolism							
Transcription factors							
Peroxisome proliferator-activated receptor α (PPARα)	*PPARA*	5465	1.0 ± 0.1	0.9 ± 0.2	1.3 ± 0.2	0.9 ± 0.1*	0.21
Peroxisome proliferator-activated receptor δ (PPARβ/δ)	*PPARD*	5467	1.0 ± 0.1	0.9 ± 0.3	1.2 ± 0.1	1.1 ± 0.2	0.76
Fatty acid transport and activation							
Lipoprotein lipase	*LPL*	4023	1.0 ± 0.2	0.7 ± 0.2*	0.7 ± 0.1#	0.6 ± 0.1	0.20
Fatty acid translocase/CD36	*CD36*	948	1.0 ± 0.1	0.7 ± 0.1*	1.2 ± 0.1#	0.9 ± 0.1*	0.17
Fatty acid binding protein 3	*FABP3*	2170	1.0 ± 0.1	0.9 ± 0.1	1.3 ± 0.2	1.2 ± 0.2	0.72
Acyl-CoA synthetase long-chain family member 1	*ACSL1*	2180	1.0 ± 0.1	0.7 ± 0.1*	1.3 ± 0.1	0.7 ± 0.1*	0.80
Acyl-CoA synthetase short-chain family member 2	*ACSS2*	55902	1.0 ± 0.1	1.2 ± 0.2	0.9 ± 0.1	0.8 ± 0.2	0.17
Acetyl-CoA carboxylase α	*ACACA*	31	1.0 ± 0.1	1.5 ± 0.3	1.4 ± 0.2#	1.5 ± 0.2	0.31
Acetyl-CoA carboxylase β	*ACACB*	32	1.0 ± 0.1	1.5 ± 0.4	1.1 ± 0.2	1.2 ± 0.3	0.40

Gene name	Gene symbol	Entrez gene	Lean		Obese		Interaction p-value
			Post-meal	48h fast	Post-meal	48h fast	
Malonyl-CoA decarboxylase	MLYCD	23417	1.0 ± 0.1	1.2 ± 0.3	1.4 ± 0.3	1.3 ± 0.3	0.87
Mitochondrial FA transport							
Carnitine palmitoyltransferase 1A	CPT1A	1374	1.0 ± 0.1	1.0 ± 0.1	1.2 ± 0.2	1.2 ± 0.2	0.76
Carnitine palmitoyltransferase 1B	CPT1B	1375	1.0 ± 0.1	0.8 ± 0.2	1.0 ± 0.1	0.9 ± 0.1	0.77
Carnitine palmitoyltransferase 2	CPT2	1376	1.0 ± 0.2	1.2 ± 0.1	1.1 ± 0.1	0.9 ± 0.2	0.19
Mitochondrial metabolism							
Mitochondrial biogenesis							
PPARγ, coactivator 1α (PGC-1α)	PPARGC1A	10891	1.0 ± 0.2	0.6 ± 0.1*	1.3 ± 0.2	0.6 ± 0.1*	0.29
PPARγ, coactivator 1β (PGC-1β)	PPARGC1B	133522	1.0 ± 0.2	1.0 ± 0.3	1.2 ± 0.1	1.1 ± 0.1	0.69
Transcription factor A	TFAM	7019	1.0 ± 0.1	0.9 ± 0.1	1.0 ± 0.0	0.8 ± 0.1	0.60
Nuclear respiratory factor 1	NRF1	4899	1.0 ± 0.1	1.2 ± 0.1	1.2 ± 0.1	0.9 ± 0.3*	0.04
TCA cycle & electron transport chain							
Pyruvate dehydrogenase kinase 4	PDK4	5166	1.0 ± 0.3	5.6 ± 1.6*	1.9 ± 0.7#	4.7 ± 1.2	0.24
Pyruvate carboxylase	PC	5091	1.0 ± 0.1	1.0 ± 0.2	1.2 ± 0.2	1.4 ± 0.2	0.19
Citrate synthase	CS	1431	1.0 ± 0.1	0.9 ± 0.1	1.0 ± 0.1	0.8 ± 0.1	0.67
Succinate dehydrogenase complex, subunit A	SDHA	6389	1.0 ± 0.1	0.8 ± 0.1	1.1 ± 0.1	1.1 ± 0.1	0.40
NADH dehydrogenase (ubiquinone) 1 beta subcomplex, 8	NDUFB8	4714	1.0 ± 0.1	0.8 ± 0.1*	1.0 ± 0.1	0.8 ± 0.1*	0.57
ATPase, Ca++ transporting, cardiac muscle, fast twitch 1	ATP2A1	487	1.0 ± 0.1	1.1 ± 0.3	1.5 ± 0.3#	1.2 ± 0.3	0.83
Uncoupling protein 3	UCP3	7352	1.0 ± 0.2	3.4 ± 0.8*	1.7 ± 0.6	3.4 ± 0.7*	0.85
FA β-oxidation							
Acyl-CoA dehydrogenase, C-2 to C-3 short chain	ACADS	35	1.0 ± 0.1	1.1 ± 0.3	1.0 ± 0.1	1.1 ± 0.2	0.83
Acyl-CoA dehydrogenase, short/branched chain	ACADSB	36	1.0 ± 0.1	1.0 ± 0.2	1.2 ± 0.1	1.2 ± 0.2	0.98
Acyl-CoA dehydrogenase, very long chain	ACADVL	37	1.0 ± 0.1	1.1 ± 0.2	1.2 ± 0.1	1.2 ± 0.2	1.00
Acyl-CoA dehydrogenase, C-4 to C-12 straight chain	ACADM	34	1.0 ± 0.2	0.9 ± 0.2	1.2 ± 0.0#	1.0 ± 0.1	0.70
Acyl-Coenzyme A oxidase 1	ACOX1	51	1.0 ± 0.1	1.1 ± 0.2	1.2 ± 0.2	1.3 ± 0.2	0.80
3-ketoacyl-Coenzyme A thiolase, α	HADHA	3030	1.0 ± 0.1	1.3 ± 0.3	1.2 ± 0.2	1.6 ± 0.2*	0.95
Ketone body metabolism							
Acetyl-CoA acetyltransferase 2	ACAT2	39	1.0 ± 0.1	0.8 ± 0.1*	1.0 ± 0.1	1.1 ± 0.1	0.04
Acyl-Coenzyme A oxidase 3	ACOX3	8310	1.0 ± 0.1	1.4 ± 0.2	1.2 ± 0.1#	1.1 ± 0.1	0.08
3-hydroxy-3-methylglutaryl-CoA synthase 2	HMGCS2	3158	1.0 ± 0.4	5.0 ± 2.5	1.7 ± 0.7	4.9 ± 1.3*	0.73

Data are shown as mean ± SEM, n=8-6. *, p<0.05 vs post-meal; #, p<0.05 vs lean subjects

2

Discussion

By contrast to the vast literature available on the signal transduction pathways involved in metabolic adaptations to exercise in human skeletal muscle, only few systematic studies have been conducted to investigate the molecular processes triggered by fasting, especially in individuals with metabolic disorders. To our knowledge, this study is the first to report the effects of prolonged fasting on whole-body substrate oxidation rates in relation with changes in signal transduction pathways and metabolic gene expression in skeletal muscle from both lean and obese subjects.

The physiological adaptation to fasting is generally marked by increased lipolysis, ketone body synthesis and lipid oxidation, and a concomitant decrease in glucose uptake and oxidation by peripheral tissues [7]. In lean individuals, we observed several of these well-known effects on whole-body substrate metabolism together with decreased plasma levels of glucose, insulin and leptin, and concomitant increase in GH. Not surprisingly, our obese subjects exhibited elevated levels of glucose, insulin, TG and leptin and lower circulating adiponectin at baseline when compared to lean individuals, and a marked whole-body metabolic inflexibility characterized by impaired fasting-induced switch from glucose toward FA oxidation. In addition, the decrease in plasma leptin and insulin levels in response to fasting was also blunted, in line with previous reports [22-24]. Among the limitations to the interpretation of these data, it should be mentioned that it cannot be totally excluded that some of the baseline differences between lean and obese individuals might partly reflect impaired metabolic adaptation to the initial standardized breakfast taken by the subjects. However, Labayen *et al.* have also reported a lower RQ and higher lipid oxidation rate at baseline in obese women after an overnight fast when compared to lean individuals [25], suggesting that these fundamental differences are independent to meal response. Interestingly, we found that the protein expression of the insulin receptor β (IRβ) was reduced at baseline in skeletal muscle from obese when compared to lean individuals. However, the IRβ protein expression was similarly increased in response to fasting in both lean and obese individuals, likely reflecting a compensatory feedback mechanism triggered by reduced plasma insulin levels. In contrast to our findings, Bergman *et al.* have found no effect of 48h-fasting on the expression of the insulin receptor [26]. This discrepancy might be explained by the fact that their baseline samples were collected after an overnight fast, a nutritional condition that might be sufficient to already induce

IR expression. Of note, IRβ downstream signaling, reflected by the phosphorylation state of IRS1, PKB, PRAS40 and AS160, was similarly reduced by fasting in both groups.

The fasting-induced increase in plasma GH levels is believed to play an important role in the regulation of whole-body substrate metabolism, notably by inhibiting glucose uptake and enhancing lipid oxidation in skeletal muscle [27]. Interestingly, we found that the change in plasma GH levels was significantly different between groups, with a much larger increase in lean compared to obese individuals. This result is in line with our previous findings showing that obese women exhibit lower plasma GH concentrations in response to a 20h-fast compared to normal weight women [28], suggesting that GH hyporesponsiveness may contribute to metabolic inflexibility. At present, it is unclear to which extent the fasting-induced increase in GH modulates signaling pathways involved in the regulation of glucose/lipid metabolism in human skeletal muscle. However, it has recently been shown that fasting induced similar up-regulation of lipid oxidation genes in skeletal muscle from wild-type and GH receptor knockout obese mice, suggesting that GHR signaling is likely not required for the control of lipid oxidation during fasting [29]. Among the fasting-induced changes in skeletal muscle metabolic gene expression observed in our study, some were previously reported, such as upregulation of PDK4 and UCP3, and are likely contributing to the whole-body shift from glucose to lipid oxidation in humans [18-21;30-32]. However, no major differences in transcriptional regulation in response to fasting were found between lean and obese individuals.

One of our initial hypotheses was that the nutrient/energy sensing AMPK pathway is activated by fasting in skeletal muscle and subsequently triggers metabolic adaptations to food deprivation. Indeed, although most of its established functions came from *in vitro* and/or rodent studies, it is largely acknowledged that AMPK activation promotes both glucose uptake and lipid oxidation in skeletal muscle through direct phosphorylation of key regulatory enzymes or transcription factors [33;34]. In the present study, we did not find any differences in basal (post-meal) AMPK activity in skeletal muscle from lean and obese subjects. This is in line with most of the previous reports [19;35-37], although one study has reported reduced AMPK activity in skeletal muscle from healthy obese and type 2 diabetes individuals [38]. Surprisingly, we showed that fasting decreases skeletal muscle AMPK activity in lean subjects, an effect lost in obese individuals. Of note, it was also recently reported that 72 hours of fasting does not significantly affect AMPK activity in healthy individuals [32]. One could therefore argue

2

that fasting-induced AMPK activation is an early regulatory event that transiently occurs in the first hours following food deprivation. Additional experiments with earlier time points are therefore required to clarify this issue.

Why does AMPK activity decrease in healthy individuals in response to fasting and why is this effect lost in obesity? The regulation of AMPK activity is complex and involves 1) adenine nucleotides binding to the γ-subunit, 2) Thr172 phosphorylation by LKB1 and/or CAMKKβ, 3) Thr172 dephosphorylation by AMPK-specific protein phosphatase(s), 4) phosphorylation of various regulatory residues on both α- and β-subunits, and 5) glycogen binding to the β-subunit [9-11]. In addition, modification in the AMPK subunits composition might also influence the kinase activity by changing the sensitivity toward AMP and/or other post-translational regulatory mechanisms. In human skeletal muscle, the majority of AMPK heterotrimers consists of either α2β2γ1 or α2β2γ3 complexes [37]. However, except for the protein expression of the marginal short AMPKγ2 isoform which was significantly lower at baseline in the obese when compared to lean individuals, all the other catalytic α and regulatory β/γ subunits were similar between groups whatever the conditions. Among the AMPK regulatory mechanisms described above, an increase in cellular energy status during fasting is rather unlikely and no differences in the phosphorylation state of AMPKα at the inhibitory Ser485/491 residue were observed (*data not shown*). A fasting-induced increase in protein phosphatase(s) activity cannot be excluded but the identity of the enzyme(s) involved in AMPK-Thr172 dephosphorylation remains uncertain [9-11]. Counter intuitively, we found an increase in LKB1 protein expression after fasting in lean but not in obese individuals that, however, merely suggests a compensatory mechanism secondary to reduced AMPK activity in the former group. On top of the cellular energy state, AMPK constantly monitors intracellular glycogen stores. Interestingly, a paradoxical increase in skeletal muscle glycogen content was reported during prolonged fasting [32]. It is therefore tempting to speculate that this physiological adaptation might be involved in reduced AMPK activity in lean subjects and altered in obese individuals with impaired glycogen metabolism. The determination of skeletal muscle glycogen content in our study would have clearly contributed to strengthen this point but the amount of available materials was unfortunately not sufficient to perform this measurement. Finally, an attractive potential explanation emerges from a recent study showing that adrenaline inhibits AMPK by a mechanism involving activation of an unidentified kinase which phosphorylates the AMPK β-subunit on a new inhibitory residue [39]. Indeed, fasting is known to increase plasma catecholamine levels [40], an effect that was reported to be

partly blunted in obese individuals [22]. Taken together, the physiological rationale for a reduced AMPK activity during prolonged fasting still remains unclear. One of the hypotheses builds on modulation of the so-called Randle cycle [41]: a reduced AMPK activity would therefore prevent glucose uptake by reducing AMPK-mediated GLUT4 translocation to the plasma membrane, leading to subsequent inhibition of glucose oxidation and the concomitant shift toward mitochondrial FA.

Finally, another striking finding is the marked decrease in protein expression of key mitochondrial respiratory-chain subunits in from obese subjects, strongly suggesting that the skeletal muscle mitochondrial content is reduced in these individuals. This may affect the capacity of skeletal muscle to adapt to increased FA availability associated with fasting and underlie the impaired shift from glucose toward mitochondrial FA oxidation. Although the underlying molecular mechanisms remains to be elucidated, this strengthens previous reports showing that mitochondrial density in skeletal muscle, assessed either by mtDNA content and/or by *ex vivo* determination of mitochondrial respiratory-chain complexes activities, was reduced in skeletal muscle from obese subjects [42;43]. In the present study, due to lack of materials, we were unfortunately not able to measure other mitochondrial markers, such as mtDNA content or activities of citrate synthase and β-hydroxyacetyl coenzyme A dehydrogenase. Additional studies are therefore required to determine additional mitochondrial parameters and clarify the (patho)physiological consequence of these findings.

In conclusion, our main findings show that obese individuals are characterized by whole-body metabolic inflexibility in response to prolonged fasting, a feature associated with apparent alteration in AMPK signaling and reduced skeletal muscle IRβ and mitochondrial content.

Acknowledgements

References

1. Corpeleijn E, Saris WH, Blaak EE. Metabolic flexibility in the development of insulin resistance and type 2 diabetes: effects of lifestyle. *Obes Rev* 2009; 10(2): 178-193.

2. Galgani JE, Moro C, Ravussin E. Metabolic flexibility and insulin resistance. *Am J Physiol Endocrinol Metab* 2008; 295(5): E1009-E1017.

3. Kelley DE, Goodpaster B, Wing RR, Simoneau JA. Skeletal muscle fatty acid metabolism in association with insulin resistance, obesity, and weight loss. *Am J Physiol* 1999; 277(6 Pt 1): E1130-E1141.

4. Storlien L, Oakes ND, Kelley DE. Metabolic flexibility. *Proc Nutr Soc* 2004; 63(2): 363-368.

5. Kelley DE. Skeletal muscle fat oxidation: timing and flexibility are everything. *J Clin Invest* 2005; 115(7): 1699-1702.

6. Cahill GF, Jr. Fuel metabolism in starvation. *Annu Rev Nutr* 2006; 26:1-22.: 1-22.

7. Soeters MR, Soeters PB, Schooneman MG, Houten SM, Romijn JA. Adaptive reciprocity of lipid and glucose metabolism in human short-term starvation. *Am J Physiol Endocrinol Metab* 2012; 303(12): E1397-E1407.

8. Inoki K, Kim J, Guan KL. AMPK and mTOR in cellular energy homeostasis and drug targets. *Annu Rev Pharmacol Toxicol* 2012; 52: 381-400.

9. Carling D, Thornton C, Woods A, Sanders MJ. AMP-activated protein kinase: new regulation, new roles? *Biochem J* 2012; 445(1): 11-27.

10. Hardie DG, Ross FA, Hawley SA. AMPK: a nutrient and energy sensor that maintains energy homeostasis. *Nat Rev Mol Cell Biol* 2012; 13(4): 251-262.

11. Steinberg GR, Kemp BE. AMPK in Health and Disease. *Physiol Rev* 2009; 89(3): 1025-1078.

12. Canto C, Jiang LQ, Deshmukh AS, Mataki C, Coste A, Lagouge M, Zierath JR, Auwerx J. Interdependence of AMPK and SIRT1 for metabolic adaptation to fasting and exercise in skeletal muscle. *Cell Metab* 2010; 11(3): 213-219.

13. Frier BC, Jacobs RL, Wright DC. Interactions between the consumption of a high-fat diet and fasting in the regulation of fatty acid oxidation enzyme gene expression: an evaluation of potential mechanisms. *Am J Physiol Regul Integr Comp Physiol* 2011; 300(2): R212-R221.

14. Snel M, Jonker JT, Hammer S, Kerpershoek G, Lamb HJ, Meinders AE, Pijl H, de RA, Romijn JA, Smit JW, Jazet IM. Long-term beneficial effect of a 16-week

very low calorie diet on pericardial fat in obese type 2 diabetes mellitus patients. *Obesity (Silver Spring)* 2012; 20(8): 1572-1576.

15. Kok P, Roelfsema F, Frolich M, van PJ, Stokkel MP, Meinders AE, Pijl H. Activation of dopamine D2 receptors simultaneously ameliorates various metabolic features of obese women. *Am J Physiol Endocrinol Metab* 2006; 291(5): E1038-E1043.

16. Friedewald WT, Levy RI, Fredrickson DS. Estimation of the concentration of low-density lipoprotein cholesterol in plasma, without use of the preparative ultracentrifuge. *Clin Chem* 1972; 18(6): 499-502.

17. Stephenne X, Foretz M, Taleux N, van der Zon GC, Sokal E, Hue L, Viollet B, Guigas B. Metformin activates AMP-activated protein kinase in primary human hepatocytes by decreasing cellular energy status. *Diabetologia* 2011; 54(12): 3101-3110.

18. Kunkel SD, Suneja M, Ebert SM, Bongers KS, Fox DK, Malmberg SE, Alipour F, Shields RK, Adams CM. mRNA expression signatures of human skeletal muscle atrophy identify a natural compound that increases muscle mass. *Cell Metab* 2011; 13(6): 627-638.

19. Pilegaard H, Saltin B, Neufer PD. Effect of short-term fasting and refeeding on transcriptional regulation of metabolic genes in human skeletal muscle. *Diabetes* 2003; 52(3): 657-662.

20. Tsintzas K, Jewell K, Kamran M, Laithwaite D, Boonsong T, Littlewood J, Macdonald I, Bennett A. Differential regulation of metabolic genes in skeletal muscle during starvation and refeeding in humans. *J Physiol* 2006; 575(Pt 1): 291-303.

21. Tunstall RJ, Mehan KA, Hargreaves M, Spriet LL, Cameron-Smith D. Fasting activates the gene expression of UCP3 independent of genes necessary for lipid transport and oxidation in skeletal muscle. *Biochem Biophys Res Commun* 2002; 294(2): 301-308.

22. Horowitz JF, Coppack SW, Paramore D, Cryer PE, Zhao G, Klein S. Effect of short-term fasting on lipid kinetics in lean and obese women. *Am J Physiol* 1999; 276(2 Pt 1): E278-E284.

23. Horowitz JF, Coppack SW, Klein S. Whole-body and adipose tissue glucose metabolism in response to short-term fasting in lean and obese women. *Am J Clin Nutr* 2001; 73(3): 517-522.

24. Klein S, Horowitz JF, Landt M, Goodrick SJ, Mohamed-Ali V, Coppack SW. Leptin production during early starvation in lean and obese women. *Am J Physiol Endocrinol Metab* 2000; 278(2): E280-E284.

2

2

25. Labayen I, Diez N, Parra D, Gonzalez A, Martinez JA. Basal and postprandial substrate oxidation rates in obese women receiving two test meals with different protein content. *Clin Nutr* 2004; 23(4): 571-578.

26. Bergman BC, Cornier MA, Horton TJ, Bessesen DH. Effects of fasting on insulin action and glucose kinetics in lean and obese men and women. *Am J Physiol Endocrinol Metab* 2007; 293(4): E1103-E1111.

27. Jorgensen JO, Moller L, Krag M, Billestrup N, Christiansen JS. Effects of growth hormone on glucose and fat metabolism in human subjects. *Endocrinol Metab Clin North Am* 2007; 36(1): 75-87.

28. Buijs MM, Burggraaf J, Wijbrandts C, de Kam ML, Frolich M, Cohen AF, Romijn JA, Sauerwein HP, Meinders AE, Pijl H. Blunted lipolytic response to fasting in abdominally obese women: evidence for involvement of hyposomatotropism. *Am J Clin Nutr* 2003; 77(3): 544-550.

29. Vijayakumar A, Wu Y, Buffin NJ, Li X, Sun H, Gordon RE, Yakar S, LeRoith D. Skeletal muscle growth hormone receptor signaling regulates basal, but not fasting-induced, lipid oxidation. *PLoS One* 2012; 7(9): e44777.

30. Norton L, Parr T, Bardsley RG, Ye H, Tsintzas K. Characterization of GLUT4 and calpain expression in healthy human skeletal muscle during fasting and refeeding. *Acta Physiol (Oxf)* 2007; 189(3): 233-240.

31. Spriet LL, Tunstall RJ, Watt MJ, Mehan KA, Hargreaves M, Cameron-Smith D. Pyruvate dehydrogenase activation and kinase expression in human skeletal muscle during fasting. *J Appl Physiol* 2004; 96(6): 2082-2087.

32. Vendelbo MH, Clasen BF, Treebak JT, Moller L, Krusenstjerna-Hafstrom T, Madsen M, Nielsen TS, Stodkilde-Jorgensen H, Pedersen SB, Jorgensen JO, Goodyear LJ, Wojtaszewski JF, Moller N, Jessen N. Insulin Resistance after a 72 hour Fast is Associated with Impaired AS160 Phosphorylation and Accumulation of Lipid and Glycogen in Human Skeletal Muscle. *Am J Physiol Endocrinol Metab* 2011.

33. Hardie DG. Energy sensing by the AMP-activated protein kinase and its effects on muscle metabolism. *Proc Nutr Soc* 2011; 70(1): 92-99.

34. Viollet B, Athea Y, Mounier R, Guigas B, Zarrinpashneh E, Horman S, Lantier L, Hebrard S, Devin-Leclerc J, Beauloye C, Foretz M, Andreelli F, Ventura-Clapier R, Bertrand L. AMPK: Lessons from transgenic and knockout animals. *Front Biosci (Landmark Ed)* 2009; 14: 19-44.

35. Hojlund K, Mustard KJ, Staehr P, Hardie DG, Beck-Nielsen H, Richter EA, Wojtaszewski JF. AMPK activity and isoform protein expression are similar in muscle of obese subjects with and without type 2 diabetes. *Am J Physiol Endocrinol Metab* 2004; 286(2): E239-E244.

36. Steinberg GR, Smith AC, van Denderen BJ, Chen Z, Murthy S, Campbell DJ, Heigenhauser GJ, Dyck DJ, Kemp BE. AMP-activated protein kinase is not down-regulated in human skeletal muscle of obese females. *J Clin Endocrinol Metab* 2004; 89(9): 4575-4580.

37. Wojtaszewski JF, Birk JB, Frosig C, Holten M, Pilegaard H, Dela F. 5'AMP activated protein kinase expression in human skeletal muscle: effects of strength training and type 2 diabetes. *J Physiol* 2005; 564(Pt 2): 563-573.

38. Bandyopadhyay GK, Yu JG, Ofrecio J, Olefsky JM. Increased malonyl-CoA levels in muscle from obese and type 2 diabetic subjects lead to decreased fatty acid oxidation and increased lipogenesis; thiazolidinedione treatment reverses these defects. *Diabetes* 2006; 55(8): 2277-2285.

39. Tsuchiya Y, Denison FC, Heath RB, Carling D, Saggerson D. 5'-AMP-activated protein kinase is inactivated by adrenergic signalling in adult cardiac myocytes. *Biosci Rep* 2012; 32(2): 197-213.

40. Beer SF, Bircham PM, Bloom SR, Clark PM, HALES CN, Hughes CM, Jones CT, Marsh DR, Raggatt PR, Findlay AL. The effect of a 72-h fast on plasma levels of pituitary, adrenal, thyroid, pancreatic and gastrointestinal hormones in healthy men and women. *J Endocrinol* 1989; 120(2): 337-350.

41. Hue L, Taegtmeyer H. The Randle cycle revisited: a new head for an old hat. *Am J Physiol Endocrinol Metab* 2009; 297(3): E578-E591.

42. Kelley DE, He J, Menshikova EV, Ritov VB. Dysfunction of mitochondria in human skeletal muscle in type 2 diabetes. *Diabetes* 2002; 51(10): 2944-2950.

43. Ritov VB, Menshikova EV, Azuma K, Wood R, Toledo FG, Goodpaster BH, Ruderman NB, Kelley DE. Deficiency of electron transport chain in human skeletal muscle mitochondria in type 2 diabetes mellitus and obesity. *Am J Physiol Endocrinol Metab* 2010; 298(1): E49-E58.

2

2

Chapter 3

Obesity is associated with an altered autonomic nervous system response to nutrient restriction

3

Marjolein Wijngaarden[1], Hanno Pijl[1], Ko Willems van Dijk[2] , Esther S. Klaassen[3], Jacobus Burggraaf[4]

[1] Department of Endocrinology and Metabolism, Leiden University Medical Center, Leiden, The Netherlands
[2] Human Genetics, Leiden University Medical Center, Leiden, The Netherlands
[3] Department of Statistics, Centre for Human Drug Research, Leiden, The Netherlands
[4] Vascular Medicine, Centre for Human Drug Research, Leiden, The Netherlands

3

Abstract

Objective

Heart rate variability (HRV) reflects the balance of activities of sympathetic and parasympathetic components of the autonomic nervous system. We compared HRV parameters in response to a prolonged fast in obese versus normal weight humans. In addition, the effect of weight-loss was evaluated in obese individuals.

Design

Intervention study

Patients

14 non-diabetic obese (12 females/2 males, aged 30 ± 3 years, Body Mass Index (BMI) 35.2 ± 1.2 kg/m^2) and 12 lean subjects(10 females/2 males, aged 27 ± 3 years, BMI of 23.3 ± 0.5 kg/m^2)

Measurements

HRV was examined 75 minutes after standardized breakfast and after a 48h fast in 14 non-diabetic obese and 12 lean subjects. The postprandial measurement was repeated in 12 obese subjects after weight-loss.

Results

In lean subjects, fasting decreased high frequency (HF) power by 43 % ($p<0.05$) and decreased low frequency (LF) power by 37% ($p=0.1$), leaving the LF/HF ratio unchanged ($p=0.7$). In the obese group, autonomic nervous system tone shifted to sympathetic dominance as the LF/HF increased from 0.61 to 1.14 ($p=0.03$). After an average weight-loss of 13.8 kg in obese subjects, a trend for sympathetic dominance was found; the LF/HF ratio increased by 56% ($p=0.06$).

Conclusion

Our data show that a 48h fast leaves autonomic nervous system balance unaltered in lean subjects. In contrast, a 48h fast as well as weight-loss induce sympathetic dominance in obese humans.

Introduction

Diabetes and obesity have been associated with an altered autonomic nervous system tone, marked by increased orthosympathetic nervous system activity and decreased parasympathetic/ vagal nervous system (PSN) tone. In the framework of energy balance, activation of the orthosympathetic nervous system generally mobilizes energy while the parasympathetic nervous system promotes digestion and energy storage. The dynamic balance between the orthosympathetic nervous system and the parasympathetic nervous system quickly responds to environmental cues, such as fasting, to appropriately adapt energy metabolism. Heart rate variability (HRV) can be used as a measure of activity of both components of the autonomic nervous system.[1] It has been shown that overall HRV, after an overnight fast, is decreased in obesity[2] and that fasting increases orthosympathetic nervous system activity in lean individuals.[3;4] Importantly, a 48h fast has different effects than prolonged fasting (starvation). Truly starved humans show symptoms of profoundly decreased orthosympathetic nervous system activity such as hypotension, bradycardia and hypothermia.[5;6]

We hypothesized that the autonomic nervous system response to a 48h fast would be different in obese compared to lean individuals, reflecting a disturbed handling of energy balance disturbances. We compared postprandial values with post-48-hours of fasting to determine the real impact of food deprivation (comparison with values after an overnight fast at baseline obviously entails 10 hours of fasting prior to the baseline measurement). We also wondered whether weight loss would reduce any potential difference in postprandial HRV between lean and obese subjects.

Material & Methods

We included 12 obese (BMI >30 kg/m^2) and 12 lean volunteers (19-25 kg/m^2), matched for gender and age. All participants were healthy, without medication, non-smoking, weight-stable (<3kg weight change in the preceding 3 months), with a negative family history for type 2 diabetes and a fasting plasma glucose ≤5.6 mmol/l. The study was approved by the medical ethics committee of the Leiden University Medical Center and executed in accordance with the Declaration of Helsinki (as amended in Seoul (2008), including the clarifications added in Washington (2002) and Tokyo (2004)). The study was registered in The Netherlands Trial Register (NTR2401). All volunteers gave written informed consent.

This study consisted of 2 interventions: a 48h fast for all participants and a weight-loss program for the obese participants. During fasting, overnight-fasted participants were admitted to our research center. Upon arrival subjects consumed a standardized breakfast (2 slices of brown bread with cheese; 300 calories, 27g carbohydrates, 18g protein and 11g fat). At 75 minutes after breakfast, a five-minute ECG-recording was made while subjects were supine, lying still and awake in a quiet environment. The second ECG was made after 48h fasting. The ECG-recordings were made with a CardioPerfect ECG recording system (Cardiocontrol, Rijswijk, The Netherlands) using a sampling rate of 500 Hz. After recording the ECG signals were scrutinized for artefacts and subsequently analyzed for the duration of the RR-intervals using the software supplied with the device. The RR-interval time series were subjected to HRV analysis according to international guidelines [7] for the frequency-domain HRV parameters. These consist of the mean RR-interval (RR-int), the power of the high-frequency (HF; vagal activity), and low-frequency (LF; sympathetic activity) band and their ratio (LF/HF; sympathovagal balance) with Kubios HRV software version 2 (Biosignal Analysis and Medical Imaging Group, University of Kuopio, Finland).

Subsequently, 12 of the 14 obese subjects participated in an 8 week dietary weight-loss program. This consisted of a high protein low calorie diet (HPLC; Prodimed®, Valkenswaard, The Netherlands), with an average intake of 600 kcal/day taken as 4-5 (females) or 5-6 (males) sachets daily with a tablespoon of vegetable oil and selected vegetables. Each sachet contained approximately 90 kcal (about 18 g protein, 2.5-5 g carbohydrates, 0.5-2 g fat). After dieting, the obese subjects underwent HRV measurements, again 75 minutes after standardized breakfast. We also collected plasma samples and muscle biopsies; these results will be presented elsewhere.

All values are expressed as median and range and variables were log-transformed prior to analysis to correct for the log-normal distribution of the data. For both groups, baseline data was compared to the 48h data using a mixed model analysis of variance with fixed factors time, group and time by group, and random factor subject. The postprandial data before and after weight-loss was compared with a mixed model analysis of variance with fixed factor time and random factor subject. The analysis is summarized as the back-transformed geometric means of the percentage difference along with the corresponding 95% confidence intervals, and the p-value of the contrasts. Analyses were performed using SAS for Windows V9.1.2 (SAS Institute, Inc., Cary, NC, USA).

Results

Lean subjects (10F/2M) were on average (±SEM) aged 27 ± 3 years with a BMI of 23.3 ± 0.5 kg/m^2. We planned to include 12 obese participants, but 2 patients who discontinued the diet were replaced. Hence, 14 obese subjects (12F/2M, aged 30 ± 3 years, BMI 35.2 ± 1.2 kg/m^2) were studied at baseline.

The HPLC program in the 12 obese subjects (10F/2M, aged 29 ± 2 years, BMI: 35.9 ± 1.3 kg/m^2) reduced weight by 13.8 ± 1.2 kg and decreased BMI by 4.4 ± 0.4 kg/m^2. For one lean and one obese subject the postprandial measurements were not performed on time, these subjects were excluded from analysis.
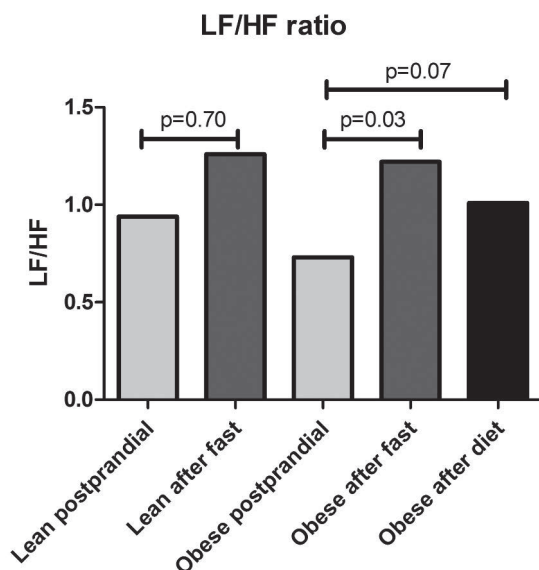
At baseline, the LF power and LF/HF ratio were lower in obese compared to lean subjects, but not significantly (p= 0.17 and p= 0.49, Tables 1 and 2).

In lean subjects, the 48h fast de-

Figure 1: LF/HF ratio after a standardized breakfast and after a 48 hour fast in lean and obese subjects.
Data are shown as median. We show the LF/HF ratio after a standardized breakfast in lean and obese subjects as well as after a 48 hour fast. The ratio after weight loss in the obese subjects was also measured after a standardized breakfast.

Table 1 HRV parameters in the frequency domain for lean and obese subjects after a standardized breakfast (postprandial) and after a 48h fast.

		N	RR-interval (ms)	CV (%)	HF power (ms^2)	LF power (ms^2)	LF/HF
Lean	Postprandial	11	941 (711 – 1307)	6.8 (3.9 – 14.4)	795 (317 - 14919)	1348 (158 - 5187)	0.94 (0.06 - 4.59)
	48h fast	12	829 (701 – 1106)	6.2 (3.1 – 13.6)	418 (224 – 15122)	780 (87 – 4253)	1.26 (0.07 - 4.80)
Obese	Postprandial	13	915 (644 – 1101)	6.4 (1.8 – 23.0)	955 (33 – 27794)	755 (22 – 2846)	0.73 (0.10 - 2.11)
	48h fast	14	922 (640 – 1165)	5.5 (2.8 – 22.6)	375 (49 – 29695)	635 (100 – 9083)	1.22 (0.31 - 6.61)
	Postprandial after weight loss	12	917 (805 – 1212)	5.7 (3.7 – 25.2)	640 (222 – 37661)	1002 (168 – 4472)	1.01 (0.12 - 2.71)

Data are depicted as median (range). Abbreviations: ms; millisecons, h; hours, RR-int; RR-interval, CV; coefficient of variation, LF; power of the low frequency band in the power spectrum, HF; power of the high frequency band in the power spectrum, LF/HF; ratio of low over high frequency power.

3

creased the RR-interval by 8.6% (p=0.02), decreased HF-power by 43% (p<0.05) and decreased LF-power by 37% (p=0.1) leaving the LF/HF ratio unchanged (p=0.7) (Tables 1 and 2).

In the obese subjects, the 48h fast decreased the RR-interval with 1.5% (p=0.7), decreased HF-power by 40% (p=0.06), increased LF-power by 20% (p=0.5) and therefore increased the LF/HF ratio by 90% (p=0.03, Tables 1 and 2).

Repeating the postprandial measurements after weight-loss in the obese subjects showed that the RR-interval and HF-power remained similar, LF power increased by 52% (p=0.12). This resulted in a 56% increase (p=0.07) in the LF/HF ratio (Figure 1, Tables 1 and 2).

Table 2 Frequency domain heart rate variability parameters for lean and obese subjects at post-prandial baseline compared to the 48h fast and in obese subjects at postprandial baseline compared to after the High Protein Low Calorie diet.

	Point estimate (95%CI) of change		p-value
RR-int (ms)			
Lean fast	-8.6%	(-15; -2%)	0.02
Obese fast	-1.5%	(-8; +6%)	0.66
Obese diet	4.3%	(-3; +12%)	0.23
HF (ms^2)			
Lean fast	-43.1%	(-67; -1%)	<0.05
Obese fast	-39.6%	(-64; +2%)	0.06
Obese diet	-4.9%	(-46; +68%)	0.86
LF (ms^2)			
Lean fast	-36.7%	(-66; +19%)	0.14
Obese fast	21.0%	(-33; +120%)	0.52
Obese diet	51.5%	(-11; +158%)	0.12
LF/HF			
Lean fast	11.8%	(-39; +105%)	0.70
Obese fast	87.8%	(9; +244%)	0.03
Obese diet	55.6%	(-3; +150%)	0.07

Data are depicted as point estimates of the percentage difference (95% confidence interval). Abbreviations: ms; milliseconds, CI; confidence interval, RR-int; RR-interval, LF; power of the low frequency band in the power spectrum, HF; power of the high frequency band in the power spectrum, LF/HF; ratio of low over high frequency power.

Discussion

We investigated the effect of 48h of fasting on HRV parameters in lean and obese subjects. First, we studied differences in HRV measurements between groups at baseline since obese humans were shown to have lower HRV. However we did not find significant differences in HRV parameters between groups at baseline, although autonomic nervous system tone in obese subjects seemed to be characterized by parasympathetic nervous system predominance. This appears to contradict earlier studies showing orthosympathetic nervous system overactivity in obese subjects after an overnight fast.[2] However, our baseline values were determined postprandially, and obesity is marked by a blunted postprandial increase in orthosympathetic nervous system tone.[8;9] Thus, the apparent discrepancy with previous findings may be explained by differences in the timing of measurements.

In lean subjects, 48 hours of subsequent fasting decreased both vagal and sympathetic tone, leaving the sympathovagal balance unaltered compared to postprandially. Accordingly, a previous study showed that 72h of fasting in lean subjects blunts both LF and HF power, leaving the LF/HF ratio unchanged.[3] In contrast, 48h of fasting decreased parasympathetic nervous system activity and increased orthosympathetic nervous system activity in the obese subjects. This shifted overall autonomic nervous system tone towards a more sympathetic state. One previous study also documents an increased orthosympathetic nervous system activity in skeletal muscle after a 48h fast in obese women.[10] Taken together, our results suggest that obese subjects cannot maintain the overall autonomic nervous system tone balanced during a 48h fast, which might reflect a disturbed response to alterations in energy balance.

The causes of autonomic nervous system tone alterations upon a prolonged fast are multifactorial. There may be effects of catecholamines; norepinephrine and dopamine levels increase during fasting.[3] Thyroid hormones might also be involved, since both hyperthyroidism and hypothyroidism are characterized by an altered sympathovagal balance.[11;12] However, it is unlikely that changes in thyroid hormones play a major role in the altered autonomic nervous system tone we observed, because fasting reduces plasma triiodothyronine levels, which is expected to reduce the LF/HF ratio.[4;12;13] Fasting enhances lipolysis and elevates FFA levels. Infusion of lipids has been shown to increase orthosympathetic nervous system activity.[14] Although the

3

rate of appearance of FFAs per unit of adipose mass is attenuated during fasting in obese subjects[15], plasma FFA levels are higher, which could underlie their increased orthosympathetic nervous system response.

Finally we studied the effect of weight-loss on HRV parameters in obese subjects. Weight-loss, 13.8kg on average, was characterized by an increased in orthosympathetic nervous system and thus overall autonomic nervous system tone. In fact, the LF/HF ratio increased to a level similar to that observed in lean subjects at baseline, suggesting that the (not significantly) altered postprandial autonomic nervous system tone in obese subjects is reversible upon weight loss.

What do these findings mean? The fact that fasting alters autonomic nervous balance in obese subjects but not in lean suggests that obese individuals distinctly process the challenge of food (energy) deprivation (at least in terms of autonomic nervous system response). The physiological meaning of that finding is unclear, but it may have endocrine and/or metabolic corollaries that hamper weight loss. The fact that weight loss tends to normalize (postprandial) autonomic balance in obese individuals suggests that autonomic balance is not critically involved in the pathogenesis of weight gain (in view of the fact that the vast majority of post-obese subjects tends to regain their weight).

Future studies should address changes in the time course of autonomic nervous system activity after food intake between lean and obese subjects. It would also be interesting to study autonomic nervous system modulation by FFAs. Limitations of the current study include that the influence of the menstrual cycle on HRV was not taken into account.[16;17]

In summary, we compared HRV parameters in the fed and fasted state between lean and obese individuals. Importantly, 48h of fasting in lean individuals similarly reduced vagal and sympathetic tone, whereas it reduced vagal and increased sympathetic tone in obese individuals. This suggests that obese subjects cannot maintain autonomic nervous system balance upon fasting. We also show that weight-loss diminishes the (non significant) difference in postprandial autonomic nervous system tone between lean and obese subjects, suggesting that the effects of obesity on postprandial HRV are reversible.

Acknowledgements

References

1. Dampney RA. Functional organization of central pathways regulating the cardiovascular system. *Physiol Rev* 1994; 74(2): 323-364.
2. Muscelli E, Emdin M, Natali A, Pratali L, Camastra S, Gastaldelli A, Baldi S, Carpeggiani C, Ferrannini E. Autonomic and hemodynamic responses to insulin in lean and obese humans. *J Clin Endocrinol Metab* 1998; 83(6): 2084-2090.
3. Chan JL, Mietus JE, Raciti PM, Goldberger AL, Mantzoros CS. Short-term fasting-induced autonomic activation and changes in catecholamine levels are not mediated by changes in leptin levels in healthy humans. *Clin Endocrinol (Oxf)* 2007; 66(1): 49-57.
4. Webber J, Macdonald IA. The cardiovascular, metabolic and hormonal changes accompanying acute starvation in men and women. *Br J Nutr* 1994; 71(3): 437-447.
5. Keys A, Henschel A, Taylor Hl. The size and function of the human heart at rest in semi-starvation and in subsequent rehabilitation. *Am J Physiol* 1947; 150(1): 153-169.
6. Peel M. Hunger strikes. *BMJ* 1997; 315(7112): 829-830.
7. Malik M. Heart rate variability. Standards of measurement, physiological interpretation, and clinical use. Task Force of the European Society of Cardiology and the North American Society of Pacing and Electrophysiology. *Eur Heart J* 1996; 17(3): 354-381.
8. Lu CL, Zou X, Orr WC, Chen JD. Postprandial changes of sympathovagal balance measured by heart rate variability. *Dig Dis Sci* 1999; 44(4): 857-861.
9. Tentolouris N, Tsigos C, Perea D, Koukou E, Kyriaki D, Kitsou E, Daskas S, Daifotis Z, Makrilakis K, Raptis SA, Katsilambros N. Differential effects of high-fat and high-carbohydrate isoenergetic meals on cardiac autonomic nervous system activity in lean and obese women. *Metabolism* 2003; 52(11): 1426-1432.

3

10. Andersson B, Wallin G, Hedner T, Ahlberg AC, Andersson OK. Acute effects of short-term fasting on blood pressure, circulating noradrenaline and efferent sympathetic nerve activity. *Acta Med Scand* 1988; 223(6): 485-490.

11. Burggraaf J, Tulen JH, Lalezari S, Schoemaker RC, De Meyer PH, Meinders AE, Cohen AF, Pijl H. Sympathovagal imbalance in hyperthyroidism. *Am J Physiol Endocrinol Metab* 2001; 281(1): E190-E195.

12. Heemstra KA, Burggraaf J, van der Klaauw AA, Romijn JA, Smit JW, Corssmit EP. Short-term overt hypothyroidism induces sympathovagal imbalance in thyroidectomized differentiated thyroid carcinoma patients. *Clin Endocrinol (Oxf)* 2010; 72(3): 417-421.

13. Chan JL, Heist K, DePaoli AM, Veldhuis JD, Mantzoros CS. The role of falling leptin levels in the neuroendocrine and metabolic adaptation to short-term starvation in healthy men. *J Clin Invest* 2003; 111(9): 1409-1421.

14. Paolisso G, Manzella D, Rizzo MR, Ragno E, Barbieri M, Varricchio G, Varricchio M. Elevated plasma fatty acid concentrations stimulate the cardiac autonomic nervous system in healthy subjects. *Am J Clin Nutr* 2000; 72(3): 723-730.

15. Horowitz JF, Coppack SW, Paramore D, Cryer PE, Zhao G, Klein S. Effect of short-term fasting on lipid kinetics in lean and obese women. *Am J Physiol* 1999; 276(2 Pt 1): E278-E284.

16. Sato N, Miyake S, Akatsu J, Kumashiro M. Power spectral analysis of heart rate variability in healthy young women during the normal menstrual cycle. *Psychosom Med* 1995; 57(4): 331-335.

17. Yildirir A, Kabakci G, Akgul E, Tokgozoglu L, Oto A. Effects of menstrual cycle on cardiac autonomic innervation as assessed by heart rate variability. *Ann Noninvasive Electrocardiol* 2002; 7(1): 60-63.

3

Chapter 4

Obesity is marked by distinct functional connectivity in neural networks involved in the control of food reward and salience

4

Marjolein A. Wijngaarden[1] , Ilya M. Veer[2,3,4], Serge A.R.B. Rombouts[2,3,4],
Mark van Buchem[2,3], Ko Willems van Dijk[1,5], Hanno Pijl[1], Jeroen van der Grond[2]

[1] Department of Endocrinology and Metabolism, Leiden University Medical Center, Leiden, The Netherlands
[2] Department of Radiology, Leiden University Medical Center, Leiden, The Netherlands
[3] Leiden Institute for Brain and Cognition (LIBC), Leiden University, Leiden, The Netherlands
[4] Institute of Psychology, Leiden University, Leiden, The Netherlands
[5] Department of Human Genetics, Leiden University Medical Center, Leiden, The Netherlands

4

Abstract

Objective

The brain plays a crucial role in controlling energy balance. We hypothesize that brain circuits involved in reward and salience respond differently to fasting in obese compared to lean individuals. We compared functional connectivity networks related to food reward and saliency, prior to and after 48 hours of fasting, in lean and obese individuals.

Subjects

We included 13 obese (2 males, 11 females, BMI 35.4 ± 1.2, age 31 ± 3) and 11 control subjects (2 males, 9 females, BMI 23.2 ± 0.5, age 28 ± 3). Resting-state functional magnetic resonance imaging (fMRI) scans were made before and after fasting. Functional connectivity of the amygdala, hypothalamus and posterior cingulate cortex was assessed using seed-based correlations.

Results

Fasting affected hypothalamus functional connectivity differently between groups. Before fasting, a stronger connectivity between hypothalamus and left insula was found in obese subjects which decreased upon fasting. Upon fasting, connectivity of the hypothalamus with the dorsal anterior cingulate cortex (dACC) increased in lean subjects and decreased in obese individuals. Amygdala connectivity with the ventromedial prefrontal cortex was stronger in lean subjects at baseline, which did not change upon fasting. No differences in posterior cingulate cortex connectivity were observed.

Conclusion

To conclude, obesity is marked by alterations in functional connectivity networks involved in food reward and salience. Fasting differentially affected hypothalamic connections with the dACC and the insula between obese and lean subjects. Our data supports the idea that food reward and nutrient deprivation are differently perceived and/or processed in obesity.

Introduction

It is currently well recognized that obesity is a growing public health concern [1;2]. Obesity results from excessive energy intake relative to actual metabolic needs. The monitoring and regulation of energy intake depends both on internal factors such as homeostatic signals and cognitive-emotional state as well as on external factors such as the availability of food and social context. The brain plays a crucial role in the decision to eat by integrating the multiple hormonal and neuronal signals [3]. Not surprisingly, there is increasing evidence that obesity is associated with changes in the central nervous system [4-8].

In normal weight subjects, hunger is associated with increased activity in the prefrontal cortex, hypothalamus, thalamus, several limbic/paralimbic areas, basal ganglia, temporal cortex, cerebellum, insula, orbitofrontal and anterior cingulate cortices, striatum, hippocampus, parahippocampal gyrus, and precuneus [6;7;9-15]. This underscores the concept that food intake is controlled by multiple neural networks and their mutual connections [16]. Therefore, it is likely that alterations in the complex interplay between multiple brain regions are involved in the pathophysiology of obesity (i.e. unbalanced food intake). To better understand this disorder, it is important to evaluate how brain regions responsible for food intake interact in healthy controls, and if changes in this circuitry are related to obesity.

Resting-state functional magnetic resonance imaging (RS-fMRI) has become an important tool to study functional interactions in the brain in absence of overt behavior [17;18]. Remote brain regions are considered to be functionally connected when showing coherent signal fluctuations over time. By now, the presence of spatially distinct resting-state networks (RSNs) has been demonstrated consistently. Interestingly, most of these networks also show a remarkable overlap with patterns of brain activity evoked by tasks probing cognitive and emotional function [19]. Thus far, we are aware of only one study that has looked at differences in RS functional connectivity between obese individuals and healthy controls after an overnight fast [20], finding increased functional connectivity of the default mode network with the cuneus and midcingulate cortex in obese participants, while a temporal network demonstrated that functional connectivity strength was decreased in the left insular cortex. Moreover, the connectivity in these networks seems to vary with increasing body mass index (BMI). While

these results shed light on integration of brain circuits after an overnight fast in obese participants, we set out to study whether RSNs involved in food homeostasis, salience and reward respond differently to a prolonged fast in obese compared to lean individuals.

To this end, RS data were acquired after an overnight fast and after a prolonged fast of 48 hours. We compared the response of three different functional connectivity networks to 48 hours of fasting between obese and normal weight volunteers using a seed-based correlation approach. First, hypothalamic functional connectivity was assessed since the hypothalamus controls energy balance by regulating food intake and energy expenditure [3;21;22]. Then we analyzed functional connectivity of the amygdala, as this is a key constituent of the brain's emotion circuitry [23] and as such involved in learning how to translate emotional and rewarding events to behavioral schemes [24]. Alterations in reward-related brain regions are possibly associated with obesity [8]. Finally, we studied the default mode network (DMN). The DMN includes regions which are active when subjects are in an awake, resting state without any task, but whose activity diminishes during specific goal-directed behaviors [25]. The DMN includes the precuneus, posterior cingulate, medial prefrontal, and inferior parietal cortices. It has been suggested previously that alterations in the DMN in obese subjects may originate from parietal and cingulate regions [26;27].

Material & Methods

Subjects

Participants were recruited by advertisements in the public space. The participants had to be Caucasian, healthy, weight-stable, with a fasting plasma glucose ≤ 5.6 mmol/l. Exclusion criteria were: a positive family history of type 2 diabetes mellitus, smoking, recent blood donation and general MRI contraindications. Participants who used medication that could affect glucose homeostasis and/or brain function were excluded. Lean and obese individuals were matched with respect to age and sex. The study was performed in accordance with the principles of the revised Declaration of Helsinki (as amended in Seoul (2008) and including the clarifications added in Washington (2002) and Tokyo (2004)). The study was approved by the Medical Ethical Committee of the Leiden University Medical Centre and registered in The Netherlands Trial Register (NTR2401). All volunteers gave written informed consent before participation.

Study Design

During the 48-hour fast, all participants were admitted to our research center after an overnight fast. On the first study day, the overnight fasted subjects underwent baseline MRI scanning. After the MRI, participants consumed a standardized breakfast – after which several metabolic parameters were assessed which will be published elsewhere - and then fasted for the next 48 hours. Drinking water and non-caffeinated tea was allowed ad libitum. The second MRI session was conducted after 48 hours of fasting. Participants were asked to lie still and relaxed with their eyes open during acquisition of each resting-state scan.

MRI data acquisition

MRI scans were acquired on a Philips Achieva 3.0 Tesla scanner using an eight-channel SENSE head coil for radiofrequency reception (Philips Healthcare, Best, The Netherlands). Whole-brain resting-state scans were acquired using T2*-weighted gradient-echo echo-planar imaging (EPI, EPI factor 29,160 volumes, 38 axial slices scanned in ascending order, repetition time (TR) 2200 ms, echo time (TE) 30 ms, flip angle 80^0, field of view 220x220 mm, 2.75 mm isotropic voxels with a 0.25 mm slice gap).

A high-resolution T_1-weighted anatomical image (ultra-fast gradient-echo acquisition, TR 9.78 ms, TE 4.59 ms, flip angle 8^0, 140 axial slices, FOV 224x224 mm, in-plane resolution 0.875x0.875 mm, slice thickness 1.2 mm) and a high resolution T_2^*-weighted EPI scan (TR 2200 ms, TE 30 ms, flip angle 80^0, 84 axial slices, FOV 220x220 mm, in-plane resolution 1.96x1.96 mm, slice thickness 2.0 mm) were acquired for registration purposes.

fMRI data preprocessing

All data was analyzed using FSL Version 4.1.3. (FMRIB's Software Library, www.fMRIb.ox.ac.uk/fsl) [28;29]. The resting-state scans were preprocessed by applying motion correction, brain extraction (to remove non-brain data), spatial smoothing (Gaussian kernel of 6mm full width at half maximum), a grand-mean intensity normalization of the entire data set by a single scaling factor, and a high pass temporal filter with a cutoff of 0.01Hz. Each resting-state data set was registered to the high resolution EPI scan, the high resolution EPI scan to the T_1-weighted anatomical image, and the T_1 image to the 2 mm isotropic MNI-152 standard space (T_1-weighted standard brain averaged over 152 subjects; Montreal Neurological Institute, Montreal,

QC, Canada). The resulting transformation matrices were concatenated to describe the registration of the resting-state data to MNI standard space, and the inverse matrix was calculated (MNI to resting-state data).

fMRI time course extraction and statistics

A seed-based correlation approach was used to study resting-state functional connectivity with the hypothalamus, amygdala, and PCC. Using the MNI standard space image, binary spherical regions of interest (ROIs) with a 2.5 mm radius were created around the center voxels of the bilateral hypothalamus (left seed: x=-4, y=-1, z=-13, right seed: x=5, y=-1, z=-13), and with a 3.5 mm radius of the amygdala (left seed: x=-23, y=-4, z=-19, right seed: x=23, y=-4, z=-19) [30], and PCC (seed: x=-5, y=-49, z=40 [31]). Using the inverse transformation matrix, ROIs were registered to each participant's preprocessed resting-state data set.

Then, the mean time course within each ROI was calculated and used as regressor in a general linear model (GLM). Separate GLMs were set up to probe each of the three networks associated with the different seeds: the first contained regressors for the left and right hypothalamus seeds, the second contained regressors for the left and right amygdala seeds, the third contained the regressor for the PCC seed. In addition, white matter signal, cerebrospinal fluid (CSF) signal, six motion parameters (3 translations and 3 rotations), and the global signal were used as nuisance regressors. For each individual the three GLMs were analyzed using FEAT (FMRI Expert Analysis Tool) version 5.98, part of FSL (FMRIB's Software Library [28]). Except for the PCC, contrasts were made for the left and right seed separately, as well as for both seeds together. The resulting parameter estimate maps and corresponding images of variance were resliced into 2 mm MNI space and fed into a higher level mixed effects analysis to assess within-group (one sample *t*-test) and between-groups (independent samples *t*-test) effects at baseline, and the difference between baseline and the post-fast time point (repeated measures analysis of variance). Whole-brain *z*-score statistical images were thresholded with an initial cluster-forming threshold of $z>2.3$ and a corrected cluster significance threshold of $p<0.05$ [32]. Regions of interests (ROIs) were drawn on significant and contiguous voxels found with the functional connectivity analysis. Average *z*-scores were calculated within these ROIs for each individual and then averaged per group to create bar graphs to illustrate the strength and directionality of the functional connectivity effects.

All data shown is depicted as mean ± standard error of the mean (SEM).

Results

Fourteen obese (BMI>30 kg/m^2) and 12 lean (BMI 19-25 kg/m^2) participants were included. Two scans were excluded because of excessive motion (>3 mm in any direction) resulting in large imaging artifacts (one of an obese and one of a lean participant). Therefore, we compared fMRI results of 13 obese (2 males, 11 females, BMI 35.4 ± 1.2, age 31 ± 3) and 11 lean individuals (2 males, 8 females, BMI 23.2 ± 0.5, age 28 ± 3).

Functional connectivity of hypothalamus

Positive connectivity analysis at baseline
Areas that were connected with the hypothalamus in both groups were: the brainstem, medial prefrontal cortex, amygdala, insula, posterior part of the middle temporal gyrus, subcallosal cortex, orbitofrontal cortex, hippocampus and the nucleus accumbens. Data for lean individuals at baseline is shown in supplementary Figure 1. At baseline there were no differences in functional connectivity between lean and obese individuals.

Negative connectivity analysis at baseline
The regions that were connected with the hypothalamus in both groups were: the cuneal cortex, the frontal poles, the lateral occipital cortices and the inferior frontal gyri (supplementary Figure 1). Again, there were no differences between obese and lean individuals at baseline.

Effects of 48-hours of fasting
After fasting, connectivity of the hypothalamus with the left insula and the superior temporal gyrus decreased in obese subjects (Figure 1A) compared with the baseline scan. Fasting did not significantly affect hypothalamic connectivity in lean individuals. An interaction between Group and Time was found for hypothalamic connectivity with the left insula and the dorsal anterior cingulate cortex (dACC), demonstrating differentially affected connectivity by the prolonged fast between lean and obese participants (Figure 2, Table 1). The (positive) connectivity between hypothalamus and left insula was reduced in the obese group to levels comparable to the lean individuals. In addition, the connectivity between the hypothalamus and the dACC increased in lean subjects, whereas it decreased in obese individuals (Figure 2).
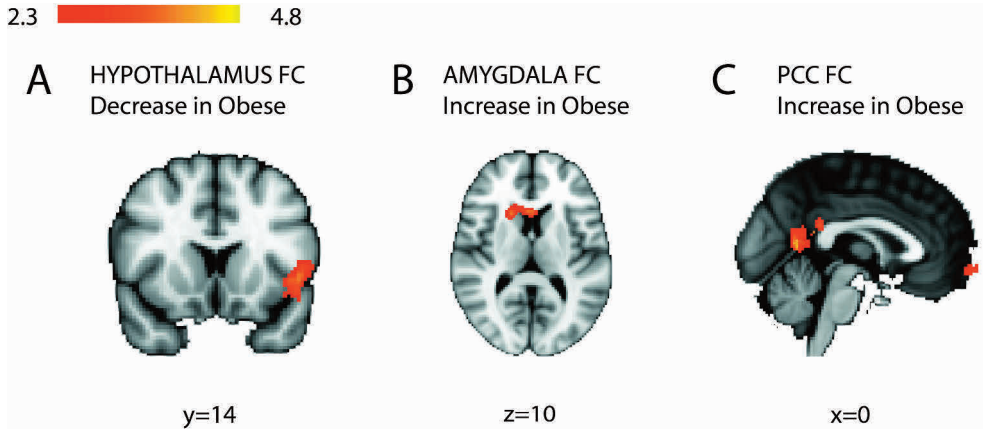
Figure 1: Fasting compared to baseline: Fasting induced changes in hypothalamus, amygdala and posterior cingulate cortex functional connectivity networks in obese subjects only.
Fasting had a significant effect on all three (positive analysis) functional connectivity networks studied, but only in the obese subjects. In this figure we show that fasting A) reduced functional connectivity between hypothalamus and left insula and hypothalamus and superior temporal gyrus in obese individuals, B) increased amygdala functional connectivity with the left caudate nucleus in obese subjects and C) increased PCC functional connectivity with the frontal pole, the precuneus cortex and the PCC itself in obese individuals. All results are projected on 2mm MNI standard space. Effects are thresholded at z>2.30, p<0.05. The left side of the brain in the figure corresponds with the right side in reality and vice versa. Abbreviations: PCC, posterior cingulated cortex; MNI standard space, T1-weighted standard brain averaged over 152 subjects; Montreal Neurological Institute, Montreal, QC, Canada.

Functional connectivity of the amygdala

Positive connectivity analysis at baseline
Areas that were connected with the amygdala in both groups included: the brainstem, hippocampus, hypothalamus, globus pallidus, fusiform gyrus, orbitofrontal cortex and both temporal lobes. Data for lean individuals at baseline is shown in supplementary Figure 2. At baseline, lean individuals demonstrated increased amygdala functional connectivity with the ventromedial prefrontal cortex (vmPFC) (Figure 3, Table 2). Moreover, increased connectivity was observed between the amygdala and superior temporal gyrus in lean individuals compared with obese individuals (Figure 3, Table 2).

Negative connectivity analysis at baseline
The following areas were connected with the amygdala in both groups: the frontal poles, the precuneal cortices and the occipital cortices (supplementary Figure 3).
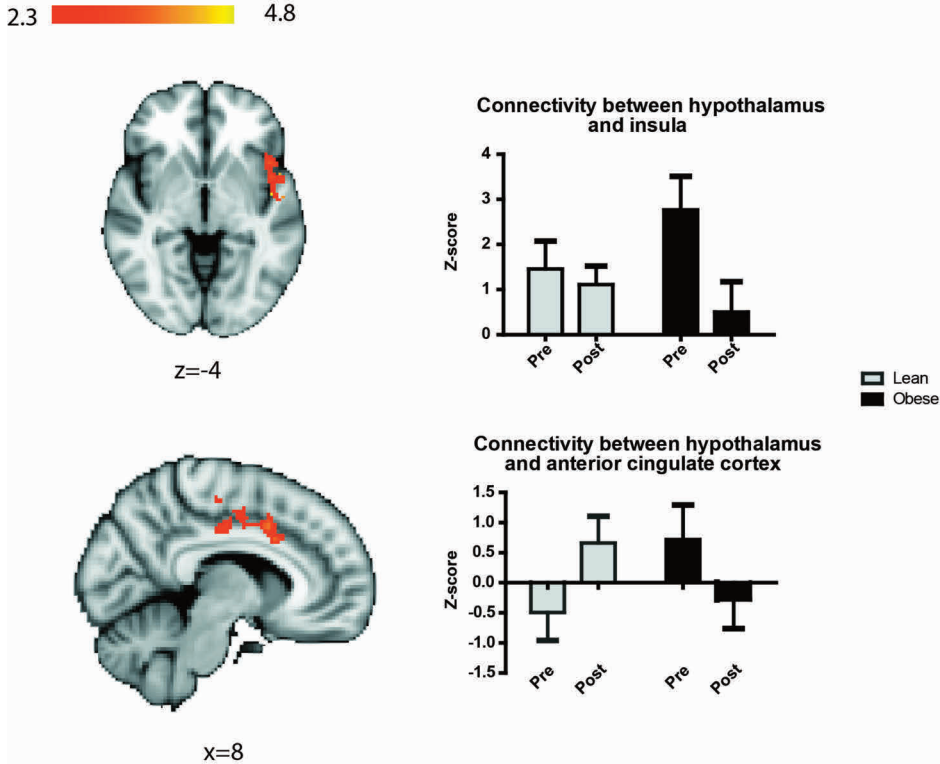
Figure 2: The effect of fasting (compared to baseline) between lean and obese subjects: Fasting affected hypothalamic connectivity with the left insula and dACC differently in lean compared to obese participants.

Fasting had a different effect on hypothalamic functional connectivity with the left insula and the dorsal anterior cingulate cortex in lean compared to obese individuals. In the top figure, the difference in hypothalamic connectivity with the insula is depicted. In the bottom figure, we show the difference in hypothalamic connectivity with the dorsal anterior cingulated cortex.

Between group effects of hypothalamus functional connectivity are projected here on 2mm MNI standard space. Between group effects are thresholded at z>2.30, p<0.05. The left side of the brain in the figure corresponds with the right side in reality and vice versa. Error bars depict standard errors of the mean. Abbreviations; MNI ,T1-weighted standard brain averaged over 152 subjects; Montreal Neurological Institute, Montreal, QC, Canada.

Effects of 48-hours of fasting

Fasting increased connectivity between the amygdala and left caudate nucleus in obese individuals (Figure 1B). Fasting did not affect the connectivity of the amygdala in lean subjects. However, these differences did not reach statistical significance.

Table 1 The effect of fasting compared to baseline between lean and obese subjects

Region	Hemisphere	Peak voxel coordinates (MNI)			Z-value
		x	y	z	
Differentially affected regions by the fast between lean and obese (interaction group x time)					
Anterior cingulate gyrus	R	4	-8	42	3.97
Posterior cingulate gyrus	R	6	-18	36	3.24
Inferior frontal gyrus	L	-50	12	0	4.57
Insula	L	-42	-10	4	3.44

Only the significant results are shown. All Z-values are corrected for multiple comparisons (p<0.05). Abbreviations: R, right; L, left; MNI standard space, T1-weighted standard brain averaged over 152 subjects; Montreal Neurological Institute, Montreal, QC, Canada.

Functional connectivity of the posterior cingulate cortex

Positive connectivity analysis at baseline

We observed PCC functional connectivity with the following regions in both groups: the posterior division of the right middle temporal gyrus, an extensive frontal area
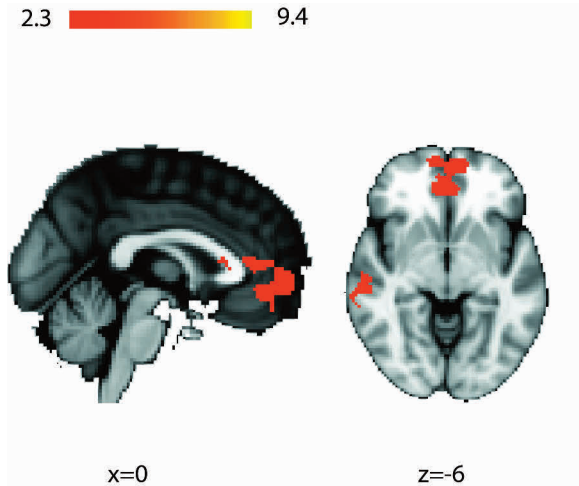
Figure 3: Differences at baseline in amygdala functional connectivity between groups: Significant functional connectivity between amygdala and mPFC was found in lean but not in obese individuals.
Here we show the difference in amygdala functional connectivity with the medial prefrontal cortex in lean compared to obese subjects at baseline. Increased connectivity was observed in the lean subjects. Results are projected on 2mm MNI standard space. Between group effects are thresholded at z>2.3, p<0.05 (cluster corrected). The left side of the brain in the figure corresponds with the right side in reality and vice versa. Abbreviations: mPFC, medial prefrontal cortex. MNI, T1-weighted standard brain averaged over 152 subjects; Montreal Neurological Institute, Montreal, QC, Canada.

Table 2 Baseline differences in amygdala functional connectivity between groups

Region	Hemisphere	Peak voxel coordinates (MNI)			Z-value
		x	y	z	
Lean > Obese					
Baseline					
Medial prefrontal cortex	R	10	62	-8	4.27
Superior temporal Gyrus	R	56	-32	2	3.75

Only the significant results are shown. All Z-values are corrected for multiple comparisons (p<0.05). Abbreviations: R, right; L, left; MNI standard space, T1-weighted standard brain averaged over 152 subjects; Montreal Neurological Institute, Montreal, QC, Canada.
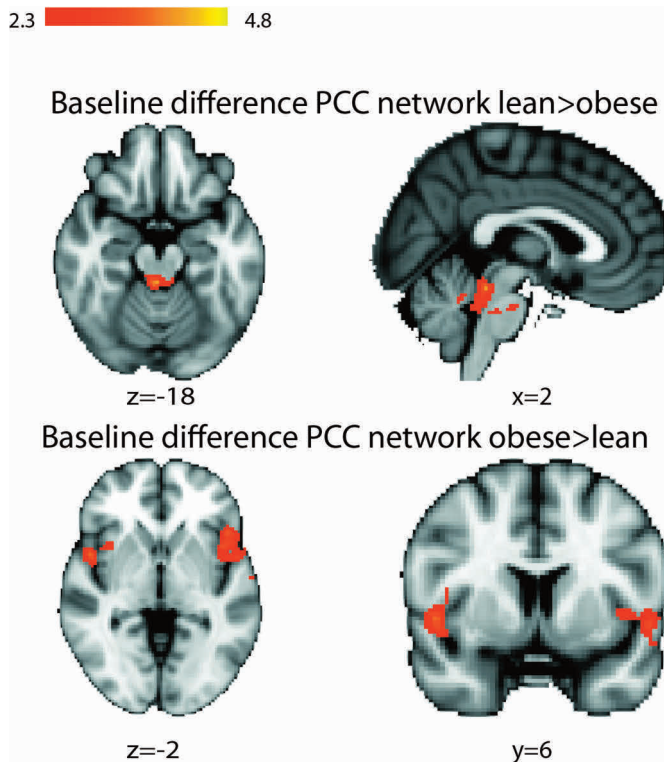
Figure 4: Differences at baseline in posterior cingulate cortex functional connectivity between groups: Stronger connectivity between the PCC and brainstem in lean subjects and stronger connectivity with the bilateral frontal opercular cortices, extending into the insula, in obese subjects. Baseline differences in posterior cingulate cortex functional connectivity between lean and obese individuals, projected on 2mm MNI standard space. Here we show that connectivity between the PCC and brainstem and between the PCC and pons were stronger in lean subjects, whereas PCC connections with left and right frontal opercular cortices were stronger in obese individuals at baseline. Between group effects are thresholded at z>2.3, p<0.05 (cluster corrected). The left side of the brain in the figure corresponds with the right side in reality and vice versa. Abbreviations: MNI standard space, T1-weighted standard brain averaged over 152 subjects; Montreal Neurological Institute, Montreal, QC, Canada.

(medial and superior frontal gyruses, frontal pole), an extensive posterior cortical area (posterior cingulate cortex, precuneus cortex) and the lateral occipital cortices. Data for lean individuals at baseline is shown in supplementary Figure 3. Connectivity between the PCC and brainstem was stronger in lean subjects, whereas PCC connections with the bilateral frontal opercular cortices, extending into the insula, were stronger in obese individuals at baseline (Figure 4, Table 3).

Negative connectivity analysis at baseline
The following areas showed connectivity with the PCC in both groups: bilateral precentral gyrus, bilateral insula, bilateral occipital fusiform gyrus, and the cerebellum (Supplementary Figure 3).

Effects of 48-hours of fasting
After fasting, PCC connectivity with the frontal pole, the posterior cingulate gyrus and the precuneus cortex was increased in the obese group (Figure 1C). Although fasting did not impact functional connections of the PCC in lean subjects, the different reactions in lean and obese individuals did not reach statistical significance.

Table 3 Baseline differences in PCC functional connectivity between groups

Region	Hemisphere	Peak voxel coordinates (MNI)			Z-value
		x	y	z	
Lean > Obese Baseline					
Brain stem	R	2	-36	-18	4.03
Pons	L	-10	-18	-28	2.74
Obese>Lean Baseline					
Central opercular cortex	L	-52	6	-2	2.62
Central opercular cortex	R	50	6	-2	3.53

Only the significant results are shown. All Z-values are corrected for multiple comparisons (p<0.05). Abbreviations: PCC, posterior cingulate cortex; R, right; L, left; MNI standard space, T1-weighted standard brain averaged over 152 subjects; Montreal Neurological Institute, Montreal, QC, Canada.
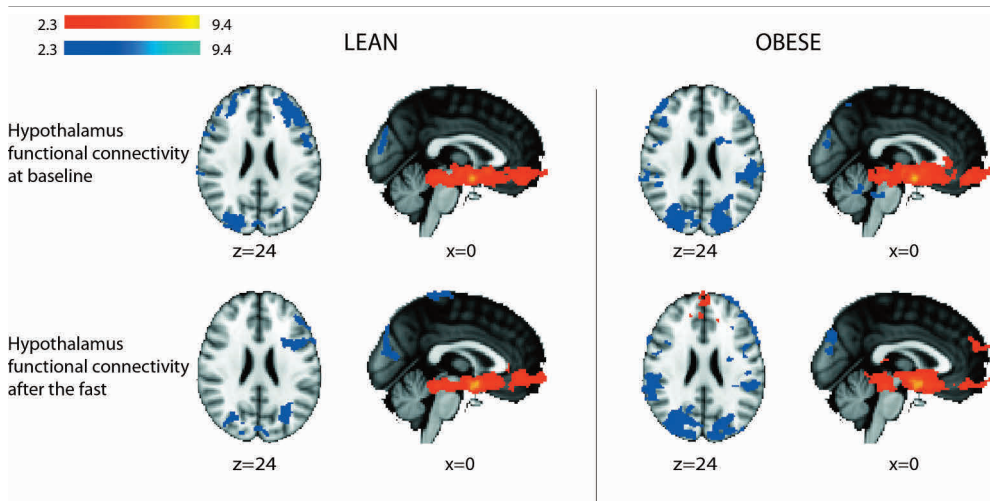
Supplementary Figure 1 Hypothalamus functional connectivity in lean and obese subjects at baseline and after the fast

Within group results of the hypothalamus functional connectivity network at baseline and after the fast. Results are projected on 2mm MNI standard space. Positive connectivity analysis results are depicted in red, negative connectivity analysis results in blue. Effects are thresholded at z>2.30, p<0.05. The left side of the brain in the figure corresponds with the right side in reality and vice versa. Abbreviations: MNI, T1-weighted standard brain averaged over 152 subjects; Montreal Neurological Institute, Montreal, QC, Canada.
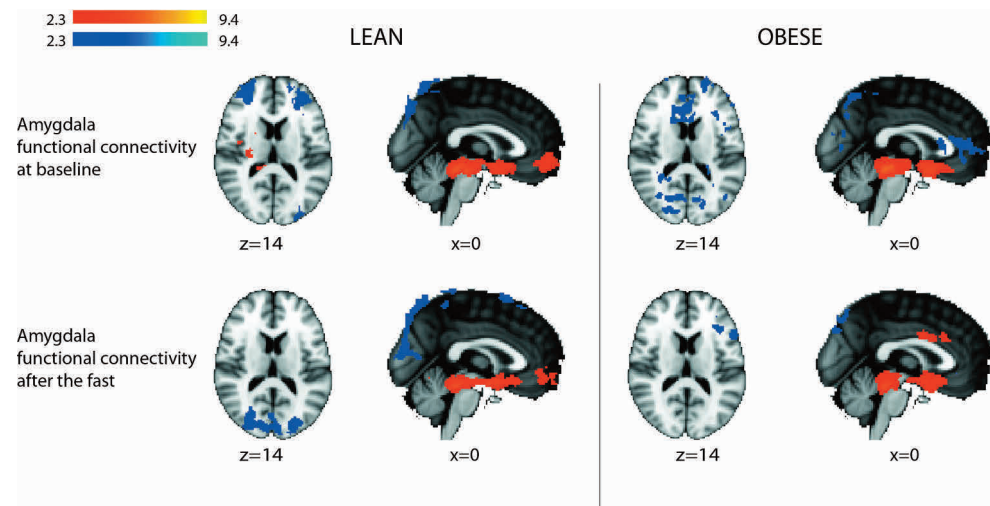
Supplementary Figure 2 Amygdala functional connectivity in lean and obese subjects at baseline and after the fast

Within group results of the amygdala functional connectivity network at baseline and after the fast. Results are projected on 2mm MNI standard space. Positive connectivity analysis results are depicted in red, negative connectivity analysis results in blue. Effects are thresholded at z>2.30, p<0.05. The left side of the brain in the figure corresponds with the right side in reality and vice versa. Abbreviations: MNI standard space, T1-weighted standard brain averaged over 152 subjects; Montreal Neurological Institute, Montreal, QC, Canada.
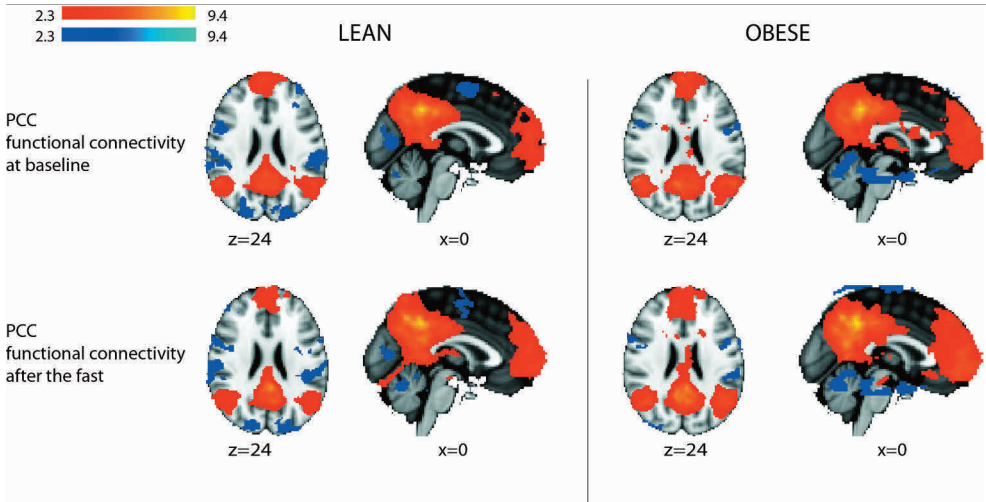
Supplementary Figure 3 Posterior cingulated cortex functional connectivity in lean and obese subjects at baseline and after the fast
Within group results of the posterior cingulated cortex functional connectivity network at baseline and after the fast. Results are projected on 2mm MNI standard space. Positive connectivity analysis results are depicted in red, negative connectivity analysis results in blue. Effects are thresholded at z>2.30, p<0.05. The left side of the brain in the figure corresponds with the right side in reality and vice versa. Abbreviations: MNI standard space, T1-weighted standard brain averaged over 152 subjects; Montreal Neurological Institute, Montreal, QC, Canada.

Discussion

We compared the effects of 48 hours of fasting on functional connectivity of the hypothalamus and amygdala, brain regions involved in homeostatic control of body weight and/or metabolism and salience, in lean and obese individuals. Additionally, the so called 'default mode network' was examined, as this network's resting state architecture has been studied extensively in both health and disease [33;34] and alterations in this network have been shown in obese subjects previously [20].

At baseline, the patterns of hypothalamus, amygdala and PCC functional connectivity in lean and obese individuals generally corresponded with what is known about these networks in the available literature [30;31;35-37]. There were no apparent differences in the hypothalamic functional connectivity of lean versus obese subjects at baseline. However, we did find differences in baseline connectivity of amygdala and PCC networks between lean and obese subjects. The amygdala was connected to the ventromedial prefrontal cortex (vmPFC) and the superior temporal gyrus in lean, but not in obese individuals. Additionally, in the default mode network, the connections be-

tween PCC and brainstem, and between PCC and pons were stronger in lean subjects, whereas the connections with left and right frontal opercular cortices were stronger in obese individuals.

Fasting induced changes in all three networks, primarily in the obese group. Obese, but not lean, participants demonstrated decreased hypothalamic connectivity with the left insula, and the superior temporal gyrus. In addition, increased functional connectivity between amygdala and left caudate nucleus was observed in obese, but not in lean individuals. Finally, increased connectivity between the PCC and frontal pole, posterior cingulate gyrus and precuneus cortex was observed in obese, but not in lean subjects.

Most importantly, the 48-hour fast affected hypothalamic connectivity with the left insula and dACC differently in lean compared to obese participants. The strong functional connectivity between hypothalamus and left insula observed at baseline was reduced to a large extent in obese subjects, to a comparable level observed in lean controls. The insula is heavily involved in interoceptive processing, connecting interoception (bodily awareness) to emotion and motivation [38;39]. In addition, functional connectivity between the hypothalamus and the dACC increased in lean subjects after fasting, whereas it decreased in obese individuals. The hypothalamus, dACC and insula are all part of the so called "salience network" [40]. This network is proposed to perceive internal and external cues and define the most relevant among them to adapt behavior and/or physiology accordingly [41]. Therefore, any difference between obese and normal weight subjects in the salience network's response to fasting may indicate that the neuronal perception or processing of calorie-imbalance is different between these phenotypes. The physiological and behavioral ramifications of the observed differences remain to be established. However, it is tempting to speculate that functional connectivity specifics of the saliency network might drive weight gain in predisposed individuals.

Our baseline analysis showed that functional connectivity between the amygdala and the vmPFC was stronger in lean than in obese individuals. Both the vmPFC and amygdala are involved in the response to motivationally relevant cues such as hunger [24]. Moreover, the amygdala plays an important role in food reward [24] and stimulation of amygdala neurons induces hyperphagia and weight-gain in rodents [42;43]. Notably, the

response of the amygdala and vmPFC to food cues is increased in obese women [44]. It is conceivable that the lack of functional connection between these nuclei in obese individuals hampers mutual control of activity which might affect reward sensations.

Our data also show that PCC functional connectivity with the brainstem is stronger in lean compared to obese participants at baseline. Neurons of the solitary tract, located in the brainstem, are involved in satiety [45] whereas the pons plays a role in tasting [46]. We also show stronger PCC functional connectivity with the left and right frontal opercular cortices in obese compared to lean individuals at baseline. The opercular cortices cover the insula and the frontal operculum is involved in gustation [47]. The physiological function of the default mode network includes cognition and tasks with an internal focus [48]. With respect to our data, it is tempting to speculate that the changes associated with obesity reflect alterations in the control of satiety and possibly taste and/or palatability in these subjects, given the well known functional properties of brainstem and opercula [46].

Our baseline (overnight fasted) results differ from those of previous studies with respect to differences between lean and obese subjects. Importantly, these previous studies mainly focused on the default-mode network. For example, it was demonstrated that the DMN of obese individuals is characterized by increased connectivity with the precuneus and decreased connectivity with the ACC [20] compared to lean subjects. In addition, it has been shown that obese individuals that lost considerable weight have enhanced activity in regions within the DMN: the PCC and the left lateral inferior parietal cortex [7]. The differences with our results might be explained by the analytical methods (independent component analysis versus our seed-based approach) [20], the inclusion of weight-reduced obese subjects [7] and differences in scanning procedure (scans acquired during picture viewing versus our "resting" paradigm) [7].

It is important to discuss some limitations. First, negative correlations might be artificially induced by global signal regression[51]. Therefore, no conclusions can be drawn from the observed sign of the connectivities (positive or negative). As such, differences in connectivity are real but no conclusions about the direction of connectivity can be drawn.

Furthermore, hypothalamic and amygdala functional connectivity may be influenced by noise from arteries surrounding these areas [49]. To reduce this effect, we used the global signal as confound regressor in our analysis, because this signal is largely re-

lated to physiological noise in fMRI data [50]. Due to the relatively low spatial resolution, it is unfortunately impossible to distinguish the different hypothalamic regions that have distinct homeostatic properties. Furthermore, quantification of hunger and other relevant behavioral and cognitive parameters during fasting in future studies would allow correlation of these features with changes in functional connectivity.

In conclusion, we studied resting-state functional connectivity of three brain regions that are related to the behavioral and metabolic control of energy balance in humans. We describe changes in these networks both at baseline and in response to fasting between lean and obese individuals. Although the ramifications of these changes in network connectivity remain to be established, our results are in keeping with the notion that food reward and nutrient deprivation are differentially perceived and /or processed by obese individuals.

References

1. Flegal KM, Graubard BI, Williamson DF, Gail MH. Cause-specific excess deaths associated with underweight, overweight, and obesity. *JAMA* 2007; 298(17): 2028-2037.
2. World Health Organization. Obesity and Overweight, Fact Sheet No 311. 2011. Ref Type: Grant
3. Schwartz MW, Woods SC, Porte D, Jr., Seeley RJ, Baskin DG. Central nervous system control of food intake. *Nature* 2000; 404(6778): 661-671.
4. Berthoud HR. Neural control of appetite: cross-talk between homeostatic and non-homeostatic systems. *Appetite* 2004; 43(3): 315-317.
5. Baskin DG, Figlewicz LD, Seeley RJ, Woods SC, Porte D, Jr., Schwartz MW. Insulin and leptin: dual adiposity signals to the brain for the regulation of food intake and body weight. *Brain Res* 1999; 848(1-2): 114-123.

6. Cornier MA, Von Kaenel SS, Bessesen DH, Tregellas JR. Effects of overfeeding on the neuronal response to visual food cues. *Am J Clin Nutr* 2007; 86(4): 965-971.

7. Tregellas JR, Wylie KP, Rojas DC, Tanabe J, Martin J, Kronberg E, Cordes D, Cornier MA. Altered Default Network Activity in Obesity. *Obesity (Silver Spring)* 2011.

8. Carnell S, Gibson C, Benson L, Ochner CN, Geliebter A. Neuroimaging and obesity: current knowledge and future directions. *Obes Rev* 2011; 10-789X.

9. Alkan A, Sahin I, Keskin L, Cikim AS, Karakas HM, Sigirci A, Erdem G. Diffusion-weighted imaging features of brain in obesity. *Magn Reson Imaging* 2008; 26(4): 446-450.

10. Del PA, Gautier JF, Chen K, Salbe AD, Ravussin E, Reiman E, Tataranni PA. Neuroimaging and obesity: mapping the brain responses to hunger and satiation in humans using positron emission tomography. *Ann N Y Acad Sci* 2002; 967:389-97.: 389-397.

11. DelParigi A, Chen K, Salbe AD, Reiman EM, Tataranni PA. Sensory experience of food and obesity: a positron emission tomography study of the brain regions affected by tasting a liquid meal after a prolonged fast. *Neuroimage* 2005; 24(2): 436-443.

12. Gautier JF, Chen K, Salbe AD, Bandy D, Pratley RE, Heiman M, Ravussin E, Reiman EM, Tataranni PA. Differential brain responses to satiation in obese and lean men. *Diabetes* 2000; 49(5): 838-846.

13. Gautier JF, Del PA, Chen K, Salbe AD, Bandy D, Pratley RE, Ravussin E, Reiman EM, Tataranni PA. Effect of satiation on brain activity in obese and lean women. *Obes Res* 2001; 9(11): 676-684.

14. Karhunen LJ, Lappalainen RI, Vanninen EJ, Kuikka JT, Uusitupa MI. Regional cerebral blood flow during food exposure in obese and normal-weight women. *Brain* 1997; 120 (Pt 9): 1675-1684.

15. Stice E, Spoor S, Bohon C, Veldhuizen MG, Small DM. Relation of reward from food intake and anticipated food intake to obesity: a functional magnetic resonance imaging study. *J Abnorm Psychol* 2008; 117(4): 924-935.

16. Shin AC, Zheng H, Berthoud HR. An expanded view of energy homeostasis: neural integration of metabolic, cognitive, and emotional drives to eat. *Physiol Behav* 2009; 97(5): 572-580.

4

17. Fox MD, Raichle ME. Spontaneous fluctuations in brain activity observed with functional magnetic resonance imaging. *Nat Rev Neurosci* 2007; 8(9): 700-711.

18. Biswal BB, Mennes M, Zuo XN, Gohel S, Kelly C, Smith SM, Beckmann CF, Adelstein JS, Buckner RL, Colcombe S, Dogonowski AM, Ernst M, Fair D, Hampson M, Hoptman MJ et al. Toward discovery science of human brain function. *Proc Natl Acad Sci U S A* 2010; 107(10): 4734-4739.

19. Smith SM, Fox PT, Miller KL, Glahn DC, Fox PM, Mackay CE, Filippini N, Watkins KE, Toro R, Laird AR, Beckmann CF. Correspondence of the brain's functional architecture during activation and rest. *Proc Natl Acad Sci U S A* 2009; 106(31): 13040-13045.

20. Kullmann S, Heni M, Veit R, Ketterer C, Schick F, Haring HU, Fritsche A, Preissl H. The obese brain: Association of body mass index and insulin sensitivity with resting state network functional connectivity. *Hum Brain Mapp* 2011; 10.

21. Sande-Lee S, Pereira FR, Cintra DE, Fernandes PT, Cardoso AR, Garlipp CR, Chaim EA, Pareja JC, Geloneze B, Li LM, Cendes F, Velloso LA. Partial reversibility of hypothalamic dysfunction and changes in brain activity after body mass reduction in obese subjects. *Diabetes* 2011; 60(6): 1699-1704.

22. Thaler JP, Yi CX, Schur EA, Guyenet SJ, Hwang BH, Dietrich MO, Zhao X, Sarruf DA, Izgur V, Maravilla KR, Nguyen HT, Fischer JD, Matsen ME, Wisse BE, Morton GJ et al. Obesity is associated with hypothalamic injury in rodents and humans. *J Clin Invest* 2012; 122(1): 153-162.

23. Pessoa L, Adolphs R. Emotion processing and the amygdala: from a 'low road' to 'many roads' of evaluating biological significance. *Nat Rev Neurosci* 2010; 11(11): 773-783.

24. Baxter MG, Murray EA. The amygdala and reward. *Nat Rev Neurosci* 2002; 3(7): 563-573.

25. Raichle ME, MacLeod AM, Snyder AZ, Powers WJ, Gusnard DA, Shulman GL. A default mode of brain function. *Proc Natl Acad Sci U S A* 2001; 98(2): 676-682.

26. Rothemund Y, Preuschhof C, Bohner G, Bauknecht HC, Klingebiel R, Flor H, Klapp BF. Differential activation of the dorsal striatum by high-calorie visual food stimuli in obese individuals. *Neuroimage* 2007; 37(2): 410-421.

27. Volkow ND, Wang GJ, Telang F, Fowler JS, Goldstein RZ, Alia-Klein N, Logan J, Wong C, Thanos PK, Ma Y, Pradhan K. Inverse association between BMI and prefrontal metabolic activity in healthy adults. *Obesity (Silver Spring)* 2009; 17(1): 60-65.

4

28. Smith SM, Jenkinson M, Woolrich MW, Beckmann CF, Behrens TE, Johansen-Berg H, Bannister PR, De LM, Drobnjak I, Flitney DE, Niazy RK, Saunders J, Vickers J, Zhang Y, De SN et al. Advances in functional and structural MR image analysis and implementation as FSL. *Neuroimage* 2004; 23 Suppl 1:S208-19.: S208-S219.

29. Woolrich MW, Jbabdi S, Patenaude B, Chappell M, Makni S, Behrens T, Beckmann C, Jenkinson M, Smith SM. Bayesian analysis of neuroimaging data in FSL. *Neuroimage* 2009; 45(1 Suppl): S173-S186.

30. Veer IM, Oei NY, Spinhoven P, van Buchem MA, Elzinga BM, Rombouts SA. Beyond acute social stress: increased functional connectivity between amygdala and cortical midline structures. *Neuroimage* 2011; 57(4): 1534-1541.

31. Fox MD, Snyder AZ, Vincent JL, Corbetta M, Van E, Raichle ME. The human brain is intrinsically organized into dynamic, anticorrelated functional networks. *Proc Natl Acad Sci U S A* 2005; 102(27): 9673-9678.

32. Worsley KJ, Jezzard P, Matthews PM, Smith S. Statistical analysis of activation images. In: *Functional Magnetic Resonance Imaging. An introduction to Methods.* Oxford University Press: 2001.

33. Rombouts SA, Barkhof F, Goekoop R, Stam CJ, Scheltens P. Altered resting state networks in mild cognitive impairment and mild Alzheimer's disease: an fMRI study. *Hum Brain Mapp* 2005; 26(4): 231-239.

34. Swanson N, Eichele T, Pearlson G, Kiehl K, Yu Q, Calhoun VD. Lateral differences in the default mode network in healthy controls and patients with schizophrenia. *Hum Brain Mapp* 2011; 32(4): 654-664.

35. Kaufmann C, Wehrle R, Wetter TC, Holsboer F, Auer DP, Pollmacher T, Czisch M. Brain activation and hypothalamic functional connectivity during human non-rapid eye movement sleep: an EEG/fMRI study. *Brain* 2006; 129(Pt 3): 655-667.

36. Roy AK, Shehzad Z, Margulies DS, Kelly AM, Uddin LQ, Gotimer K, Biswal BB, Castellanos FX, Milham MP. Functional connectivity of the human amygdala using resting state fMRI. *Neuroimage* 2009; 45(2): 614-626.

37. Greicius MD, Krasnow B, Reiss AL, Menon V. Functional connectivity in the resting brain: a network analysis of the default mode hypothesis. *Proc Natl Acad Sci U S A* 2003; 100(1): 253-258.

38. Volkow ND, Wang GJ, Fowler JS, Tomasi D, Baler R. Food and Drug Reward: Overlapping Circuits in Human Obesity and Addiction. *Curr Top Behav Neurosci* 2011.

4

39. Critchley HD, Wiens S, Rotshtein P, Ohman A, Dolan RJ. Neural systems supporting interoceptive awareness. *Nat Neurosci* 2004; 7(2): 189-195.

40. Seeley WW, Menon V, Schatzberg AF, Keller J, Glover GH, Kenna H, Reiss AL, Greicius MD. Dissociable intrinsic connectivity networks for salience processing and executive control. *J Neurosci* 2007; 27(9): 2349-2356.

41. Menon V, Uddin LQ. Saliency, switching, attention and control: a network model of insula function. *Brain Struct Funct* 2010; 214(5-6): 655-667.

42. Ahn S, Phillips AG. Modulation by central and basolateral amygdalar nuclei of dopaminergic correlates of feeding to satiety in the rat nucleus accumbens and medial prefrontal cortex. *J Neurosci* 2002; 22(24): 10958-10965.

43. Loscher W, Brandt C, Ebert U. Excessive weight gain in rats over extended kindling of the basolateral amygdala. *Neuroreport* 2003; 14(14): 1829-1832.

44. Stoeckel LE, Weller RE, Cook EW, III, Twieg DB, Knowlton RC, Cox JE. Widespread reward-system activation in obese women in response to pictures of high-calorie foods. *Neuroimage* 2008; 41(2): 636-647.

45. Berthoud HR. The vagus nerve, food intake and obesity. *Regul Pept* 2008; 149(1-3): 15-25.

46. Spector AC. Gustatory function in the parabrachial nuclei: implications from lesion studies in rats. *Rev Neurosci* 1995; 6(2): 143-175.

47. Scott TR, Yaxley S, Sienkiewicz ZJ, Rolls ET. Gustatory responses in the frontal opercular cortex of the alert cynomolgus monkey. *J Neurophysiol* 1986; 56(3): 876-890.

48. Buckner RL, Andrews-Hanna JR, Schacter DL. The brain's default network: anatomy, function, and relevance to disease. *Ann N Y Acad Sci* 2008; 1124: 1-38.

49. Laufs H, Walker MC, Lund TE. 'Brain activation and hypothalamic functional connectivity during human non-rapid eye movement sleep: an EEG/fMRI study'—its limitations and an alternative approach. *Brain* 2007; 130(Pt 7): e75.

50. Fox MD, Zhang D, Snyder AZ, Raichle ME. The global signal and observed anticorrelated resting state brain networks. *J Neurophysiol* 2009; 101(6): 3270-3283.

51. Murphy K, Birn RM, Handwerker DA, Jones TB, Bandettini PA. The impact of global signal regression on resting state correlations: are anti-correlated networks introduced? *Neuroimage* 2009; 44/3: 893-905.

4

Chapter 5

Regulation of skeletal muscle energy/nutrient-sensing pathways during metabolic adaptation to fasting in healthy humans

Marjolein A. Wijngaarden[1*], Leontine E.H. Bakker[2*], Gerard C. van der Zon[3], Peter A.C. 't Hoen[4], Ko Willems van Dijk[1,5], Ingrid M. Jazet[2], Hanno Pijl[1], Bruno Guigas[3,6]

* These authors contributed equally to this work

5

[1] Department of Endocrinology and Metabolism, Leiden University Medical Center, Leiden, The Netherlands
[2] Department of Internal Medicine, Leiden University Medical Center, Leiden, The Netherlands
[3] Department of Molecular Cell Biology, Leiden University Medical Center, Leiden, The Netherlands
[4] Center for Human and Clinical Genetics, Leiden University Medical Center, Leiden, The Netherlands
[5] Department of Human Genetics, Leiden University Medical Center, Leiden, The Netherlands
[6] Department of Parasitology, Leiden University Medical Center, Leiden, The Netherlands

5

Abstract

During fasting, rapid metabolic adaptations are required to maintain energy home-ostasis. This occurs by a coordinated regulation of energy/nutrient-sensing pathways leading to transcriptional activation and repression of specific sets of genes. The aim of the study was to investigate how short-term fasting affects whole-body energy homeostasis and skeletal muscle energy/nutrient-sensing pathways and transcrip-tome in humans. For this purpose, twelve young healthy men were studied during a 24-hour fast. Whole-body glucose/lipid oxidation rates were determined by indirect calorimetry and blood and skeletal muscle biopsies were collected and analyzed at baseline and after 10 and 24h of fasting. As expected, fasting induced a time-depen-dent decrease in plasma insulin and leptin levels, whereas levels of ketone bodies and free fatty acids increased. This was associated with a metabolic shift from glu-cose towards lipid oxidation. At the molecular level, activation of the protein kinase B (PKB/Akt) and mammalian target of rapamycin (mTOR) pathways was time-depen-dently reduced in skeletal muscle during fasting, whereas the AMP-activated protein kinase (AMPK) activity remained unaffected. Furthermore, we report some changes in the phosphorylation and/or content of forkhead protein 1 (FoxO1), sirtuins 1 (SIRT1) and class IIa histone deacetylase 4 (HDAC4), suggesting that these path-ways might be involved in the transcriptional adaptation to fasting. Finally, transcrip-tome profiling identified genes that were significantly regulated by fasting in skeletal muscle at both early and late time-points. Collectively, our study provides a compre-hensive map of the main energy/nutrient-sensing pathways and transcriptomic changes during short-term adaptation to fasting in human skeletal muscle.

5

Introduction

During evolution, an integrated system regulating substrate storage and utilization at the whole organism level has developed by means of nutrient and energy sensors that constantly gauge the change in metabolic or environmental conditions. One example is the decrease in glycogen storage observed during fasting, which is associated with a concomitant shift in substrate utilization from carbohydrate to lipid oxidation, aiming to preserve glucose for use by the brain and maintain whole-body energy homeostasis [1].

As a metabolically flexible tissue, skeletal muscle contributes to a large extent to this whole-body metabolic adaptation that occurs through complex and coordinated regulation of several energy/nutrient-sensing pathways [2]. Among them, the serine/threonine AMP-activated protein kinase (AMPK) is considered one of the main sensors of energy depletion. Once activated, AMPK acts to restore energy balance by switching off energy-consuming pathways and promoting ATP-generating processes [3-5]. AMPK consists of a heterotrimeric complex containing a catalytic subunit α and two regulatory β and γ subunits. Phosphorylation of the α subunit at Thr172 by upstream AMPK kinases (AMPKKs), such as the liver kinase B (LKB1) or calmodulin-dependent protein kinase kinase β (CAMKKβ), is required for AMPK activation. The β subunit acts as a scaffold to which the two other subunits are bound, and contains a carbohydrate binding site which allows AMPK to sense energy reserves in the form of glycogen [3-5]. When cellular energy status is threatened, the binding of AMP and/or ADP to the γ subunit activates AMPK via a complex mechanism involving direct allosteric activation, phosphorylation on Thr172 by AMPKKs, and inhibition of dephosphorylation by protein phosphatase(s) [3-5]. Interestingly, animal studies suggest that skeletal muscle AMPK activation rapidly occurs during fasting [6], triggering the transcriptional modulation of genes involved in lipid and glucose metabolism [7].

Other energy/nutrient-sensing pathways, such as the mammalian target of rapamycin (mTOR) [8], some forkhead protein (FoxO) family members [9;10], sirtuins 1 (SIRT1) [11] and the class IIa histone deacetylase 4 (HDAC4) [12], were also suggested to be involved in the metabolic shift towards lipid oxidation during fasting in peripheral tissues. Interestingly, all these pathways are tightly interconnected with AMPK [13-15], suggesting that the kinase could play a central role in skeletal muscle metabolic flexibility.

Modulation of energy/nutrient-sensing pathways are likely to be involved in health

and diseases. Indeed, calorie restriction was shown to extend lifespan and delay the onset of age-related diseases in a wide spectrum of organisms [16], partly by inducing acute and long-lasting changes in energy/nutrient-sensing signaling pathways [17-20]. A better understanding of the energy/nutrient-sensing machinery in humans would therefore provide important insight into the pathophysiology of various age-related diseases, including type 2 diabetes and cancer. To the best of our knowledge, there is currently no data available reporting the kinetic of response of energy/nutrient-sensing pathways in human skeletal muscle during fasting. The purpose of the present study was therefore to investigate how short-term fasting affects whole-body energy homeostasis and skeletal muscle energy/nutrient-sensing pathways and transcriptome in healthy humans.

5

Methods

Ethical approval

The present study (Clinical Trial Registration Number: NCT01387919) was approved by the Medical Ethical Committee of the Leiden University Medical Center and performed in accordance with the principles of the revised Declaration of Helsinki. All volunteers gave written informed consent before participation.

Subjects

Twelve lean male volunteers (body mass index (BMI) 21.3 ± 0.6 kg/m^2, age 22 ± 1 year-old) were included. All of them were healthy weight-stable non-smoking Caucasians with a fasting plasma glucose ≤5.6 mmol/l and without family history of diabetes. Height, weight and body mass index (BMI) were measured according to World Health Organization recommendations.

Study design

All participants were instructed not to perform physical activity in the last 48 hours before the study day and were admitted to our research center after an overnight fast. The intervention study started after a standardized breakfast (t=0, two slices of brown bread with cheese; 300 calories), followed by 24 hours of fasting. Water and caffeine-free tea were allowed *ad libitum*. Blood samples were taken after breakfast (t=90 min), and after 10 and 24 hours of fasting by the means of an intravenous cannula, which was inserted in the elbow just before breakfast. Muscle biopsies from *musculus vastus lateralis* were collected after breakfast (baseline, t=105 min), and after 10 and 24 hours of fasting under localized 1% lidocain anesthesia, as previously described[21].

Indirect calorimetry

Subjects were placed under the ventilated hood after ~75 min, 10 and 24 hours of fasting (OxyconPro, Mijnhardt Jaegher, The Netherlands). Respiratory quotient and substrate oxidation were calculated from CO_2 and O_2 concentrations in the exhaled air, as previously described[22].

Laboratory analysis

Serum glucose, total cholesterol, triglycerides (TG), free fatty acids (FFA), alkaline

phosphatase and creatinine were measured on a Modular Analytics P-800 system (Roche Diagnostics, Germany). Serum insulin and insulin-like growth factor 1 (IGF-1) were measured by immunoluminometric assay on an Immulite 2500 automated system (Siemens Healthcare Diagnostics, The Netherlands). Cortisol, free T4 (FT4) and thyroid stimulating hormone (TSH) were measured by electrochemolumines-cence immunoassay on a Modular Analytics E-170 system (Roche Diagnostics, Germany). Triiodothyronine (T3) was measured with by fluorescence polarization immunoassay on an AxSym system (Abbott, US). Growth hormone (GH) was measured by immunofluorometric assay (Wallac, Finland). Serum active ghrelin, leptin and adiponectin were determined by radioimmunoassay (Millipore, USA). Testosterone was determined by a direct RIA of Siemens Healthcare Diagnostics, Sex hormone-binding globulin (SHBG) was measured on an automated Immulite 2500 (Siemens, Breda, The Netherlands). Ketone bodies were measured using test strips on the Precision XtraTM Blood Glucose and Ketone Monitoring System (Abbott, North Chicago, Illinois)

Western Blot

Skeletal muscle biopsies (~30-45 mg) were homogenized by Ultra-Turrax (22 000 rpm; 2x5 sec) in a 6:1 (v/w) ratio of ice-cold buffer containing: 50 mM HEPES (pH 7.6), 50 mM NaF, 50 mM KCl, 5 mM NaPPi, 1 mM EDTA, 1 mM EGTA, 5 mM β-GP, 1 mM Na3VO4, 1 mM DTT, 1% NP40 and protease inhibitors cocktail (Complete, Roche, The Netherlands). Western blots were performed using phospho-specific (Ser473-PKB, phospho-Akt substrate, Ser2448-mTOR, Ser235/236-S6, Thr172-AMPKα, Ser221-ACC, Ser498-HDAC4, Ser47-SIRT1 and Thr24-FoxO1 from Cell Signaling) or total primary antibodies (Tubulin, AMPKα, ACC and FoxO1 from Cell Signaling; HDAC4, SIRT1 and MitoProfile OXPHOS from AbCam; IRβ from Santa Cruz; NAMPT from Bethyl Laboratories), as previously described[23].

AMPK activity

AMPK heterotrimeric complexes were immunoprecipitated from 500 µg of muscle lysate using protein A-agarose beads (GE Healthcare, The Netherlands) and a pan α-specific AMPK antibody (Santa Cruz) incubated together at 4°C overnight on a rotating wheel. The AMPK activity was measured in the immunoprecipitate by radioactive assay using [γ-32P]ATP, as previously described [24].

RNA isolation

Total RNA was isolated from skeletal muscle biopsies (~25-30 mg) using the phenol-chloroform extraction method (Tripure RNA Isolation reagent, Roche, Germany), treated with the TurboDNAse kit according to manufacturer protocol (TurboDNAse, Life Technologies, The Netherlands) and quantified by NanoDrop (ND1000, Thermo Scientific, The Netherlands). The quality and integrity of RNA was tested using 2100 Bioanalyzer (Agilent Technologies, Waldbronn, Germany) and all the samples had a RNA integrity number score >8.

Microarray and real-time RT-PCR

For microarray analysis, Illumina TotalPrep-96 RNA Amplification kit was used to generate biotin labeled, amplified cRNA starting from 200ng total RNA. 750 ng of the obtained biotinylated cRNA samples was hybridized onto the Illumina HumanHT-12 v4 BeadChip array. Primary gene expression analysis of the scanned BeadChip arrays was performed using Illumina's Genomestudio v.2011.1. Analysis was performed with the lumi package version 2.4.0 in R[25]. Data was subjected to a *variance stabilizing transformation (VST function)*, and subjected to quantile normalization. The difference relative to the post-meal (baseline) condition was calculated from the mean normalized intensities for each condition, assuming a log2 scale, and fold-change were calculated after back-transformation to the linear scale. The significance of difference in gene expression relative to the post-meal condition was calculated from a hierarchical linear model, as implemented in the limma package version 3.8.3, with expression as dependent variable and time point and individual as categorical, independent variables. The fold change *versus* post-meal condition was calculated as the absolute ratio of normalized intensities between the mean values of all individual fold changes (post-meal/10h or 24h fasting). Two cutoff values were used to select the regulated genes and minimize the chances of false positives: fold changes >1.25 and p≤0.05 (up-regulated) and fold changes <0.75 and p≤0.05 (down-regulated). The gene lists of interest were next generated and analyzed for enriched gene ontology (GO) terms for biological processes, molecular functions, protein classes and pathways using the Web-based software PANTHER 8.1 [26]. The microarray data have been deposited in the NCBI Gene Expression Omnibus (GEO) repository under no. GSE55924. For real-time RT-PCR, first-strand cDNA was synthesized from 1 µg total RNA using a Superscript first strand synthesis kit (Invitrogen, The Netherlands). Real-time PCR assays were performed using specific primers sets (sequences provided on request)

and SYBR Green on a StepOne Plus Real-time PCR system (Applied Biosystems, US). mRNA expression was normalized to ribosomal protein S18 (*Rps18*) and expressed as mean log2 change *versus* post-meal group.

Statistical analysis

All data are presented as mean ± standard error of the mean (SEM). A mixed model was used to compare all measurements during fasting with the baseline (post-meal) values: time was modeled as fixed effect while random intercepts were used to model the subject-specific deviation from the mean. Within each analysis, a Bonferroni post hoc test was used to adjust for multiple comparisons. All the statistical analysis were performed using SPSS 18.0 for Windows (SPSS Inc., US).

5

Results

Effects of fasting on body weight and metabolic parameters

The anthropometric and metabolic characteristics of the subjects were determined at baseline (post-meal, ~90 min after a standardized breakfast of 300 Kcal), and after 10 and 24 hours of fasting (Table 1). Body weight decreased upon fasting (-1.9%; $p<0.05$). As expected, a significant time-dependent decrease in plasma insulin, leptin

Table 1. Anthropometric and metabolic parameters at baseline and during fasting

	Post-meal	10h fast	24h fast
Age (years)	22 ± 1		
Length (cm)	184 ± 1		
Weight (kg)	72 ± 2	nd	71 ± 2*
Body mass index (kg/m^2)	21.3 ± 0.6	nd	20.9 ± 0.5*
Glucose (mmol/l)	4.0 ± 0.1	4.2 ± 0.1	3.8 ± 0.1
Insulin (mU/l)	3.8 ± 1.0	1.0 ± 0.2*	1.0 ± 0.2*
Growth Hormone (mU/l)	0.3 ± 0.1	2.8 ± 0.9	4.8 ± 2.2*
IGF-1 (nmol/l)	24.9 ± 1.9	25.8 ± 2.3	26.4 ± 2.3
Leptin (µg/l)	1.4 ± 0.4	1.0 ± 0.3	0.5 ± 0.2*
Adiponectin (µg/l)	7.4 ± 0.8	7.3 ± 0.8	7.9 ± 1.1
Ghrelin (pg/ml)	79 ± 4	83 ± 4	69 ± 3
Cholesterol (mmol/l)	3.1 ± 0.2	3.1 ± 0.1	3.2 ± 0.2
Triglycerides (mmol/l)	0.83 ± 0.07	0.61 ± 0.04*	0.71 ± 0.06*
Free fatty acids (mmol/l)	0.19 ± 0.02	0.76 ± 0.06*	0.83 ± 0.11*
Ketone bodies (mmol/l)	0.11 ± 0.01	0.44 ± 0.06*	1.18 ± 0.26*
T3 (nmol/l)	1.45 ± 0.04	1.44 ± 0.06	1.33 ± 0.06*
FT4 (pmol/l)	15.9 ± 0.6	15.9 ± 0.6	16.6 ± 0.7*
TSH (mU/l)	1.8 ± 0.2	1.4 ± 0.2	1.5 ± 0.2
Testosterone (nmol/l)	19.7 ± 1.1	15.1 ± 1.8*	21.2 ± 2.2
SHBG (nmol/l)	27.2 ± 1.7	28.0 ± 1.7	29.6 ± 1.7*
Cortisol (µmol/l)	0.33 ± 0.03	0.20 ± 0.02*	0.51 ± 0.02*
Alkaline Phosphatase (U/l)	59 ± 5	58 ± 5	64 ± 5*
Creatinine (mmol/l)	71 ± 1	66 ± 2*	76 ± 3*

Data are shown as mean ± SEM, n=12. *, $p<0.05$ vs post-meal ; nd, not determined.

5

and T3 levels was observed, whereas circulating growth hormone, free fatty acid, ketone bodies, cortisol, alkaline phosphatase and creatinine increased (Table 1).

Effects of fasting on whole-body glucose and lipid oxidation rates
The substrate oxidation rates were determined by indirect calorimetry at baseline and after 10 and 24 hours of fasting (Table 2). The resting energy expenditure (REE), either expressed as absolute or corrected for lean body mass, remained unaffected throughout the fasting period. As expected, fasting led to significant decrease in respiratory quotient (RQ), indicating a shift in substrate metabolism from glucose toward lipid oxidation (- 48% and +702% after 24h, respectively; $p<0.05$).

Table 2. Substrate oxidation rates at baseline and during fasting

	Post-meal	10h fast	24h fast
Resting energy expenditure (kcal/day)	1627 ± 43	1573 ± 47	1585 ± 70
Resting energy expenditure (kcal/kgFFM/day)	28.8 ± 0.8	27.9 ± 0.8	28.3 ± 1.2
Respiratory quotient	0.99 ± 0.02	0.84 ± 0.02*	0.86 ± 0.03*
Lipid oxidation (µmol/kgFFM/min)	0.49 ± 0.63	4.13 ± 0.50*	3.93 ± 0.70*
Glucose oxidation (µmol/kgFFM/min)	28.2 ± 2.2	13.5 ± 1.9*	14.7 ± 2.0*

Data are shown as mean ± SEM, n=12. *, $p<0.05$ vs post-meal; kgFFM, kilogram fat free mass.

5

Effect of fasting on insulin/mTORC1 signaling pathways in human skeletal muscle
The protein expression and phosphorylation state of key molecules involved in the insulin/mTOR signaling pathway were determined in skeletal muscle biopsies at baseline and after 10 and 24h of fasting (Figure 1). Tubulin expression, used as a housekeeping protein, as well as PKB α/β, Akt substrate of 160 kDa (AS160), mTOR, 4Ebinding protein-1 (4E-BP1), S6, ERK1/2, and cAMP response element-binding protein (CREB) were not affected no matter what the conditions (Fig. 1A and data not shown). Although the insulin receptor β (IRβ) expression remained unaltered (Figure 1B), the phosphorylation of protein kinase B (PKB, also called Akt) and of its downstream target Akt Substrate of 160 kDa (AS160) were significantly reduced in response to fasting (Figure 1C-D), in line with the time-dependent decrease in plasma insulin levels. In addition, the phosphorylation state of mTOR on its Ser2448 residue was lowered by fasting (Figure 1E), together with phosphorylation of mTOR complex1
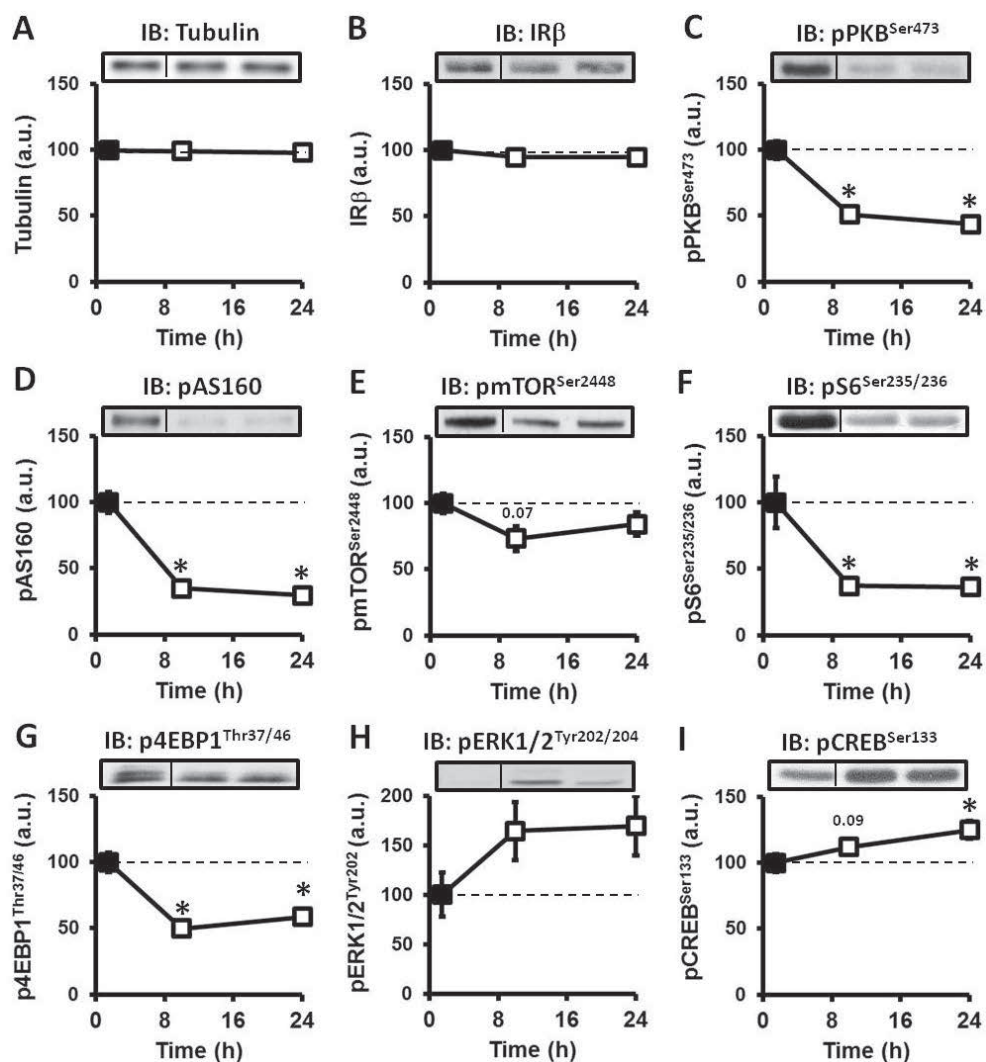
Figure 1. Effect of fasting on skeletal muscle insulin/mTOR signaling pathways.
The expression of tubulin (A), insulin receptor β (B) and the phosphorylation states of Ser473-PKB (C), AS160 (D), Ser2448-mTOR (E), Ser235/235-S6 (F), Thr37/46-4EBP1 (G), Tyr202/204-ERK1/2 (H), and Ser133-CREB (I) were assessed by Western Blot in skeletal muscle from healthy subjects before (black square) and after 10h and 24h of fasting (open squares). Representative blots for one subject are shown. Results are normalized to baseline and expressed as mean ± SEM; n=12; *p<0.05 compared with base-line.IB, immunoblot. a.u., arbitrary units.

(mTORC1) downstream targets ribosomal protein S6 kinase/S6 and eukaryotic initi-ation factor 4E binding protein (4EBP1) (Figure 1F-G). By contrast, fasting induced a time-dependent increase in both extracellular signal-regulated kinase (ERK) and cAMP response element-binding protein (CREB) phosphorylation on their respective

regulatory residues (Figure 1H-I). Of note, protein expression of PKBα/β, AS160, mTOR, 4EBP1, S6, ERK1/2 and CREB were not affected whatever the conditions (*data not shown*).

Effect of fasting on AMPK expression and signaling in human skeletal muscle

We next assessed whether fasting affects the protein expression, phosphorylation state and activity of AMPK. As shown in Figure 2A-B, neither AMPK phosphorylation on its activating Thr^{172} residue nor AMPKα protein expression differed from baseline after 10 and 24h of fasting. The stoichiometry of AMPK-Thr^{172} phosphorylation, assessed by the phosphorylated-to-total protein ratio, was therefore not affected during fasting (Figure 2C). This was confirmed by unchanged AMPK activity measured by kinase assay (0.38±0.02, 0.39±0.02 and 0.43±0.03 mU/mg protein at baseline, 10 and 24h of fasting, respectively). Surprisingly, the phosphorylation state of acetyl-
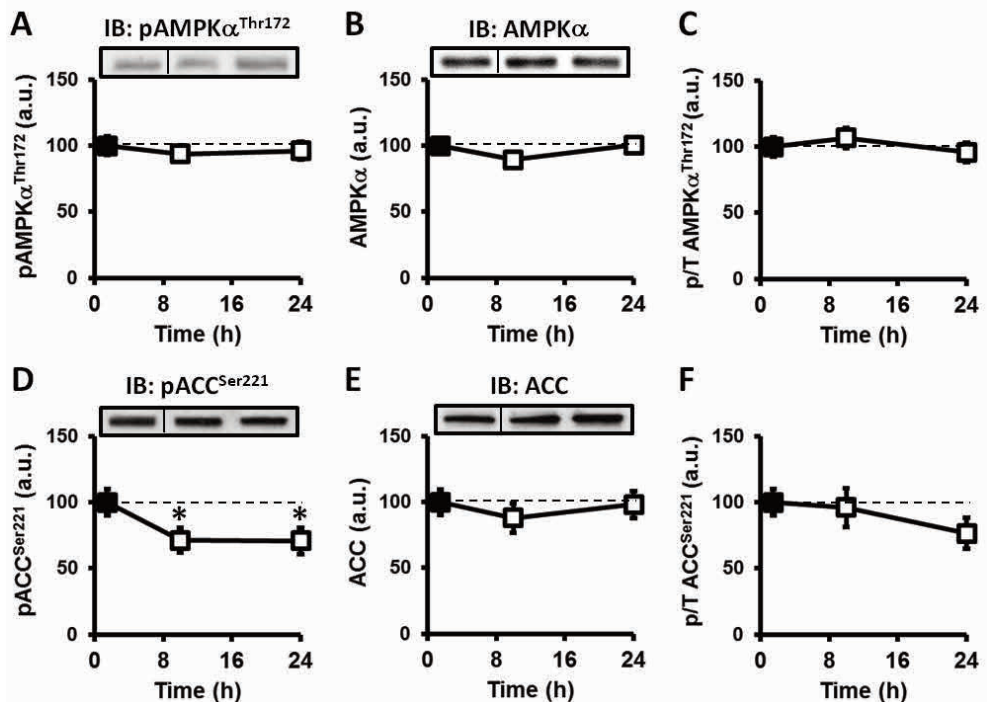
Figure 2. Effect of fasting on skeletal muscle AMPK signaling.
The phosphorylation state of Thr172-AMPKα (A) and Ser221-ACC (D), and the expression of AMPK(pan)α (B) and ACC (E) were assessed by Western Blot in skeletal muscle from healthy subjects before (black square) and after 10h and 24h of fasting (open squares). The phospho-to-total ratio for Thr172-AMPKα (C) and Ser221-ACC (F) were calculated. Representative blots for one subject are shown. Results are normalized to baseline and expressed as mean ± SEM; n=12; *p<0.05 compared with baseline. IB, immunoblot. a.u., arbitrary units.

CoA carboxylase (ACC) on Ser221, one of the main AMPK downstream targets, was found to be significantly decreased during fasting whereas the expression of ACC was not affected (Figure 2C-D). The stoichiometry of ACC-Ser221 phosphorylation, i.e the phospho-to-total ratio, followed the same pattern although not reaching significance (Figure 2E, -23% at 24h; p=0.17). Of note, the mRNA expression of the AMPK upstream kinases liver kinase B (LKB1) and Ca^{2+}/calmodulin-dependent protein kinase kinase (CAMKK) α/β and of the different isoforms of AMPK catalytic α and regulatory β and γ subunits did not change during fasting, except for the AMPKγ3 isoform that was significantly lowered after 24h when compared to baseline (Supplementary Table 1).

Effect of fasting on FoxO1 and SIRT1/HDAC4 histone deacetylases in skeletal muscle

In addition to the insulin/mTOR and AMPK pathways, other energy/nutrient-sensing pathways, such as FoxO1[9], SIRT1[11] and HDAC4[12] were also suggested to be involved in the regulation of skeletal muscle substrate metabolism. The fasting-induced changes in skeletal muscle expression and phosphorylation state of these molecules were therefore determined. The phosphorylation of Thr24-FoxO1 was significantly reduced in response to fasting (Figure 3A). Intriguingly, total FoxO1 protein levels were also decreased, leaving the stoichiometry of phosphorylation unaffected and suggesting fasting-induced change in subcellular localization of the protein (Figure 3B-C). The phosphorylation and content of SIRT 1 followed the same pattern as FoxO1, i.e a decrease in response to fasting, although not reaching significance (Figure 3D-F). Furthermore, the phosphorylation of Ser632-HDAC4, but not the protein content, was found to be transiently reduced in skeletal muscle after 10h of fasting (Figure 3G-I).

Effect of fasting on mitochondrial content in skeletal muscle

Since modulation of nutrient-sensing pathways, including mTOR, AMPK and SIRT1, is linked to regulation of mitochondrial biogenesis, the protein expression of citrate synthase (CS) and of several mitochondrial respiratory-chain complex subunits were determined in skeletal muscle. However, no differences in the expression of these classical markers used for assessing mitochondrial tissue content were observed in response to short-term fasting (Figure 4).
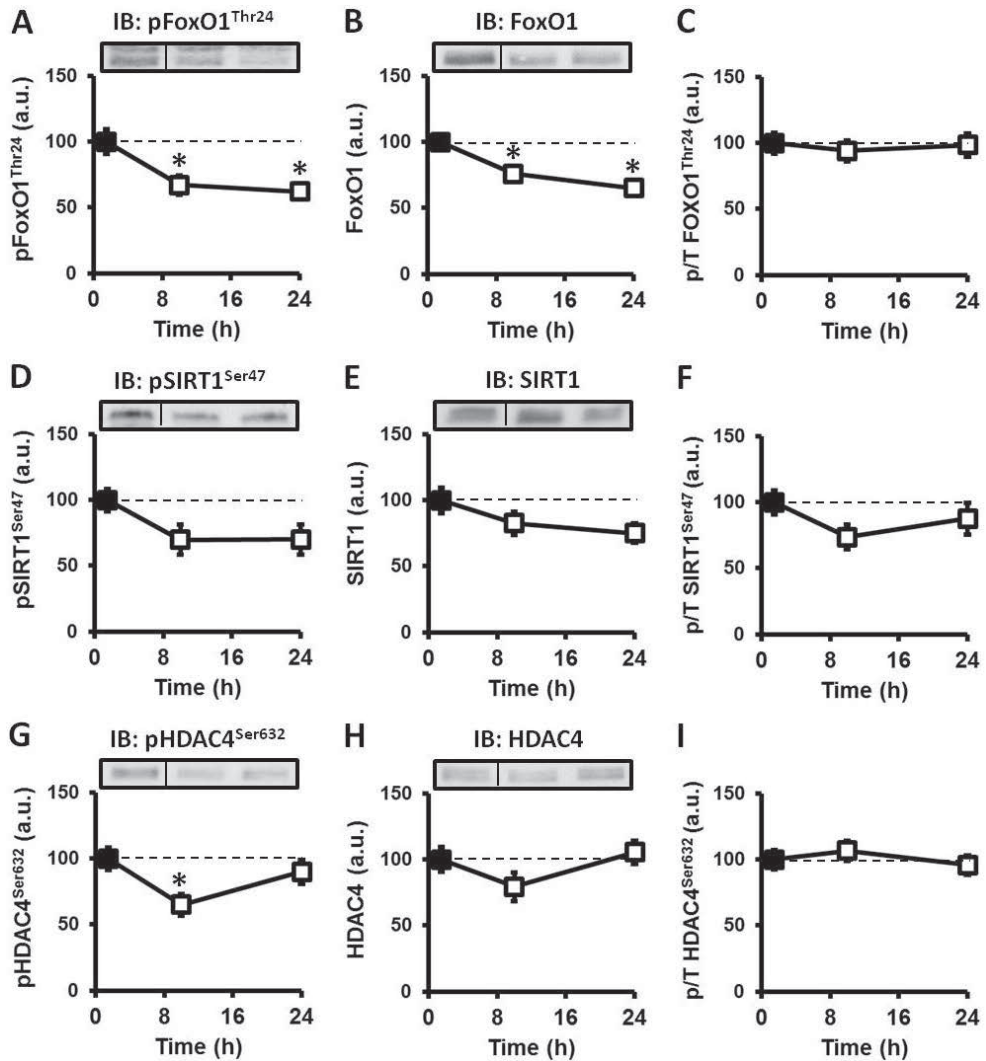
Figure 3: Effect of fasting on skeletal muscle FoxO1 and histone deacetylases.
The phosphorylation state of Thr24-FoxO1 (A), Ser47-SIRT1 (D) and Ser632-HDAC4 (G), and expression of FoxO1 (B), SIRT1 (E) and HDAC4 (H) were assessed by Western Blot in skeletal muscle from healthy subjects before (black square) and after 10h and 24h of fasting (open squares). The phospho-to-total ratio for Thr24-FoxO1 (C), Ser47-SIRT1 (F) and Ser632-HDAC4 (I) were calculated. Representative blots for one subject are shown. Results are normalized to baseline and expressed as mean ± SEM; n=12; *$p<0.05$ compared with baseline. IB, immunoblot. a.u., arbitrary units.

Effect of fasting on skeletal muscle transcriptome

Gene expression profiling was carried out to gain insight into the mechanisms of the adaptive processes that take place in skeletal muscle during fasting (Figure 5). Among the 34696 genes present on the microarray (47323 transcripts), we found

that 12410 (36 %) were expressed in skeletal muscle in at least one of the samples. Using a detection P value threshold of 0.05 and a Log2 mean fold change lower than 0.75 or higher than 1.25, a total of 44 (24 up-regulated and 20 down-regulated) and 901 (432 up-regulated and 469 down-regulated) differentially expressed genes (DEGs) from baseline were identified after 10 and 24h of fasting, respectively. Analysis of the overlapping DEGs revealed that only 23 genes were significantly affected by fasting at both time points. Microarray data validation of genes selected among the top regulated ones (Table 3) was performed using real-time quantitative PCR (RT-qPCR), confirming the significant changes observed for all the genes tested (Table 4). Finally, to gain insight into the biological implication of the observed transcriptional changes after 10 and 24h of fasting, the significant DEGs were analyzed for over-represented GO terms using the PANTHER® software. Interestingly, the GO anno-
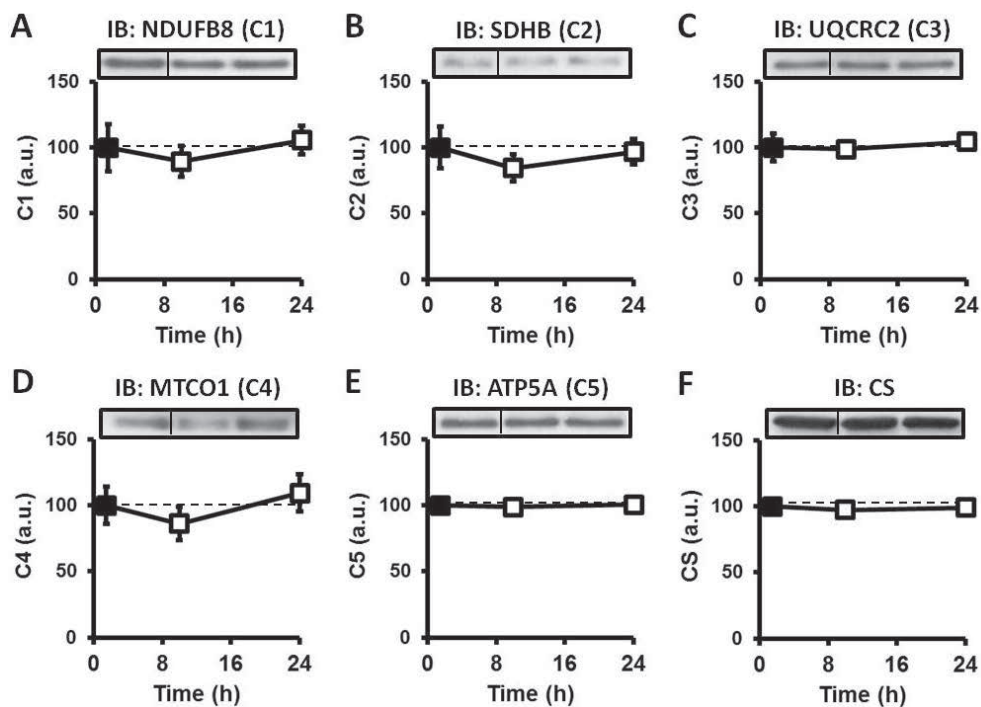
Figure 4: Effect of fasting on skeletal muscle citrate synthase (CS) and mitochondrial respiratory chain subunit expression

The expression of various mitochondrial respiratory-chain subunits (A: NDUFB8; B: SDHB; C: UQCRC2; D: MTCO1; E:ATP5A) and CS (F) were assessed by Western Blot in skeletal muscle from healthy subjects before (black square) and after 10h and 24h of fasting (open squares). Representative blots for one subject are shown. Results are normalized to baseline and expressed as mean ± SEM; n=12; *$p<0.05$ compared with baseline. IB, immunoblot. a.u., arbitrary units.

Table 3. Top 10 up- and down-regulated genes after 10 and 24h of fasting in human skeletal muscle

	10h		24h
Gene symbol	**Gene name**	**Gene symbol**	**Gene name**
Up		**Up**	
PDK4	pyruvate dehydrogenase kinase, isozyme 4	SERPINA3	serpin peptidase inhibitor, clade A, member 3
PFKFB3	6-phosphofructo-2-kinase/fructose-2,6-biphosphatase 3	CEBPD	CCAAT/enhancer binding protein, delta
ANGPTL4	angiopoietin-like 4	HMOX1	heme oxygenase 1
TXNIP	thioredoxin interacting protein	MT2A	metallothionein 2A
NFIL3	nuclear factor, interleukin 3 regulated	GADD45A	growth arrest and DNA-damage-inducible, alpha
CITED2	Cbp/p300-interacting transactivator, with Glu/Asp-rich carboxy-terminal domain, 2	PDK4	pyruvate dehydrogenase kinase, isozyme 4
UCP3	uncoupling protein 3	PFKFB3	6-phosphofructo-2-kinase/fructose-2,6-biphosphatase 3
PDE4D	phosphodiesterase 4D	NNMT	nicotinamide N-methyltransferase
HDAC4	histone deacetylase 4	SERPINB1	serpin peptidase inhibitor, clade B, member 1
TSC22D1	TSC22 domain family, member 1	RRAD	Ras-related associated with diabetes
Down		**Down**	
SLC25A25	solute carrier family 25, member 25	SLC25A25	solute carrier family 25, member 25
PER2	period homolog 2	TFRC	transferrin receptor
DBP	D site of albumin promoter binding protein	ACTA2	actin, alpha 2, smooth muscle, aorta
KLF15	Kruppel-like factor 15	SLC16A3	solute carrier family 16, member 3
PER3	period homolog 3	SBK1	SH3-binding domain kinase 1
BHLHB3	basic helix-loop-helix family, member e41	G0S2	G0/G1switch 2
NR1D2	nuclear receptor subfamily 1, group D, member 2	TAGLN	transgelin
SERTAD3	SERTA domain containing 3	PPARGC1A	peroxisome proliferator-activated receptor gamma, coactivator 1 alpha
TEF	thyrotrophic embryonic factor	FSD2	fibronectin type III and SPRY domain containing 2
PTPN3	protein tyrosine phosphatase, non-receptor type 3	PPP1R3C	protein phosphatase 1, regulatory subunit 3C

Genes are presented by hierarchical order. The whole sets of significantly regulated genes can be found in the Supplementary Table 2.

5

Tabel 4. Validation of microarray data by real-time RT-PCR

Gene symbol	Entrez gene	Gene name	10h		24h	
			qPCR	Microarray	qPCR	Microarray
Up						
ANGPTL4	51129	angiopoietin-like 4	3.0 ± 0.5*	1.38*	2.0 ± 0.4*	0.91*
CITED2	187	Cbp/p300-interacting transactivator, with Glu/Asp-rich carboxy-terminal domain 2	1.7 ± 0.4*	1.08*	1.1 ± 0.3*	0.90*
GADD45A	1647	growth arrest and DNA-damage-inducible, alpha	0.9 ± 0.5	1.37	3.5 ± 0.8*	1.85*
PDK4	10777	pyruvate dehydrogenase kinase, isozyme 4	2.4 ± 0.4*	1.93*	2.5 ± 0.5*	1.83*
PFKFB3	10370	6-phosphofructo-2-kinase/fructose-2,6-biphosphatase 3	1.7 ± 0.3*	1.03	2.5 ± 0.5*	1.75*
TXNIP	285527	thioredoxin interacting protein	1.9 ± 0.2*	1.33*	1.7 ± 0.3*	1.21*
UCP3	4783	uncoupling protein 3 (mitochondrial, proton carrier)	0.7 ± 0.2*	0.79*	0.7 ± 0.3*	0.54*
Down						
ARX	170302	aristaless related homeobox	-1.0 ± 0.3*	-0.30*	-2.0 ± 0.3*	-0.36*
ATP2A1	487	ATPase, Ca++ transporting, cardiac muscle, fast twitch 1	-0.2 ± 0.1	-0.26*	-0.3 ± 0.1*	-0.17*
PPARGC1A	10891	peroxisome proliferator-activated receptor gamma, coactivator 1 alpha	-0.6 ± 0.2*	-0.29	-1.7 ± 0.3*	-1.10*
SLC1A7	6512	solute carrier family 1 (glutamate transporter), member 7	-1.7 ± 0.4*	-0.45*	-2.5 ± 0.7	-0.55*

Data are shown as mean Log2 change vs postmeal condition ± SEM (RT-PCR), n=12. *, $p < 0.05$ vs post-meal.

5
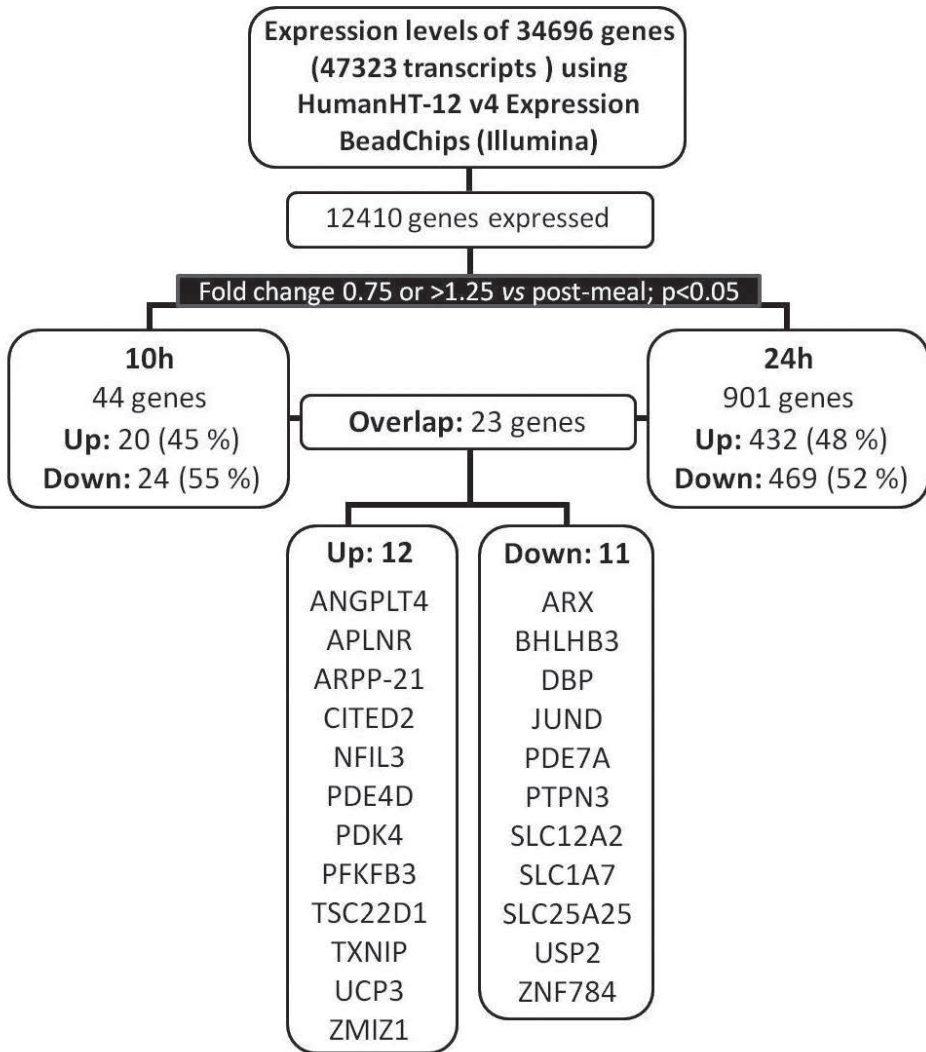
Figure 5: Flow chart of genes changes during fasting in microarray analysis.
The complete set of fasting-responsive mRNAs is shown in Supplementary Table 2.

tations found to be significantly over-represented in both gene sets revealed that most of the biological categories identified belonged to the regulation of metabolic processes, although no specific related pathways were identified (Table 5). To note, the GO term "Primary metabolic process" was found to be the only one significantly over-represented in the gene set constituted by the 23 overlapping DEGs (p=8.5E-03, *data not shown*) when compared to the human skeletal muscle transcriptome.

5

Table 5. PANTHER gene function categories significantly over-represented in human skeletal muscle gene sets during fasting.

GO Biological Process Category

	10h				24h		
	actual	expected	p-value		actual	expected	p-value
acyl-CoA metabolic process	4	0	1.1E-03 (+)	metabolic process	490	411	1.4E-05 (+)
primary metabolic process	42	25	2.3E-03 (+)	primary metabolic process	417	344	7.4E-05 (+)
fatty acid beta-oxidation	4	0	2.4E-03 (+)	generation of precursor metabolites and energy	34	13	2.6E-04 (+)
metabolic process	46	29	5.4E-03 (+)	coenzyme metabolic process	19	5	3.1E-04 (+)
coenzyme metabolic process	5	0	8.0E-03 (+)	respiratory electron transport chain	27	11	6.6E-03 (+)
generation of precursor metabolites and energy	7	1	1.2E-02 (+)				
protein acetylation	3	0	2.2E-02 (+)				
regulation of biological process	19	8	2.7E-02 (+)				

GO Molecular Function Category

	10h				24h		
	actual	expected	p-value		actual	expected	p-value
				catalytic activity	331	262	6.8E-05 (+)
				G-protein coupled receptor activity	1	14	1.4E-03 (-)
				TGF-beta-activated receptor activity	7	1	2.1E-03 (+)
				transmembrane receptor serine/threonine protein kinase activity	8	1	3.5E-03 (+)
				transferase activity	110	77	2.1E-02 (+)
				cytokine receptor activity	12	3	2.6E-02 (+)

GO PANTHER Protein Class

	10h				24h		
	actual	expected	p-value		actual	expected	p-value
				G-protein coupled receptor	1	21	1.7E-06 (-)
				TGF-beta receptor	7	1	2.3E-03 (+)
				serine/threonine protein kinase receptor	8	1	1.3E-02 (+)
				actin family cytoskeletal protein	40	21	1.5E-02 (+)
				dehydrogenase	28	12	1.6E-02 (+)
				KRAB box transcription factor	5	19	2.3E-02 (-)
				ribonucleoprotein	16	6	3.6E-02 (+)

Pathways

	10h				24h		
	actual	expected	p-value		actual	expected	p-value
Circadian clock system	3	0	1.1E-03 (+)				

The PANTHER classification of biological processes, molecular functions, protein classes and pathways significantly over-represented in differentially expressed gene sets after 10 and 24h of fasting compared to the background set of all genes expressed in human skeletal muscle are shown. The statistical analysis includes a stringent Bonferroni correction for multiple testing. The sign next to the p-value indicates whether the category is enriched (+) or depleted (−) compared to the background gene set for each time point.

Supplementary Table 1. Effects of fasting on skeletal muscle mRNA expression of AMPKKs and AMPK subunits

Gene symbol	Entrez gene	Gene name	10h Mean Log2 Change	24h Mean Log2 Change
CAMKK1	10645	Calcium/calmodulin-dependent protein kinase kinase α (CAMKK α)	0.00	0.06
CAMKK2	84254	Calcium/calmodulin-dependent protein kinase kinase β (CAMKK β)	-0.08	0.05
CAB39	51719	Calcium binding protein 39 (MO25a)	-0.05	-0.24
CAB39L	81617	Calcium binding protein 39-like (MO25b)	-0.05	-0.05
STRADA	92335	STE20-related kinase adaptor alpha	0.02	-0.06
STK11	6794	Liver Kinase B1 (LKB1)	0.00	-0.03
PRKAA1	5562	AMP-activated protein kinase α1	0.03	0.10
PRKAA2	5563	AMP-activated protein kinase α2	0.05	0.10
PRKAB1	5564	AMP-activated protein kinase β1	0.08	0.09
PRKAB2	5565	AMP-activated protein kinase β2	0.06	0.09
PRKAG1	5571	AMP-activated protein kinase γ1	-0.07	-0.19
PRKAG2	51422	AMP-activated protein kinase γ2	0.10	-0.11
PRKAG3	53632	AMP-activated protein kinase γ3	-0.12	-0.38*

Data are shown as mean Log2 change vs postmeal condition, n=12. *, $p < 0.05$ vs post-meal.

5

Discussion

In the present study, we investigated the time-dependent effects of fasting on whole-body substrate oxidation rates in relation to changes in energy/nutrient-sensing pathways and gene expression in skeletal muscle from healthy men. To our knowledge, this is the first study providing a comprehensive map of the main signal transduction pathways as well as transcriptomic changes during short-term adaptation to fasting in human skeletal muscle.

In healthy individuals who exhibit a high degree of metabolic flexibility, the adaptation to short-term fasting is characterized by a rapid decrease in glucose oxidation associated with a concomitant increase in lipid oxidation by peripheral tissues, mostly in skeletal muscle[1]. In our cohort of lean young men, we observed this expected fasting-induced shift in whole-body substrate metabolism, together with a time-dependent decrease in plasma levels of insulin and leptin, and simultaneous increase in ketone bodies, free fatty acids and growth hormone levels, as previously reported [27;28]. In line with the decrease in circulating insulin levels, we found that the phosphorylation state of (Akt)/PKB was time-dependently reduced by fasting in skeletal muscle, whereas the protein expression of both IRβ and PKB was not affected. Moreover, the phosphorylation of AS160, one of the main PKB downstream targets, which is involved in the insulin-mediated translocation of the glucose transporter 4 (GLUT4) from intravesicular pool to plasma membrane, was similarly diminished. These findings are in line with our previous report in lean individuals subjected to prolonged (48h) fasting [24] and may suggest that part of the fasting-induced shift from whole-body glucose toward lipid oxidation is secondary to an early reduction of insulin-mediated glucose uptake by skeletal muscle. Of note, Soeters *et al.* did not find significant differences on PKB and AS160 phosphorylation in skeletal muscle from healthy individuals when comparing 14h to 62h of fasting [29], most likely due to the fact that the inhibition of the pathway was already maximal after 14h.

AMPK is a cellular energy sensor, located at the crossroads of several metabolic pathways, which acts as a master regulator of energy balance. Once activated, AMPK increases insulin-independent glucose uptake, promotes lipid oxidation and enhances mitochondrial biogenesis in skeletal muscle through direct phosphorylation of key regulatory enzymes or transcription factors [30;31]. Since previous studies in rodents have shown that skeletal muscle AMPK is activated in response to fasting [6], we investigated whether the AMPK pathway was also affected in humans. In the present

study, we did not find any differences in skeletal muscle AMPK expression, phosphorylation and activity after 10 and 24h of fasting when compared to the baseline (post-meal) condition. In line with this finding, Vendelbo *et al.* have recently reported that long-term fasting (72h) did not affect AMPK activity in healthy individuals [32]. As already discussed elsewhere [24], it is conceivable that fasting-induced AMPK activation constitutes an early regulatory event that transiently occurs in the first hours following food deprivation. Additional experiments including earlier time points are therefore required to clarify this issue.

Another important component in the energy and nutrient-sensing pathways is the mammalian target of rapamycin (mTOR), a kinase that integrates both intracellular and extracellular signals and serves as a central regulator of cell metabolism, growth, proliferation and survival [33]. The mTOR complex 1 (mTORC1), which is one of the two protein complexes containing mTOR, plays an important role in coordinating anabolic and catabolic processes in response to growth factors and nutrients [33]. In response to fasting, we found that phosphorylation of skeletal muscle mTOR and mTORC1 downstream targets S6K/S6 and 4E-BP1 were reduced, an effect which is likely due to reduced PKB signaling. Indeed, active PKB promotes mTORC1 action by phosphorylating and inactivating proline-rich Akt substrate of 40 kDa (PRAS40) and tuberous sclerosis protein 2 (TSC2) [33]. AMPK can also inhibit mTOR signaling by direct phosphorylation of either TSC2 [34] or raptor [35], but the kinase is not likely to be involved in our condition, as its activity was not affected in response to fasting. On top of negatively regulating protein synthesis, one of the most ATP-consuming pathways, mTORC1 controls the transcriptional activity of PPARγ coactivator-1 (PGC1α), a nuclear cofactor that regulates mitochondrial biogenesis and oxidative metabolism [36]. Although PPARGC1A (the gene encoding PGC1α) was among the most extensively down-regulated transcripts after 24h of fasting, we did not find any obvious differences in other key genes involved in mitochondrial biogenesis, nor in the skeletal muscle protein contents of both CS and the main respiratory-chain complexes subunits. Of note, PGC1 α is not only regulated at the mRNA level but also by post-translational modifications, such as phosphorylation and acetylation [13], meaning that a decrease in gene expression does not necessarily implicate that its transcriptional activity is switched off.

FoxO1 belongs to a subfamily of the forkhead transcription factors regulating a variety of biological processes, such as metabolism, cell proliferation and differentiation, and stress response [9;37;38]. FoxO1 is phosphorylated by active PKB, thereby causing its

cytoplasmic sequestration through binding to the protein 14-3-3 [39]. Thus, in the absence of insulin/growth factors, FoxO1 translocates to the nucleus where it can trigger expression of specific genes. In our condition, we found that the total FoxO1 protein content was rapidly decreased in response to fasting whereas the stoichiometry of phosphorylation of FoxO1 at Thr24, one of the residue directly phosphorylate by active PKB, was not affected. The transcription of FoxO1 was not affected in our condition (data not shown) meaning that the time-dependent decrease observed in FoxO1 should either be due to change in protein stability or in its subcellular localization. FoxO transcription factors are relatively stable proteins which are degraded in a proteasome-dependent manner, notably in response to insulin [40]. As plasma insulin levels are low during fasting, an increase in protein turnover is unlikely, rather suggesting a change in FoxO1 subcellular localization in favor of its nuclear retention. Interestingly, PDK4 which is involved in the regulation of lipid metabolism and up-regulated by fasting [41;42;our study], has been identified as a FoxO1 target gene in skeletal muscle [43]. Taken together, our finding suggests that the fasting-induced drop in plasma insulin levels might promote FoxO1 nuclear retention, leading to upregulation of FoxO1 target genes, such as PDK4, and ultimately to enhanced skeletal muscle lipid oxidation. Further studies, including extensive analysis of the subcellular localization of skeletal muscle FoxO isoforms in response to fasting, are however required to strengthen this point.

Finally, the deacetylases SIRT1 and HDAC4 were recently shown to be involved in the metabolic shift towards lipid oxidation during fasting in peripheral tissues [11;12]. For instance, SIRT1 can modulate metabolic processes in response to fasting through deacetylation of key transcription factors, such as PGC1 α and FoxO1 [44]. The nuclear translocation of SIRT1 and HDAC4, like FoxO1, has been shown to alter the expression of metabolic genes [12;45;46]. As mentioned above, the decrease in SIRT-1 and HDAC4 protein content in response to fasting likely results from their nuclear translocation upon dephosphorylation. Further studies are however required to strengthen this finding.

In the present study, we reported that more than 900 genes were altered in human skeletal muscle after 24h of fasting representing ~7% of the genes expressed in this tissue. However, only 23 genes, mostly involved in the regulation of metabolic processes, were found to be significantly affected by fasting at both early (10h) and late (24h) time points. Some of them have previously been reported to be up-regulated (ANGPLT4, CITED2, PDK4, PFKFB3, TXNIP and UCP3) or down-regulated

(SLC25A25) in response to fasting in human skeletal muscle and are likely contributing to the shift from glucose to lipid oxidation at the whole-body level [41;42;47;48]. In addition, we identified new candidate genes that are rapidly and consistently affected by fasting, suggesting that they might also play a role in the initial adaptation of skeletal muscle to energy deprivation. Unfortunately, few data are available on the functions of most of these genes, especially with respect to skeletal muscle. Among them, the APLNR gene encoding the apelin receptor was found to be significantly up-regulated in response to fasting [49]. Interestingly, the expression of APLNR has been shown to be reduced in skeletal muscle from both high-fat fed and db/db mice [50], whereas apelin treatment increases FA oxidation, mitochondrial oxidative capacity, and biogenesis in muscle of insulin-resistant mice [51]. In addition, some genes involved in the cAMP (ARPP-21, PDE4D, PDE7A) or TGFβ (TSC22D1, ZMIZ1) signaling pathways, which play crucial roles in the regulation of multiple cellular functions and physiological processes in skeletal muscle, were also found to be regulated by fasting. Clearly, additional studies are required to investigate whether these proteins are actually involved in the skeletal muscle metabolic adaptation to fasting, and whether specific or common upstream pathways mediated their transcriptional regulation. Among the study limitations, we cannot exclude that some of the effects of fasting on signal transduction and/or protein/gene expression we observed are specific to *musculus vastus lateralis*, which contains a mix of slow and fast fibers, and would have been different in muscles with other fiber type composition. In addition, the only pathway that was found to be significantly over-represented in the two gene sets was the circadian clock after 10h of fasting. Although very little is known in skeletal muscle, the core molecular clock plays an important role in the transcriptional regulation of metabolic processes [52]. It is therefore conceivable that some of the changes observed in gene expression can partly be secondary to circadian rhythms.

Collectively, our study provides a comprehensive map of the main energy/nutrient-sensing pathways and transcriptomic changes during short-term adaptation to fasting in human skeletal muscle. Future studies are necessary to determine whether the observed changes are relevant in disease development as well as (healthy) aging and longevity.

5

References

1. Soeters MR, Soeters PB, Schooneman MG, Houten SM, Romijn JA. Adaptive reciprocity of lipid and glucose metabolism in human short-term starvation. *Am J Physiol Endocrinol Metab* 2012; 303(12): E1397-E1407.

2. de LP, Moreno M, Silvestri E, Lombardi A, Goglia F, Lanni A. Fuel economy in food-deprived skeletal muscle: signaling pathways and regulatory mechanisms. *FASEB J* 2007; 21(13): 3431-3441.

3. Steinberg GR, Kemp BE. AMPK in Health and Disease. *Physiol Rev* 2009; 89(3): 1025-1078.

4. Carling D, Thornton C, Woods A, Sanders MJ. AMP-activated protein kinase: new regulation, new roles? *Biochem J* 2012; 445(1): 11-27.

5. Hardie DG, Ross FA, Hawley SA. AMPK: a nutrient and energy sensor that maintains energy homeostasis. *Nat Rev Mol Cell Biol* 2012; 13(4): 251-262.

6. de LP, Farina P, Moreno M, Ragni M, Lombardi A, Silvestri E, Burrone L, Lanni A, Goglia F. Sequential changes in the signal transduction responses of skeletal muscle following food deprivation. *FASEB J* 2006; 20(14): 2579-2581.

7. Canto C, Jiang LQ, Deshmukh AS, Mataki C, Coste A, Lagouge M, Zierath JR, Auwerx J. Interdependence of AMPK and SIRT1 for metabolic adaptation to fasting and exercise in skeletal muscle. *Cell Metab* 2010; 11(3): 213-219.

8. Um SH, Frigerio F, Watanabe M, Picard F, Joaquin M, Sticker M, Fumagalli S, Allegrini PR, Kozma SC, Auwerx J, Thomas G. Absence of S6K1 protects against age- and diet-induced obesity while enhancing insulin sensitivity. *Nature* 2004; 431(7005): 200-205.

9. Gross DN, van den Heuvel AP, Birnbaum MJ. The role of FoxO in the regulation of metabolism. *Oncogene* 2008; 27(16): 2320-2336.

10. Lovreglio P, Carrieri M, Barbieri A, Sabatini L, Fustinoni S, Andreoli R, D'Errico MN, Basso A, Bartolucci GB, Soleo L. [Monitoring of the occupational and environmental exposure to low doses of benzene]. *G Ital Med Lav Ergon* 2013; 35(4): 251-255.

11. Gerhart-Hines Z, Rodgers JT, Bare O, Lerin C, Kim SH, Mostoslavsky R, Alt FW, Wu Z, Puigserver P. Metabolic control of muscle mitochondrial function and fatty acid oxidation through SIRT1/PGC-1alpha. *EMBO J* 2007; 26(7): 1913-1923.

12. Mihaylova MM, Vasquez DS, Ravnskjaer K, Denechaud PD, Yu RT, Alvarez JG, Downes M, Evans RM, Montminy M, Shaw RJ. Class IIa histone deacetylases

5

are hormone-activated regulators of FOXO and mammalian glucose homeostasis. *Cell* 2011; 145(4): 607-621.

13. Canto C, Auwerx J. PGC-1alpha, SIRT1 and AMPK, an energy sensing network that controls energy expenditure. *Curr Opin Lipidol* 2009; 20(2): 98-105.

14. Mihaylova MM, Shaw RJ. The AMPK signalling pathway coordinates cell growth, autophagy and metabolism. *Nat Cell Biol* 2011; 13(9): 1016-1023.

15. Inoki K, Kim J, Guan KL. AMPK and mTOR in cellular energy homeostasis and drug targets. *Annu Rev Pharmacol Toxicol* 2012; 52: 381-400.

16. Fontana L, Partridge L, Longo VD. Extending healthy life span—from yeast to humans. *Science* 2010; 328(5976): 321-326.

17. Greer EL, Brunet A. Signaling networks in aging. *J Cell Sci* 2008; 121(Pt 4): 407-412.

18. Chalkiadaki A, Guarente L. Sirtuins mediate mammalian metabolic responses to nutrient availability. *Nat Rev Endocrinol* 2012; 8(5): 287-296.

19. Lapierre LR, Hansen M. Lessons from C. elegans: signaling pathways for longevity. *Trends Endocrinol Metab* 2012; 23(12): 637-644.

20. Yuan HX, Xiong Y, Guan KL. Nutrient sensing, metabolism, and cell growth control. *Mol Cell* 2013; 49(3): 379-387.

21. Snel M, Jonker JT, Hammer S, Kerpershoek G, Lamb HJ, Meinders AE, Pijl H, de RA, Romijn JA, Smit JW, Jazet IM. Long-term beneficial effect of a 16-week very low calorie diet on pericardial fat in obese type 2 diabetes mellitus patients. *Obesity (Silver Spring)* 2012; 20(8): 1572-1576.

22. Kok P, Roelfsema F, Frolich M, van PJ, Stokkel MP, Meinders AE, Pijl H. Activation of dopamine D2 receptors simultaneously ameliorates various metabolic features of obese women. *Am J Physiol Endocrinol Metab* 2006; 291(5): E1038-E1043.

23. Stephenne X, Foretz M, Taleux N, van der Zon GC, Sokal E, Hue L, Viollet B, Guigas B. Metformin activates AMP-activated protein kinase in primary human hepatocytes by decreasing cellular energy status. *Diabetologia* 2011; 54(12): 3101-3110.

24. Wijngaarden MA, van der Zon GC, van Dijk KW, Pijl H, Guigas B. Effects of prolonged fasting on AMPK signaling, gene expression, and mitochondrial respiratory chain content in skeletal muscle from lean and obese individuals. *Am J Physiol Endocrinol Metab* 2013; 304(9): E1012-E1021.

25. Du P, Kibbe WA, Lin SM. lumi: a pipeline for processing Illumina microarray. *Bioinformatics* 2008; 24(13): 1547-1548.

5

26. Mi H, Muruganujan A, Casagrande JT, Thomas PD. Large-scale gene function analysis with the PANTHER classification system. *Nat Protoc* 2013; 8(8): 1551-1566.

27. Webber J, Macdonald IA. The cardiovascular, metabolic and hormonal changes accompanying acute starvation in men and women. *Br J Nutr* 1994; 71(3): 437-447.

28. Chan JL, Heist K, DePaoli AM, Veldhuis JD, Mantzoros CS. The role of falling leptin levels in the neuroendocrine and metabolic adaptation to short-term starvation in healthy men. *J Clin Invest* 2003; 111(9): 1409-1421.

29. Soeters MR, Sauerwein HP, Dubbelhuis PF, Groener JE, Ackermans MT, Fliers E, Aerts JM, Serlie MJ. Muscle adaptation to short-term fasting in healthy lean humans. *J Clin Endocrinol Metab* 2008; 93(7): 2900-2903.

30. Viollet B, Athea Y, Mounier R, Guigas B, Zarrinpashneh E, Horman S, Lantier L, Hebrard S, Devin-Leclerc J, Beauloye C, Foretz M, Andreelli F, Ventura-Clapier R, Bertrand L. AMPK: Lessons from transgenic and knockout animals. *Front Biosci (Landmark Ed)* 2009; 14: 19-44.

31. Hardie DG. Energy sensing by the AMP-activated protein kinase and its effects on muscle metabolism. *Proc Nutr Soc* 2011; 70(1): 92-99.

32. Vendelbo MH, Clasen BF, Treebak JT, Moller L, Krusenstjerna-Hafstrom T, Madsen M, Nielsen TS, Stodkilde-Jorgensen H, Pedersen SB, Jorgensen JO, Goodyear LJ, Wojtaszewski JF, Moller N, Jessen N. Insulin Resistance after a 72 hour Fast is Associated with Impaired AS160 Phosphorylation and Accumulation of Lipid and Glycogen in Human Skeletal Muscle. *Am J Physiol Endocrinol Metab* 2011.

33. Laplante M, Sabatini DM. Regulation of mTORC1 and its impact on gene expression at a glance. *J Cell Sci* 2013; 126(Pt 8): 1713-1719.

34. Inoki K, Li Y, Zhu T, Wu J, Guan KL. TSC2 is phosphorylated and inhibited by Akt and suppresses mTOR signalling. *Nat Cell Biol* 2002; 4(9): 648-657.

35. Gwinn DM, Shackelford DB, Egan DF, Mihaylova MM, Mery A, Vasquez DS, Turk BE, Shaw RJ. AMPK phosphorylation of raptor mediates a metabolic checkpoint. *Mol Cell* 2008; 30(2): 214-226.

36. Cunningham JT, Rodgers JT, Arlow DH, Vazquez F, Mootha VK, Puigserver P. mTOR controls mitochondrial oxidative function through a YY1-PGC-1alpha transcriptional complex. *Nature* 2007; 450(7170): 736-740.

37. Greer EL, Brunet A. FOXO transcription factors in ageing and cancer. *Acta Phys-*

5

iol (Oxf) 2008; 192(1): 19-28.

38. Hay N. Interplay between FOXO, TOR, and Akt. *Biochim Biophys Acta* 2011; 1813(11): 1965-1970.

39. Rena G, Guo S, Cichy SC, Unterman TG, Cohen P. Phosphorylation of the transcription factor forkhead family member FKHR by protein kinase B. *J Biol Chem* 1999; 274(24): 17179-17183.

40. Calnan DR, Brunet A. The FoxO code. *Oncogene* 2008; 27(16): 2276-2288.

41. Pilegaard H, Saltin B, Neufer PD. Effect of short-term fasting and refeeding on transcriptional regulation of metabolic genes in human skeletal muscle. *Diabetes* 2003; 52(3): 657-662.

42. Tsintzas K, Jewell K, Kamran M, Laithwaite D, Boonsong T, Littlewood J, Macdonald I, Bennett A. Differential regulation of metabolic genes in skeletal muscle during starvation and refeeding in humans. *J Physiol* 2006; 575(Pt 1): 291-303.

43. Furuyama T, Kitayama K, Yamashita H, Mori N. Forkhead transcription factor FOXO1 (FKHR)-dependent induction of PDK4 gene expression in skeletal muscle during energy deprivation. *Biochem J* 2003; 375(Pt 2): 365-371.

44. Canto C, Auwerx J. Targeting sirtuin 1 to improve metabolism: all you need is NAD(+)? *Pharmacol Rev* 2012; 64(1): 166-187.

45. Finkel T, Deng CX, Mostoslavsky R. Recent progress in the biology and physiology of sirtuins. *Nature* 2009; 460(7255): 587-591.

46. Wang B, Moya N, Niessen S, Hoover H, Mihaylova MM, Shaw RJ, Yates JR, III, Fischer WH, Thomas JB, Montminy M. A hormone-dependent module regulating energy balance. *Cell* 2011; 145(4): 596-606.

47. Tunstall RJ, Mehan KA, Hargreaves M, Spriet LL, Cameron-Smith D. Fasting activates the gene expression of UCP3 independent of genes necessary for lipid transport and oxidation in skeletal muscle. *Biochem Biophys Res Commun* 2002; 294(2): 301-308.

48. Kunkel SD, Suneja M, Ebert SM, Bongers KS, Fox DK, Malmberg SE, Alipour F, Shields RK, Adams CM. mRNA expression signatures of human skeletal muscle atrophy identify a natural compound that increases muscle mass. *Cell Metab* 2011; 13(6): 627-638.

49. Boucher J, Masri B, Daviaud D, Gesta S, Guigne C, Mazzucotelli A, Castan-Laurell I, Tack I, Knibiehler B, Carpene C, Audigier Y, Saulnier-Blache JS, Valet P. Apelin, a newly identified adipokine up-regulated by insulin and obesity. *Endocrinology* 2005; 146(4): 1764-1771.

5

50. Dray C, Debard C, Jager J, Disse E, Daviaud D, Martin P, Attane C, Wanecq E, Guigne C, Bost F, Tanti JF, Laville M, Vidal H, Valet P, Castan-Laurell I. Apelin and APJ regulation in adipose tissue and skeletal muscle of type 2 diabetic mice and humans. *Am J Physiol Endocrinol Metab* 2010; 298(6): E1161-E1169.

51. Attane C, Foussal C, Le GS, Benani A, Daviaud D, Wanecq E, Guzman-Ruiz R, Dray C, Bezaire V, Rancoule C, Kuba K, Ruiz-Gayo M, Levade T, Penninger J, Burcelin R et al. Apelin treatment increases complete Fatty Acid oxidation, mito-chondrial oxidative capacity, and biogenesis in muscle of insulin-resistant mice. *Diabetes* 2012; 61(2): 310-320.

52. Doherty CJ, Kay SA. Circadian control of global gene expression patterns. *Annu Rev Genet* 2010; 44: 419-444.

Acknowledgements

5

Supplementary Table 2
mRNAs regulated by fasting in human skeletal muscle, as assessed by exon expression arrays
The table includes all mRNAs whose levels were increased (gray) or decreased (black) by fasting (P ≤ 0.02 by paired t-test).

10h

EntrezID	Symbol	Gene Name	Mean Log2 Change	AdjPvalue
5166	PDK4	pyruvate dehydrogenase kinase, isozyme 4	1,93	0,00
5209	PFKFB3	6-phosphofructo-2-kinase/fructose-2,6-biphosphatase 3	1,59	0,02
51129	ANGPTL4	angiopoietin-like 4	1,38	0,01
10628	TXNIP	thioredoxin interacting protein	1,33	0,00
4783	NFIL3	nuclear factor, interleukin 3 regulated	1,16	0,05
10370	CITED2	Cbp/p300-interacting transactivator, with Glu/Asp-rich carboxy-terminal domain, 2	1,08	0,01
7352	UCP3	uncoupling protein 3 (mitochondrial, proton carrier)	0,79	0,02
5144	PDE4D	phosphodiesterase 4D, cAMP-specific (phosphodiesterase E3 dunce homolog, Drosophila)	0,55	0,01
9759	HDAC4	histone deacetylase 4	0,52	0,00
8848	TSC22D1	TSC22 domain family, member 1	0,48	0,01
406	ARNTL	aryl hydrocarbon receptor nuclear translocator-like	0,46	0,02
1195	CLK1	CDC-like kinase 1	0,45	0,02
187	APLNR	apelin receptor	0,42	0,00
220963	SLC16A9	solute carrier family 16, member 9 (monocarboxylic acid transporter 9)	0,40	0,00
114818	KLHL29	kelch-like 29 (Drosophila)	0,40	0,01
57178	ZMIZ1	zinc finger, MIZ-type containing 1	0,40	0,00
10777	ARPP-21	cyclic AMP-regulated phosphoprotein, 21 kD	0,32	0,03
79843	FAM124B	family with sequence similarity 124B	0,29	0,00
56243	KIAA1217	KIAA1217	0,29	0,03
4649	MYO9A	myosin IXA	0,26	0,05
5898	**RALA**	v-ral simian leukemia viral oncogene homolog A (ras related)	-0,26	0,00

5

EntrezID	Symbol	Gene Name	Mean Log2 Change	AdjPvalue
487	ATP2A1	ATPase, Ca++ transporting, cardiac muscle, fast twitch 1	-0,26	0,01
170302	ARX	aristaless related homeobox	-0,30	0,01
23462	HEY1	hairy/enhancer-of-split related with YRPW motif 1	-0,34	0,02
89797	NAV2	neuron navigator 2	-0,36	0,00
9099	USP2	ubiquitin specific peptidase 2	-0,37	0,01
79971	GPR177	G protein-coupled receptor 177	-0,37	0,00
23355	VPS8	vacuolar protein sorting 8 homolog (S. cerevisiae)	-0,38	0,01
147808	ZNF784	zinc finger protein 784	-0,39	0,05
5150	PDE7A	phosphodiesterase 7A	-0,41	0,02
7088	TLE1	similar to transducin-like enhancer of split 1 (E(sp1) homolog, Drosophila); transducin-like enhancer of split 1 (E(sp1) homolog, Drosophila)	-0,41	0,05
6558	SLC12A2	solute carrier family 12 (sodium/potassium/chloride transporters), member 2	-0,45	0,01
3727	JUND	jun D proto-oncogene	-0,45	0,03
6512	SLC1A7	solute carrier family 1 (glutamate transporter), member 7	-0,45	0,00
5774	PTPN3	protein tyrosine phosphatase, non-receptor type 3	-0,46	0,04
7008	TEF	thyrotrophic embryonic factor	-0,47	0,03
29946	SERTAD3	SERTA domain containing 3	-0,50	0,00
9975	NR1D2	nuclear receptor subfamily 1, group D, member 2	-0,53	0,00
79365	BHLHB3	basic helix-loop-helix family, member e41	-0,57	0,01
8863	PER3	period homolog 3 (Drosophila)	-0,58	0,00
28999	KLF15	Kruppel-like factor 15	-0,66	0,00
1628	DBP	D site of albumin promoter (albumin D-box) binding protein	-0,77	0,00
8864	PER2	period homolog 2 (Drosophila)	-0,78	0,03
114789	SLC25A25	solute carrier family 25 (mitochondrial carrier; phosphate carrier), member 25	-1,59	0,00

24h

EntrezID	Symbol	Gene Name	Mean Log2 Change	AdjPvalue
12	SERPINA3	serpin peptidase inhibitor, clade A (alpha-1 antiproteinase, antitrypsin), member 3	2,27	0,02

1052	CEBPD	CCAAT/enhancer binding protein (C/EBP), delta	2,15	0,00
3162	HMOX1	heme oxygenase (decycling) 1	2,05	0,00
4502	MT2A	metallothionein 2A	1,93	0,00
1647	GADD45A	growth arrest and DNA-damage-inducible, alpha	1,85	0,01
5166	PDK4	pyruvate dehydrogenase kinase, isozyme 4	1,83	0,00
5209	PFKFB3	6-phosphofructo-2-kinase/fructose-2,6-biphosphatase 3	1,75	0,00
4837	NNMT	nicotinamide N-methyltransferase	1,73	0,01
1992	SERPINB1	serpin peptidase inhibitor, clade B (ovalbumin), member 1	1,71	0,02
6236	RRAD	Ras-related associated with diabetes	1,69	0,04
4609	MYC	v-myc myelocytomatosis viral oncogene homolog (avian)	1,67	0,03
5142	PDE4B	phosphodiesterase 4B, cAMP-specific (phosphodiesterase E4 dunce homolog, Drosophila)	1,55	0,02
70	ACTC1	actin, alpha, cardiac muscle 1	1,44	0,01
23516	SLC39A14	solute carrier family 39 (zinc transporter), member 14	1,28	0,02
5621	PRNP	prion protein	1,23	0,00
10628	TXNIP	thioredoxin interacting protein	1,21	0,00
4489	MT1A	metallothionein 1A	1,20	0,00
23109	DDN	dendrin	1,16	0,00
10135	NAMPT	nicotinamide phosphoribosyltransferase	1,11	0,02
29982	NRBF2	nuclear receptor binding factor 2	1,06	0,01
29970	SCHIP1	schwannomin interacting protein 1	1,03	0,00
8048	CSRP3	cysteine and glycine-rich protein 3 (cardiac LIM protein)	1,02	0,00
4783	NFIL3	nuclear factor, interleukin 3 regulated	0,99	0,02
1545	CYP1B1	cytochrome P450, family 1, subfamily B, polypeptide 1	0,99	0,02
9188	DDX21	DEAD (Asp-Glu-Ala-Asp) box polypeptide 21	0,98	0,01
58480	RHOU	ras homolog gene family, member U	0,98	0,03
123	PLIN2	adipose differentiation-related protein	0,95	0,01
9976	CLEC2B	C-type lectin domain family 2, member B	0,95	0,00
644314	MTE	metallothionein 1I (pseudogene)	0,94	0,00
3929	LBP	lipopolysaccharide binding protein	0,92	0,01
4493	MT1E	metallothionein 1L (gene/pseudogene); metallothionein 1E; metallothionein 1 pseudogene	0,91	0,00

5

5

		3; metallothionein 1J (pseudogene)		
51129	ANGPTL4	angiopoietin-like 4	0,91	0,03
2745	GLRX	glutaredoxin (thioltransferase)	0,91	0,00
10370	CITED2	Cbp/p300-interacting transactivator, with Glu/Asp-rich carboxy-terminal domain, 2	0,90	0,01
84676	TRIM63	tripartite motif-containing 63	0,89	0,04
4618	MYF6	myogenic factor 6 (herculin)	0,87	0,01
4501	MT1X	metallothionein 1X	0,87	0,00
144453	BEST3	bestrophin 3	0,86	0,00
124935	SLC43A2	solute carrier family 43, member 2	0,86	0,00
7132	TNFRSF1A	tumor necrosis factor receptor superfamily, member 1A	0,85	0,02
2634	GBP2	guanylate binding protein 2, interferon-inducible	0,85	0,00
11142	PKIG	protein kinase (cAMP-dependent, catalytic) inhibitor gamma	0,85	0,00
7122	CLDN5	claudin 5	0,85	0,00
10410	IFITM3	interferon induced transmembrane protein 3 (1-8U)	0,83	0,02
58526	MID1IP1	MID1 interacting protein 1 (gastrulation specific G12 homolog (zebrafish))	0,82	0,01
2114	ETS2	v-ets erythroblastosis virus E26 oncogene homolog 2 (avian)	0,82	0,03
56975	FAM20C	family with sequence similarity 20, member C	0,81	0,01
6648	SOD2	superoxide dismutase 2, mitochondrial	0,79	0,03
55281	TMEM140	transmembrane protein 140	0,79	0,00
23082	PPRC1	peroxisome proliferator-activated receptor gamma, coactivator-related 1	0,79	0,04
7371	UCK2	uridine-cytidine kinase 2	0,77	0,01
602	BCL3	B-cell CLL/lymphoma 3	0,77	0,05
9903	KLHL21	kelch-like 21 (Drosophila)	0,77	0,00
23452	ANGPTL2	angiopoietin-like 2	0,77	0,02
6547	SLC8A3	solute carrier family 8 (sodium/calcium exchanger), member 3	0,77	0,00
54438	GFOD1	glucose-fructose oxidoreductase domain containing 1	0,77	0,01
861	RUNX1	runt-related transcription factor 1	0,77	0,03
3987	LIMS1	LIM and senescent cell antigen-like domains 1	0,75	0,00
694	BTG1	B-cell translocation gene 1, anti-proliferative	0,74	0,00
7494	XBP1	X-box binding protein 1	0,71	0,01

83786	FRMD8	FERM domain containing 8	0,71	0,03
10581	IFITM2	interferon induced transmembrane protein 2 (1-8D)	0,71	0,04
5918	RARRES1	retinoic acid receptor responder (tazarotene induced) 1	0,70	0,04
26267	FBXO10	F-box protein 3	0,70	0,00
7045	TGFBI	transforming growth factor, beta-induced, 68kDa	0,70	0,01
57132	CHMP1B	chromatin modifying protein 1B	0,70	0,00
11177	BAZ1A	bromodomain adjacent to zinc finger domain, 1A	0,69	0,00
23710	GABARAPL1	GABA(A) receptors associated protein like 3 (pseudogene); GABA(A) receptor-associated protein like 1	0,69	0,02
64786	TBC1D15	TBC1 domain family, member 15	0,68	0,00
8848	TSC22D1	TSC22 domain family, member 1	0,68	0,00
3487	IGFBP4	insulin-like growth factor binding protein 4	0,67	0,00
26354	GNL3	cyclin M4	0,67	0,01
705	BYSL	bystin-like	0,66	0,00
2512	FTL	similar to ferritin, light polypeptide; ferritin, light polypeptide	0,66	0,01
3656	IRAK2	interleukin-1 receptor-associated kinase 2	0,66	0,00
9334	B4GALT5	UDP-Gal:betaGlcNAc beta 1,4- galactosyltransferase, polypeptide 5	0,65	0,03
4780	NFE2L2	nuclear factor (erythroid-derived 2)-like 2	0,65	0,00
4217	MAP3K5	mitogen-activated protein kinase kinase kinase 5	0,64	0,03
7763	ZFAND5	similar to zinc finger, AN1-type domain 5; zinc finger, AN1-type domain 5	0,64	0,00
377007	KLHL30	kelch-like 30 (Drosophila)	0,64	0,00
303	ANXA2P1	annexin A2 pseudogene 3; annexin A2; annexin A2 pseudogene 1	0,63	0,02
7103	TSPAN8	tetraspanin 8	0,63	0,00
7465	WEE1	WEE1 homolog (S. pombe)	0,63	0,00
51491	NOP16	NOP16 nucleolar protein homolog (yeast)	0,62	0,02
79026	AHNAK	AHNAK nucleoprotein	0,62	0,00
4234	METTL1	methyltransferase like 1	0,61	0,03
64778	FNDC3B	fibronectin type III domain containing 3B	0,61	0,01
476	ATP1A1	ATPase, Na+/K+ transporting, alpha 1 polypeptide	0,61	0,04
2878	GPX3	glutathione peroxidase 3 (plasma)	0,61	0,02

5

5

54880	BCOR	BCL6 co-repressor	0,61	0,00
24145	PANX1	pannexin 1	0,60	0,03
27106	ARRDC2	arrestin domain containing 2	0,60	0,00
84365	MKI67IP	MKI67 (FHA domain) interacting nucleolar phosphoprotein	0,59	0,02
2730	GCLM	glutamate-cysteine ligase, modifier subunit	0,59	0,00
396	ARHGDIA	Rho GDP dissociation inhibitor (GDI) alpha	0,59	0,01
55636	CHD7	chromodomain helicase DNA binding protein 7	0,58	0,02
6890	TAP1	transporter 1, ATP-binding cassette, sub-family B (MDR/TAP)	0,58	0,03
84888	SPPL2A	signal peptide peptidase-like 2A	0,58	0,01
55608	ANKRD10	ankyrin repeat domain 10	0,58	0,01
1497	CTNS	cystinosis, nephropathic	0,58	0,02
10057	ABCC5	ATP-binding cassette, sub-family C (CFTR/MRP), member 5	0,57	0,00
8519	IFITM1	interferon induced transmembrane protein 1 (9-27)	0,57	0,02
55174	INTS10	integrator complex subunit 10	0,57	0,02
1950	EGF	epidermal growth factor (beta-urogastrone)	0,57	0,00
604	BCL6	B-cell CLL/lymphoma 6	0,56	0,01
6776	STAT5A	signal transducer and activator of transcription 5A	0,56	0,01
57563	KLHL8	kelch-like 8 (Drosophila)	0,55	0,00
196527	ANO6	anoctamin 6	0,55	0,00
84448	ABLIM2	actin binding LIM protein family, member 2	0,55	0,02
55240	STEAP3	STEAP family member 3	0,55	0,02
677838	SNORA61	small nucleolar RNA, H/ACA box 61	0,55	0,05
79080	CCDC86	coiled-coil domain containing 86	0,55	0,00
8511	MMP23A	matrix metallopeptidase 23A (pseudogene); matrix metallopeptidase 23B	0,55	0,01
5770	PTPN1	protein tyrosine phosphatase, non-receptor type 1	0,54	0,03
1729	DIAPH1	diaphanous homolog 1 (Drosophila)	0,54	0,00
23612	PHLDA3	pleckstrin homology-like domain, family A, member 3	0,54	0,00
7352	UCP3	uncoupling protein 3 (mitochondrial, proton carrier)	0,54	0,00
7351	UCP2	uncoupling protein 2 (mitochondrial, proton carrier)	0,53	0,00
117177	RAB3IP	RAB3A interacting protein (rabin3)	0,53	0,02

5914	RARA	retinoic acid receptor, alpha	0,52	0,04
81894	SLC25A28	solute carrier family 25, member 28	0,52	0,03
3158	HMGCS2	3-hydroxy-3-methylglutaryl-Coenzyme A synthase 2 (mitochondrial)	0,52	0,05
8406	SRPX	sushi-repeat-containing protein, X-linked	0,52	0,00
54780	NSMCE4A	non-SMC element 4 homolog A (S. cerevisiae)	0,52	0,00
115123	MARCH3	membrane-associated ring finger (C3HC4) 3	0,52	0,03
58489	FAM108C1	family with sequence similarity 108, member C1	0,51	0,02
84916	CIRH1A	cirrhosis, autosomal recessive 1A (cirhin)	0,51	0,01
140809	SRXN1	sulfiredoxin 1 homolog (S. cerevisiae)	0,50	0,03
80306	MED28	mediator complex subunit 28	0,50	0,03
57630	SH3RF1	SH3 domain containing ring finger 1	0,50	0,01
3700	ITIH4	inter-alpha (globulin) inhibitor H4 (plasma Kallikrein-sensitive glycoprotein)	0,50	0,00
85464	SSH2	slingshot homolog 2 (Drosophila)	0,50	0,01
6774	STAT3	signal transducer and activator of transcription 3 (acute-phase response factor)	0,50	0,02
84940	CORO6	coronin 6	0,49	0,00
79188	TMEM43	transmembrane protein 43	0,49	0,04
4953	ODC1	ornithine decarboxylase 1	0,48	0,04
26959	HBP1	poly(A) binding protein, cytoplasmic pseudogene 5; poly(A) binding protein, cytoplasmic 1	0,48	0,00
5144	PDE4D	phosphodiesterase 4D, cAMP-specific (phosphodiesterase E3 dunce homolog, Drosophila)	0,48	0,00
23013	SPEN	spen homolog, transcriptional regulator (Drosophila)	0,48	0,00
5954	RCN1	reticulocalbin 1, EF-hand calcium binding domain	0,48	0,02
865	CBFB	core-binding factor, beta subunit	0,48	0,00
7048	TGFBR2	transforming growth factor, beta receptor II (70/80kDa)	0,47	0,02
6584	SLC22A5	solute carrier family 22 (organic cation/carnitine transporter), member 5	0,47	0,05
51602	NOP58	NOP58 ribonucleoprotein homolog (yeast)	0,47	0,03
55127	HEATR1	HEAT repeat containing 1	0,47	0,01
54517	PUS7	pseudouridylate synthase 7 homolog (S. cerevisiae)	0,47	0,02
3099	HK2	hexokinase 2 pseudogene; hexokinase 2	0,47	0,03
10606	PAICS	phosphoribosylaminoimidazole carboxylase, phosphoribosylaminoimidazole succinocarboxamide synthetase	0,47	0,03

5

5

4302	MLLT6	myeloid/lymphoid or mixed-lineage leukemia (trithorax homolog, Drosophila); translocated to, 6	0,47	0,01
7052	TGM2	transglutaminase 2 (C polypeptide, protein-glutamine-gamma-glutamyltransferase)	0,46	0,01
8291	DYSF	dysferlin, limb girdle muscular dystrophy 2B (autosomal recessive)	0,46	0,03
3182	HNRNPAB	heterogeneous nuclear ribonucleoprotein A/B	0,46	0,03
684959	SNORA25	TATA box binding protein (TBP)-associated factor, RNA polymerase I, D, 41kDa; small nucleolar RNA, H/ACA box 32; small nucleolar RNA, H/ACA box 25	0,46	0,03
4691	NCL	nucleolin	0,46	0,00
26986	PABPC1	poly(A) binding protein, cytoplasmic pseudogene 5; poly(A) binding protein, cytoplasmic 1	0,46	0,04
10528	NOP56	NOP56 ribonucleoprotein homolog (yeast)	0,46	0,01
1912	PHC2	polyhomeotic homolog 2 (Drosophila)	0,46	0,02
50999	TMED5	transmembrane emp24 protein transport domain containing 5	0,45	0,00
1837	DTNA	dystrobrevin, alpha	0,45	0,02
9284	NPIP	nuclear pore complex interacting protein	0,45	0,00
3597	IL13RA1	interleukin 13 receptor, alpha 1	0,45	0,01
9214	FAIM3	Fas apoptotic inhibitory molecule 3	0,45	0,01
10432	RBM14	RNA binding motif protein 14; RNA binding motif protein 4	0,45	0,02
84549	MAK16	MAK16 homolog (S. cerevisiae)	0,45	0,01
10656	KHDRBS3	KH domain containing, RNA binding, signal transduction associated 3	0,45	0,03
7920	BAT5	HLA-B associated transcript 5	0,45	0,00
23558	WBP2	WW domain binding protein 2	0,44	0,00
9933	KIAA0020	KIAA0020	0,44	0,05
9533	POLR1C	polymerase (RNA) I polypeptide C, 30kDa	0,44	0,05
10068	IL18BP	interleukin 18 binding protein	0,44	0,03
26018	LRIG1	acyl-CoA thioesterase 11	0,44	0,02
6780	STAU1	staufen, RNA binding protein, homolog 1 (Drosophila)	0,44	0,01
10079	ATP9A	ATPase, class II, type 9A	0,44	0,02
7050	TGIF1	TGFB-induced factor homeobox 1	0,43	0,03
8204	NRIP1	nuclear receptor interacting protein 1	0,43	0,01
311	ANXA11	annexin A11	0,43	0,02

4790	NFKB1	nuclear factor of kappa light polypeptide gene enhancer in B-cells 1	0,43	0,01
9564	BCAR1	similar to breast cancer anti-estrogen resistance 1; breast cancer anti-estrogen resistance 1	0,43	0,01
54458	PRR13	proline rich 13	0,43	0,01
8408	ULK1	unc-51-like kinase 1 (C. elegans)	0,43	0,00
4864	NPC1	Niemann-Pick disease, type C1	0,43	0,02
337867	UBAC2	UBA domain containing 2	0,43	0,05
7994	MYST3	MYST histone acetyltransferase (monocytic leukemia) 3	0,43	0,01
6583	SLC22A4	solute carrier family 22 (organic cation/ergothioneine transporter), member 4	0,43	0,01
2531	FVT1	3-ketodihydrosphingosine reductase	0,42	0,02
51104	FAM108B1	family with sequence similarity 108, member B1	0,42	0,02
283635	FAM177A1	family with sequence similarity 177, member A1	0,42	0,02
85456	TNKS1BP1	tankyrase 1 binding protein 1, 182kDa	0,42	0,01
4282	MIF	macrophage migration inhibitory factor (glycosylation-inhibiting factor)	0,42	0,00
6059	ABCE1	similar to ATP-binding cassette, sub-family E, member 1; ATP-binding cassette, sub-family E (OABP), member 1	0,42	0,02
55559	UCHL5IP	three prime repair exonuclease 2; HAUS augmin-like complex, subunit 7	0,42	0,02
3588	IL10RB	interleukin 10 receptor, beta	0,42	0,02
8428	STK24	serine/threonine kinase 24 (STE20 homolog, yeast)	0,42	0,02
29889	GNL2	guanine nucleotide binding protein-like 2 (nucleolar)	0,41	0,01
80820	EEPD1	endonuclease/exonuclease/phosphatase family domain containing 1	0,41	0,01
81631	MAP1LC3B	microtubule-associated protein 1 light chain 3 beta	0,40	0,00
206358	SLC36A1	solute carrier family 36 (proton/amino acid symporter), member 1	0,40	0,01
9354	UBE4A	ubiquitination factor E4A (UFD2 homolog, yeast)	0,40	0,00
79042	TSEN34	tRNA splicing endonuclease 34 homolog (S. cerevisiae)	0,40	0,00
3964	LGALS8	lectin, galactoside-binding, soluble, 8	0,40	0,01
6780	STAU1	serine/threonine kinase 3 (STE20 homolog, yeast)	0,40	0,01
56940	DUSP22	similar to mitogen-activated protein kinase phosphatase x; dual specificity phosphatase 22	0,40	0,02
3665	IRF7	interferon regulatory factor 7	0,40	0,01
9416	DDX23	DEAD (Asp-Glu-Ala-Asp) box polypeptide 23	0,40	0,00
22863	KIAA0831	KIAA0831	0,39	0,00

5

4170	MCL1	myeloid cell leukemia sequence 1 (BCL2-related)	0,39	0,01
8819	SAP30	Sin3A-associated protein, 30kDa	0,39	0,00
6507	SLC1A3	solute carrier family 1 (glial high affinity glutamate transporter), member 3	0,39	0,03
3251	HPRT1	hypoxanthine phosphoribosyltransferase 1	0,39	0,00
768211	RELL1	RELT-like 1	0,39	0,03
9589	WTAP	Wilms tumor 1 associated protein	0,39	0,01
4839	NOP2	NOP2 nucleolar protein homolog (yeast)	0,39	0,02
124402	FAM100A	family with sequence similarity 100, member A	0,38	0,01
4673	NAP1L1	nucleosome assembly protein 1-like 1	0,38	0,01
83719	YPEL3	yippee-like 3 (Drosophila)	0,38	0,00
26094	WDR21A	ribosomal L1 domain containing 1	0,38	0,00
9991	ROD1	ROD1 regulator of differentiation 1 (S. pombe)	0,38	0,03
64718	UNKL	unkempt homolog (Drosophila)-like	0,38	0,00
57700	FAM160B1	family with sequence similarity 160, member B1	0,38	0,00
1736	DKC1	dyskeratosis congenita 1, dyskerin	0,38	0,05
54915	YTHDF1	YTH domain family, member 1	0,38	0,04
1454	CSNK1E	casein kinase 1, epsilon	0,38	0,00
3148	HMGB2	high-mobility group box 2	0,38	0,00
6675	UAP1	UDP-N-acteylglucosamine pyrophosphorylase 1	0,37	0,04
56902	PNO1	partner of NOB1 homolog (S. cerevisiae)	0,37	0,02
780	DDR1	discoidin domain receptor tyrosine kinase 1	0,37	0,00
5718	PSMD12	proteasome (prosome, macropain) 26S subunit, non-ATPase, 12	0,37	0,01
23531	MMD	monocyte to macrophage differentiation-associated	0,37	0,00
29121	CLEC2D	C-type lectin domain family 2, member D	0,37	0,00
79693	YRDC	yrdC domain containing (E. coli)	0,37	0,02
81929	SEH1L	SEH1-like (S. cerevisiae)	0,37	0,04
5036	PA2G4	proliferation-associated 2G4, 38kDa; proliferation-associated 2G4 pseudogene 4	0,37	0,01
5905	RANGAP1	Ran GTPase activating protein 1	0,37	0,04
9961	MVP	major vault protein	0,37	0,03
9332	CD163	CD163 molecule	0,37	0,02

ID	Symbol	Description		
135293	PM20D2	peptidase M20 domain containing 2	0,37	0,00
114907	FBXO32	F-box protein 32	0,37	0,01
25829	TMEM184B	ASF1 anti-silencing function 1 homolog A (S. cerevisiae)	0,37	0,02
2274	FHL2	four and a half LIM domains 2	0,37	0,02
5175	PECAM1	platelet/endothelial cell adhesion molecule	0,36	0,04
26258	PLDN	F-box protein 10	0,36	0,04
113791	PIK3IP1	major facilitator superfamily domain containing 3	0,36	0,04
65979	PHACTR4	phosphatase and actin regulator 4	0,36	0,04
121260	SLC15A4	solute carrier family 15, member 4	0,36	0,01
378805	FLJ43663	hypothetical LOC378805	0,36	0,01
84248	FYTTD1	forty-two-three domain containing 1	0,36	0,02
54663	WDR74	WD repeat domain 74	0,36	0,01
83743	GRWD1	glutamate-rich WD repeat containing 1	0,36	0,02
9057	SLC7A6	solute carrier family 7 (cationic amino acid transporter, y+ system), member 6	0,36	0,00
10768	AHCYL1	adenosylhomocysteinase-like 1	0,36	0,01
29799	YPEL1	yippee-like 1 (Drosophila)	0,36	0,01
129303	TMEM150A	transmembrane protein 150A	0,36	0,00
3570	IL6R	interleukin 6 receptor	0,36	0,01
10758	TRAF3IP2	TRAF3 interacting protein 2	0,36	0,01
7705	ZNF146	zinc finger protein 146	0,35	0,04
57178	ZMIZ1	zinc finger, MIZ-type containing 1	0,35	0,00
715	C1R	complement component 1, r subcomponent	0,35	0,05
54432	YIPF1	Yip1 domain family, member 1	0,35	0,00
10777	ARPP-21	cyclic AMP-regulated phosphoprotein, 21 kD	0,35	0,02
3615	IMPDH2	IMP (inosine monophosphate) dehydrogenase 2	0,35	0,02
10144	FAM13A	family with sequence similarity 13, member A	0,35	0,02
6950	TCP1	hypothetical gene supported by BC000665; t-complex 1	0,35	0,01
59338	PLEKHA1	pleckstrin homology domain containing, family A (phosphoinositide binding specific) member 1	0,35	0,05
83666	PARP9	poly (ADP-ribose) polymerase family, member 9	0,35	0,00

5

5

1017	CDK2	cyclin-dependent kinase 2	0,35	0,03
8882	ZNF259	zinc finger protein 259	0,35	0,01
79791	FBXO31	F-box protein 31	0,35	0,00
55646	LYAR	Ly1 antibody reactive homolog (mouse)	0,34	0,05
81603	TRIM8	tripartite motif-containing 8	0,34	0,00
10196	PRMT3	protein arginine methyltransferase 3	0,34	0,01
6009	RHEB	Ras homolog enriched in brain	0,34	0,03
57169	ZNFX1	zinc finger, NFX1-type containing 1	0,34	0,00
4927	NUP88	nucleoporin 88kDa	0,34	0,00
137492	VPS37A	vacuolar protein sorting 37 homolog A (S. cerevisiae)	0,34	0,03
8312	AXIN1	axin 1	0,34	0,00
8613	PPAP2B	phosphatidic acid phosphatase type 2B	0,34	0,01
8890	EIF2B4	eukaryotic translation initiation factor 2B, subunit 4 delta, 67kDa	0,34	0,02
8624	PSMG1	proteasome (prosome, macropain) assembly chaperone 1	0,34	0,02
23560	GTPBP4	GTP binding protein 4	0,34	0,05
57658	CALCOCO1	calcium binding and coiled-coil domain 1	0,34	0,00
187	APLNR	apelin receptor	0,34	0,00
84640	USP38	ubiquitin specific peptidase 38	0,34	0,01
2618	GART	phosphoribosylglycinamide formyltransferase, phosphoribosylglycinamide synthetase, phosphoribosylaminoimidazole synthetase	0,33	0,01
6229	RPS24	ribosomal protein S24	0,33	0,04
7844	RNF103	vacuolar protein sorting 24 homolog (S. cerevisiae); ring finger protein 103	0,33	0,01
10509	SEMA4B	sema domain, immunoglobulin domain (Ig), transmembrane domain (TM) and short cytoplasmic domain, (semaphorin) 4B	0,33	0,04
140885	SIRPA	signal-regulatory protein alpha	0,33	0,02
22926	ATF6	activating transcription factor 6	0,33	0,03
4008	LMO7	LIM domain 7	0,33	0,00
8824	CES2	carboxylesterase 2 (intestine, liver)	0,33	0,01
140890	SFRS12	splicing factor, arginine/serine-rich 12	0,33	0,00
23253	ANKRD12	ankyrin repeat domain 12	0,33	0,01

55810	FOXJ2	forkhead box J2	0,33	0,04
84085	FBXO30	F-box protein 30	0,33	0,00
54935	DUSP23	dual specificity phosphatase 23	0,33	0,05
3675	ITGA3	integrin, alpha 3 (antigen CD49C, alpha 3 subunit of VLA-3 receptor)	0,32	0,01
138428	PTRH1	peptidyl-tRNA hydrolase 1 homolog (S. cerevisiae)	0,32	0,04
27075	TSPAN13	tetraspanin 13	0,32	0,02
7528	YY1	YY1 transcription factor	0,32	0,00
80135	RPF1	brix domain containing 5	0,32	0,00
51678	MPP6	membrane protein, palmitoylated 6 (MAGUK p55 subfamily member 6)	0,32	0,00
114882	OSBPL8	oxysterol binding protein-like 8	0,32	0,00
80216	ALPK1	alpha-kinase 1	0,32	0,00
29110	TBK1	TANK-binding kinase 1	0,32	0,00
25996	REXO2	leucine-rich repeats and immunoglobulin-like domains 1	0,32	0,01
1116	CHI3L1	chitinase 3-like 1 (cartilage glycoprotein-39)	0,31	0,04
91	ACVR1B	activin A receptor, type IB	0,31	0,02
4097	MAFG	v-maf musculoaponeurotic fibrosarcoma oncogene homolog G (avian)	0,31	0,00
1942	EFNA1	ephrin-A1	0,31	0,01
54675	CRLS1	cardiolipin synthase 1	0,31	0,01
157697	ERICH1	glutamate-rich 1	0,31	0,01
343990	MGC42367	chromosome 2 open reading frame 55	0,31	0,03
4666	NACA	nascent polypeptide-associated complex alpha subunit	0,31	0,01
3790	KCNS3	potassium voltage-gated channel, delayed-rectifier, subfamily S, member 3	0,31	0,02
26156	RSL1D1	pallidin homolog (mouse)	0,31	0,00
1665	DHX15	DEAH (Asp-Glu-Ala-His) box polypeptide 15	0,31	0,02
6520	SLC3A2	solute carrier family 3 (activators of dibasic and neutral amino acid transport), member 2	0,31	0,02
64393	ZMAT3	zinc finger, matrin type 3	0,31	0,01
9727	RAB11FIP3	RAB11 family interacting protein 3 (class II)	0,31	0,04
22880	MORC2	MORC family CW-type zinc finger 2	0,30	0,01
54707	GPN2	GPN-loop GTPase 2	0,30	0,04
6710	SPTB	spectrin, beta, erythrocytic	0,30	0,01

5

5

ID	Symbol	Description		
9972	NUP153	nucleoporin 153kDa	0,30	0,01
259217	HSPA12A	heat shock 70kDa protein 12A	0,30	0,02
63876	PKNOX2	PBX/knotted 1 homeobox 2	0,30	0,02
83593	RASSF5	Ras association (RalGDS/AF-6) domain family member 5	0,30	0,03
4779	NFE2L1	nuclear factor (erythroid-derived 2)-like 1	0,30	0,02
23411	SIRT1	sirtuin (silent mating type information regulation 2 homolog) 1 (S. cerevisiae)	0,30	0,01
84128	WDR75	WD repeat domain 75	0,30	0,01
135112	NCOA7	nuclear receptor coactivator 7	0,30	0,02
29097	CNIH4	cornichon homolog 4 (Drosophila)	0,30	0,02
85358	SHANK3	SH3 and multiple ankyrin repeat domains 3	0,30	0,01
9988	DMTF1	cyclin D binding myb-like transcription factor 1	0,30	0,02
90850	ZNF598	zinc finger protein 598	0,30	0,02
55205	ZNF532	similar to zinc finger protein 347; zinc finger protein 532	0,29	0,02
88455	ANKRD13A	ankyrin repeat domain 13A	0,29	0,02
56919	DHX33	DEAH (Asp-Glu-Ala-His) box polypeptide 33	0,29	0,05
51010	EXOSC3	exosome component 3	0,29	0,03
4286	MITF	microphthalmia-associated transcription factor	0,29	0,02
51283	BFAR	bifunctional apoptosis regulator	0,29	0,02
5757	PTMA	hypothetical LOC728026; prothymosin, alpha; hypothetical gene supported by BC013859; prothymosin, alpha pseudogene 4 (gene sequence 112)	0,29	0,01
50640	PNPLA8	patatin-like phospholipase domain containing 8	0,29	0,03
5936	RBM4	RNA binding motif protein 14; RNA binding motif protein 4	0,29	0,02
285704	RGMB	RGM domain family, member B	0,29	0,01
3431	SP110	SP110 nuclear body protein	0,29	0,01
10964	IFI44L	interferon-induced protein 44-like	0,29	0,01
55718	POLR3E	polymerase (RNA) III (DNA directed) polypeptide E (80kD)	0,29	0,01
9766	KIAA0247	KIAA0247	0,29	0,03
79733	E2F8	E2F transcription factor 8	0,29	0,03
1464	CSPG4	chondroitin sulfate proteoglycan 4	0,29	0,02
2028	ENPEP	glutamyl aminopeptidase (aminopeptidase A)	0,28	0,05

23177	CEP68	centrosomal protein 68kDa	0,28	0,01
26511	CHIC2	olfactory receptor, family 7, subfamily E, member 37 pseudogene	0,28	0,02
57510	XPO5	exportin 5	0,28	0,01
5478	PPIA	similar to TRIMCyp; peptidylprolyl isomerase A (cyclophilin A); peptidylprolyl isomerase A (cyclophilin A)-like 3	0,28	0,01
84171	LOXL4	lysyl oxidase-like 4	0,28	0,02
84312	BRMS1L	breast cancer metastasis-suppressor 1-like	0,28	0,00
6310	ATXN1	ataxin 1	0,28	0,01
56984	PSMG2	proteasome (prosome, macropain) assembly chaperone 2	0,28	0,00
25942	SIN3A	dehydrogenase/reductase (SDR family) member 7B	0,28	0,01
6777	STAT5B	signal transducer and activator of transcription 5B	0,28	0,05
9718	ECE2	endothelin converting enzyme 2	0,28	0,02
23011	RAB21	RAB21, member RAS oncogene family	0,28	0,01
81567	TXNDC5	thioredoxin domain containing 5 (endoplasmic reticulum); muted homolog (mouse)	0,28	0,01
29954	POMT2	protein-O-mannosyltransferase 2	0,28	0,01
25778	DSTYK	dual serine/threonine and tyrosine protein kinase	0,28	0,01
51082	POLR1D	polymerase (RNA) I polypeptide D, 16kDa	0,28	0,00
8662	EIF3B	eukaryotic translation initiation factor 3, subunit B	0,27	0,04
677	ZFP36L1	zinc finger protein 36, C3H type-like 1	0,27	0,01
8473	OGT	O-linked N-acetylglucosamine (GlcNAc) transferase (UDP-N-acetylglucosamine:polypeptide-N-acetylglucosaminyl transferase)	0,27	0,00
9180	OSMR	oncostatin M receptor	0,27	0,05
84665	MYPN	myopalladin	0,27	0,05
191	AHCY	adenosylhomocysteinase	0,27	0,01
84864	MINA	MYC induced nuclear antigen	0,27	0,03
6788	STK3	aurora kinase A; aurora kinase A pseudogene 1	0,27	0,02
3620	INDO	indoleamine 2,3-dioxygenase 1	0,27	0,03
9043	SPAG9	sperm associated antigen 9	0,27	0,02
54881	TEX10	testis expressed 10	0,27	0,01
6772	STAT1	signal transducer and activator of transcription 1, 91kDa	0,27	0,01

5

5

ID	Symbol	Description		
27309	ZNF330	zinc finger protein 330	0,27	0,00
57685	CACHD1	cache domain containing 1	0,27	0,03
1362	CPD	carboxypeptidase D	0,27	0,00
9911	TMCC2	transmembrane and coiled-coil domain family 2	0,27	0,01
51315	KRCC1	lysine-rich coiled-coil 1	0,27	0,01
79139	DERL1	Der1-like domain family, member 1	0,26	0,01
7005	TEAD3	TEA domain family member 3	0,26	0,03
84918	LRP11	low density lipoprotein receptor-related protein 11	0,26	0,00
272	AMPD3	adenosine monophosphate deaminase (isoform E)	0,26	0,00
10597	TRAPPC2P1	trafficking protein particle complex 2; trafficking protein particle complex 2 pseudogene 1	0,26	0,04
5937	RBMS1	RNA binding motif, single stranded interacting protein 1	0,26	0,03
5516	PPP2CB	protein phosphatase 2 (formerly 2A), catalytic subunit, beta isoform	0,26	0,03
2104	ESRRG	estrogen-related receptor gamma	0,26	0,00
92912	UBE2Q2	ubiquitin-conjugating enzyme E2Q family member 2	0,26	0,03
55800	SCN3B	sodium channel, voltage-gated, type III, beta	0,26	0,01
63893	UBE2O	ubiquitin-conjugating enzyme E2O	0,26	0,01
80325	ABTB1	ankyrin repeat and BTB (POZ) domain containing 1	0,26	0,02
55813	UTP6	UTP6, small subunit (SSU) processome component, homolog (yeast)	0,26	0,01
10952	SEC61B	Sec61 beta subunit	0,26	0,04
114793	FMNL2	formin-like 2	0,26	0,05
57664	PLEKHA4	pleckstrin homology domain containing, family A (phosphoinositide binding specific) member 4	0,26	0,04
83787	ARMC10	armadillo repeat containing 10	0,26	0,04
23214	XPO6	exportin 6	0,26	0,03
3066	HDAC2	histone deacetylase 2	0,26	0,01
51065	RPS27L	ribosomal protein S27-like	0,26	0,04
64782	AEN	apoptosis enhancing nuclease	0,26	0,03
55207	ARL8B	ADP-ribosylation factor-like 8B	0,26	0,03
535	ATP6V0A1	ATPase, H+ transporting, lysosomal V0 subunit a1	0,25	0,03
11091	WDR5	WD repeat domain 5	0,25	0,01

58490	RPRD1B	regulation of nuclear pre-mRNA domain containing 1B	0,25	0,01
114908	TMEM123	transmembrane protein 123	0,25	0,00
51056	LAP3	leucine aminopeptidase 3	0,25	0,04
55349	CHDH	choline dehydrogenase	0,25	0,00
831	CAST	calpastatin	0,25	0,03
10865	ARID5A	AT rich interactive domain 5A (MRF1-like)	0,25	0,00
6840	SVIL	supervillin	0,25	0,02
817	CAMK2D	calcium/calmodulin-dependent protein kinase II delta	0,25	0,01
2752	GLUL	glutamate-ammonia ligase (glutamine synthetase)	0,25	0,04
3189	HNRPH3	heterogeneous nuclear ribonucleoprotein H3 (2H9)	0,25	0,03
10436	EMG1	EMG1 nucleolar protein homolog (S. cerevisiae)	0,25	0,04
6103	RPGR	retinitis pigmentosa GTPase regulator	0,25	0,01
23162	MAPK8IP3	mitogen-activated protein kinase 8 interacting protein 3	0,25	0,00
10413	YAP1	Yes-associated protein 1, 65kDa	0,25	0,05
31	ACACA	acetyl-Coenzyme A carboxylase alpha	0,25	0,00
2665	GDI2	GDP dissociation inhibitor 2	0,25	0,03
4430	MYO1B	myosin IB	0,25	0,05
5887	RAD23B	RAD23 homolog B (S. cerevisiae)	0,25	0,05
25825	BACE2	transmembrane protein 184B	0,25	0,02
10199	MPHOSPH10	M-phase phosphoprotein 10 (U3 small nucleolar ribonucleoprotein)	0,25	0,03
23392	KIAA0368	KIAA0368	0,25	0,04
54464	XRN1	5'-3' exoribonuclease 1	0,25	0,01
10782	ZNF274	zinc finger protein 274	0,25	0,02
54865	GPATCH4	G patch domain containing 4	0,25	0,03
25778	RIPK5	RAS guanyl releasing protein 3 (calcium and DAG-regulated)	0,25	0,03
64951	**MRPS24**	**mitochondrial ribosomal protein S24**	**-0,25**	**0,04**
9491	**PSMF1**	**proteasome (prosome, macropain) inhibitor subunit 1 (PI31)**	**-0,25**	**0,00**
5787	**PTPRB**	**protein tyrosine phosphatase, receptor type, B**	**-0,25**	**0,02**
8087	**FXR1**	**fragile X mental retardation, autosomal homolog 1**	**-0,25**	**0,03**
22913	**RALY**	**RNA binding protein, autoantigenic (hnRNP-associated with lethal yellow homolog**	**-0,25**	**0,02**

5

		(mouse))		
122622	ADSSL1	adenylosuccinate synthase like 1	-0,25	0,00
6687	SPG7	spastic paraplegia 7 (pure and complicated autosomal recessive)	-0,25	0,02
1512	CTSH	cathepsin H	-0,25	0,00
114876	OSBPL1A	oxysterol binding protein-like 1A	-0,25	0,03
92106	MGC15763	oxidoreductase NAD-binding domain containing 1	-0,25	0,01
6549	SLC9A2	solute carrier family 9 (sodium/hydrogen exchanger), member 2	-0,25	0,01
6563	SLC14A1	solute carrier family 14 (urea transporter), member 1 (Kidd blood group)	-0,25	0,01
339123	JMJD8	jumonji domain containing 8	-0,25	0,03
29911	HOOK2	hook homolog 2 (Drosophila)	-0,25	0,01
10138	YAF2	YY1 associated factor 2	-0,25	0,02
55788	LMBRD1	LMBR1 domain containing 1	-0,25	0,03
79077	DCTPP1	dCTP pyrophosphatase 1	-0,25	0,04
92259	MRPS36	mitochondrial ribosomal protein S36	-0,25	0,02
79894	ZNF672	zinc finger protein 672; hypothetical LOC100130262	-0,25	0,03
55755	CDK5RAP2	CDK5 regulatory subunit associated protein 2	-0,25	0,03
389257	LRRC14B	leucine-rich repeat-containing protein 14-like	-0,25	0,03
498	ATP5A1	ATP synthase, H+ transporting, mitochondrial F1 complex, alpha subunit 1, cardiac muscle	-0,25	0,01
5250	SLC25A3	solute carrier family 25 (mitochondrial carrier; phosphate carrier), member 3	-0,25	0,01
126306	JSRP1	junctional sarcoplasmic reticulum protein 1	-0,25	0,00
374291	NDUFS7	NADH dehydrogenase (ubiquinone) Fe-S protein 7, 20kDa (NADH-coenzyme Q reductase)	-0,25	0,01
9604	RNF14	ring finger protein 14	-0,25	0,02
253738	EBF3	early B-cell factor 3	-0,25	0,03
64285	RHBDF1	rhomboid 5 homolog 1 (Drosophila)	-0,25	0,01
54205	CYCS	cytochrome c, somatic	-0,25	0,01
139285	FLJ39827	family with sequence similarity 123B	-0,25	0,03
118472	ZNF511	zinc finger protein 511	-0,25	0,02
6237	RRAS	related RAS viral (r-ras) oncogene homolog	-0,25	0,01
51530	ZC3HC1	zinc finger, C3HC-type containing 1	-0,26	0,01

5

4802	NFYC	nuclear transcription factor Y, gamma	-0,26	0,01
55486	PARL	presenilin associated, rhomboid-like	-0,26	0,00
5583	PRKCH	protein kinase C, eta	-0,26	0,02
9552	SPAG7	sperm associated antigen 7	-0,26	0,00
219749	ZNF25	zinc finger protein 25	-0,26	0,00
53826	FXYD6	FXYD domain containing ion transport regulator 6	-0,26	0,01
7867	MAPKAPK3	mitogen-activated protein kinase-activated protein kinase 3	-0,26	0,01
6596	HLTF	helicase-like transcription factor	-0,26	0,03
90624	LYRM7	Lyrm7 homolog (mouse)	-0,26	0,04
112724	RDH13	retinol dehydrogenase 13 (all-trans/9-cis)	-0,26	0,02
8605	PLA2G4C	phospholipase A2, group IVC (cytosolic, calcium-independent)	-0,26	0,02
55052	MRPL20	similar to mitochondrial ribosomal protein L20; mitochondrial ribosomal protein L20	-0,26	0,01
3312	HSPA8	heat shock 70kDa protein 8	-0,26	0,02
22921	MSRB2	methionine sulfoxide reductase B2	-0,26	0,01
26827	RNU6-1	5-oxoprolinase (ATP-hydrolysing)	-0,26	0,02
26275	HIBCH	guanine nucleotide binding protein-like 3 (nucleolar)	-0,26	0,02
10817	FRS3	fibroblast growth factor receptor substrate 3	-0,26	0,01
26508	HEYL	cysteine-rich hydrophobic domain 2	-0,26	0,01
54795	TRPM4	transient receptor potential cation channel, subfamily M, member 4	-0,26	0,04
5296	PIK3R2	phosphoinositide-3-kinase, regulatory subunit 2 (beta)	-0,27	0,02
9781	RNF144	ring finger protein 144A	-0,27	0,01
529	ATP6V1E1	ATPase, H+ transporting, lysosomal 31kDa, V1 subunit E1	-0,27	0,05
1163	CKS1B	CDC28 protein kinase regulatory subunit 1B	-0,27	0,00
51016	FAM158A	family with sequence similarity 158, member A	-0,27	0,01
28958	CCDC56	coiled-coil domain containing 56	-0,27	0,00
79956	ERMP1	endoplasmic reticulum metallopeptidase 1	-0,27	0,01
26636	OR7E37P	RNA, U6 small nuclear 2; RNA, U6 small nuclear 1	-0,27	0,01
10099	TSPAN3	tetraspanin 3	-0,27	0,01
79005	SCNM1	sodium channel modifier 1	-0,27	0,01
7169	TPM2	tropomyosin 2 (beta)	-0,27	0,02

5

5

10890	RAB10	RAB10, member RAS oncogene family	-0,27	0,01
81618	ITM2C	integral membrane protein 2C	-0,27	0,01
57153	SLC44A2	solute carrier family 44, member 2	-0,27	0,03
55745	MUDENG	MU-2/AP1M2 domain containing, death-inducing	-0,27	0,02
1355	COX15	COX15 homolog, cytochrome c oxidase assembly protein (yeast)	-0,27	0,00
23553	HYAL4	hyaluronoglucosaminidase 4	-0,27	0,03
285193	DUSP28	dual specificity phosphatase 28	-0,27	0,03
5699	PSMB10	proteasome (prosome, macropain) subunit, beta type, 10	-0,27	0,01
5358	PLS3	plastin 3 (T isoform)	-0,27	0,03
51075	TXNDC14	thioredoxin-related transmembrane protein 2	-0,27	0,00
10295	BCKDK	branched chain ketoacid dehydrogenase kinase	-0,27	0,03
1593	CYP27A1	cytochrome P450, family 27, subfamily A, polypeptide 1	-0,27	0,05
516	ATP5G1	ATP synthase, H+ transporting, mitochondrial F0 complex, subunit C1 (subunit 9)	-0,28	0,03
523	ATP6V1A	ATPase, H+ transporting, lysosomal 70kDa, V1 subunit A	-0,28	0,02
5524	PPP2R4	protein phosphatase 2A activator, regulatory subunit 4	-0,28	0,00
4005	LMO2	LIM domain only 2 (rhombotin-like 1)	-0,28	0,01
1352	COX10	COX10 homolog, cytochrome c oxidase assembly protein, heme A: farnesyltransferase (yeast)	-0,28	0,00
6242	RTKN	rhotekin	-0,28	0,00
57107	PDSS2	prenyl (decaprenyl) diphosphate synthase, subunit 2	-0,28	0,00
2021	ENDOG	endonuclease G	-0,28	0,00
123169	LEO1	Leo1, Paf1/RNA polymerase II complex component, homolog (S. cerevisiae)	-0,28	0,00
55347	ABHD10	abhydrolase domain containing 10	-0,28	0,02
147184	TMEM99	transmembrane protein 99	-0,28	0,04
51734	SEPX1	selenoprotein X, 1	-0,28	0,01
3385	ICAM3	intercellular adhesion molecule 3	-0,28	0,01
2882	GPX7	glutathione peroxidase 7	-0,28	0,05
952	CD38	CD38 molecule	-0,28	0,03
858	CAV2	caveolin 2	-0,28	0,05
6482	ST3GAL1	ST3 beta-galactoside alpha-2,3-sialyltransferase 1	-0,28	0,05

7390	UROS	uroporphyrinogen III synthase	-0,28	0,01
5859	QARS	glutaminyl-tRNA synthetase	-0,28	0,01
84816	RTN4IP1	reticulon 4 interacting protein 1	-0,29	0,00
169611	OLFML2A	olfactomedin-like 2A	-0,29	0,02
360132	FKBP9L	FK506 binding protein 9-like	-0,29	0,04
57060	PCBP4	poly(rC) binding protein 4	-0,29	0,01
23446	SLC44A1	solute carrier family 44, member 1	-0,29	0,00
4856	NOV	nephroblastoma overexpressed gene	-0,29	0,03
51455	REV1	REV1 homolog (S. cerevisiae)	-0,29	0,01
80207	OPA3	optic atrophy 3 (autosomal recessive, with chorea and spastic paraplegia)	-0,29	0,03
5210	PFKFB4	6-phosphofructo-2-kinase/fructose-2,6-biphosphatase 4	-0,29	0,02
64975	MRPL41	mitochondrial ribosomal protein L41	-0,29	0,04
155066	ATP6V0E2	ATPase, H+ transporting V0 subunit e2	-0,29	0,01
2592	GALT	galactose-1-phosphate uridylyltransferase	-0,29	0,04
79135	APOO	apolipoprotein O	-0,29	0,01
29074	MRPL18	mitochondrial ribosomal protein L18	-0,29	0,01
90313	TP53I13	tumor protein p53 inducible protein 13	-0,29	0,00
522	ATP5J	ATP synthase, H+ transporting, mitochondrial F0 complex, subunit F6	-0,29	0,04
29928	TIMM22	translocase of inner mitochondrial membrane 22 homolog (yeast)	-0,29	0,00
6100	RP9	retinitis pigmentosa 9 (autosomal dominant)	-0,29	0,01
55852	TEX2	testis expressed 2	-0,29	0,05
51069	MRPL2	mitochondrial ribosomal protein L2	-0,29	0,02
23187	PHLDB1	pleckstrin homology-like domain, family B, member 1	-0,30	0,01
1632	DCI	dodecenoyl-Coenzyme A delta isomerase (3,2 trans-enoyl-Coenzyme A isomerase)	-0,30	0,02
7263	TST	thiosulfate sulfurtransferase (rhodanese)	-0,30	0,03
3337	DNAJB1	DnaJ (Hsp40) homolog, subfamily B, member 1	-0,30	0,05
369	ARAF	v-raf murine sarcoma 3611 viral oncogene homolog	-0,30	0,03
9717	SEC14L5	SEC14-like 5 (S. cerevisiae)	-0,30	0,03
84967	LSM10	LSM10, U7 small nuclear RNA associated	-0,30	0,01
5420	PODXL	podocalyxin-like	-0,30	0,03

5

5

11344	TWF2	twinfilin, actin-binding protein, homolog 2 (Drosophila)	-0,30	0,05
201140	DHRS7C	dehydrogenase/reductase (SDR family) member 7C	-0,30	0,00
5207	PFKFB1	6-phosphofructo-2-kinase/fructose-2,6-biphosphatase 1	-0,30	0,00
23294	ANKS1A	ankyrin repeat and sterile alpha motif domain containing 1A	-0,30	0,02
7079	TIMP4	TIMP metallopeptidase inhibitor 4	-0,30	0,02
55186	SLC25A36	solute carrier family 25, member 36	-0,30	0,04
8869	ST3GAL5	ST3 beta-galactoside alpha-2,3-sialyltransferase 5	-0,30	0,00
140456	ASB11	ankyrin repeat and SOCS box-containing 11	-0,30	0,05
6697	SPR	sepiapterin reductase (7,8-dihydrobiopterin:NADP+ oxidoreductase)	-0,30	0,01
3280	HES1	hairy and enhancer of split 1, (Drosophila)	-0,30	0,02
25979	DHRS7B	REX2, RNA exonuclease 2 homolog (S. cerevisiae)	-0,30	0,01
29803	REPIN1	replication initiator 1	-0,30	0,02
84266	ALKBH7	alkB, alkylation repair homolog 7 (E. coli)	-0,30	0,01
10651	MTX2	metaxin 2	-0,30	0,01
29089	UBE2T	ubiquitin-conjugating enzyme E2T (putative)	-0,30	0,01
51004	COQ6	coenzyme Q6 homolog, monooxygenase (S. cerevisiae)	-0,30	0,01
4713	NDUFB7	NADH dehydrogenase (ubiquinone) 1 beta subcomplex, 7, 18kDa	-0,30	0,00
3858	KRT10	keratin 10	-0,30	0,00
65009	NDRG4	NDRG family member 4	-0,30	0,00
56963	RGMA	RGM domain family, member A	-0,30	0,04
23051	ZHX3	zinc fingers and homeoboxes 3	-0,31	0,03
79675	FASTKD1	FAST kinase domains 1	-0,31	0,01
57048	PLSCR3	phospholipid scramblase 3	-0,31	0,00
23543	RBM9	RNA binding motif protein 9	-0,31	0,03
22911	WDR47	WD repeat domain 47	-0,31	0,02
157310	PEBP4	phosphatidylethanolamine-binding protein 4	-0,31	0,02
8214	DGCR6	DiGeorge syndrome critical region gene 6	-0,31	0,01
112464	PRKCDBP	protein kinase C, delta binding protein	-0,31	0,04
79944	L2HGDH	L-2-hydroxyglutarate dehydrogenase	-0,31	0,00
5201	PFDN1	prefoldin subunit 1	-0,31	0,02

1347	COX7A2	cytochrome c oxidase subunit VIIa polypeptide 2 (liver)	-0,31	0,02
56937	PMEPA1	prostate transmembrane protein, androgen induced 1	-0,31	0,01
4594	MUT	methylmalonyl Coenzyme A mutase	-0,31	0,04
51728	POLR3K	polymerase (RNA) III (DNA directed) polypeptide K, 12.3 kDa	-0,31	0,00
51070	NOSIP	nitric oxide synthase interacting protein	-0,31	0,05
4728	NDUFS8	NADH dehydrogenase (ubiquinone) Fe-S protein 8, 23kDa (NADH-coenzyme Q reductase)	-0,31	0,00
7172	TPMT	thiopurine S-methyltransferase	-0,31	0,01
55268	ECHDC2	enoyl Coenzyme A hydratase domain containing 2	-0,31	0,04
3338599	DUPD1	dual specificity phosphatase and pro isomerase domain containing 1	-0,31	0,00
26504	CNNM4	hairy/enhancer-of-split related with YRPW motif-like	-0,31	0,01
55508	SLC35E3	solute carrier family 35, member E3	-0,31	0,02
66000	TMEM108	transmembrane protein 108	-0,31	0,00
54749	EPDR1	ependymin related protein 1 (zebrafish)	-0,31	0,05
404093	CUEDC1	CUE domain containing 1	-0,31	0,02
727956	SDHAP2	succinate dehydrogenase complex, subunit A, flavoprotein pseudogene 2	-0,32	0,01
5789	PTPRD	protein tyrosine phosphatase, receptor type, D	-0,32	0,00
80144	FRAS1	Fraser syndrome 1	-0,32	0,01
51106	TFB1M	transcription factor B1, mitochondrial	-0,32	0,00
64710	NUCKS1	nuclear casein kinase and cyclin-dependent kinase substrate 1	-0,32	0,02
203	AK1	adenylate kinase 1	-0,32	0,05
51334	PRR16	proline rich 16	-0,32	0,00
9612	NCOR2	nuclear receptor co-repressor 2	-0,32	0,04
122786	FRMD6	FERM domain containing 6	-0,32	0,01
6558	SLC12A2	solute carrier family 12 (sodium/potassium/chloride transporters), member 2	-0,32	0,02
255812	SDHALP1	succinate dehydrogenase complex, subunit A, flavoprotein pseudogene 1	-0,32	0,04
8266	UBL4A	ubiquitin-like 4A	-0,32	0,01
154091	SLC2A12	solute carrier family 2 (facilitated glucose transporter), member 12	-0,32	0,01
339344	MYPOP	Myb-related transcription factor, partner of profilin	-0,32	0,01
3157	HMGCS1	3-hydroxy-3-methylglutaryl-Coenzyme A synthase 1 (soluble)	-0,32	0,00

5

5

57146	TMEM159	transmembrane protein 159	-0,32	0,03
8635	RNASET2	ribonuclease T2	-0,32	0,03
8604	SLC25A12	solute carrier family 25 (mitochondrial carrier, Aralar), member 12	-0,32	0,04
252995	FNDC5	fibronectin type III domain containing 5	-0,32	0,00
10217	CTDSPL	CTD (carboxy-terminal domain, RNA polymerase II, polypeptide A) small phosphatase-like	-0,32	0,01
27101	CACYBP	similar to calcyclin binding protein; calcyclin binding protein	-0,32	0,01
55090	MED9	mediator complex subunit 9	-0,32	0,01
8404	SPARCL1	SPARC-like 1 (hevin)	-0,32	0,03
65010	SLC26A6	solute carrier family 26, member 6; cadherin, EGF LAG seven-pass G-type receptor 3 (flamingo homolog, Drosophila)	-0,32	0,02
1070	CETN3	centrin, EF-hand protein, 3 (CDC31 homolog, yeast)	-0,33	0,00
9586	CREB5	cAMP responsive element binding protein 5	-0,33	0,00
491	ATP2B2	ATPase, Ca++ transporting, plasma membrane 2	-0,33	0,01
201164	PLD6	phospholipase D family, member 6	-0,33	0,01
3927	LASP1	LIM and SH3 protein 1	-0,33	0,03
3145	HMBS	hydroxymethylbilane synthase	-0,33	0,01
80212	CCDC92	coiled-coil domain containing 92	-0,33	0,00
388650	FAM69A	family with sequence similarity 69, member A	-0,33	0,00
55168	MRPS18A	mitochondrial ribosomal protein S18A	-0,33	0,00
91687	CENPL	centromere protein L	-0,33	0,03
9452	ITM2A	integral membrane protein 2A	-0,33	0,04
8925	HERC1	hect (homologous to the E6-AP (UBE3A) carboxyl terminus) domain and RCC1 (CHC1)-like domain (RLD) 1	-0,33	0,01
348093	RBPMS2	RNA binding protein with multiple splicing 2	-0,33	0,00
65003	MRPL11	mitochondrial ribosomal protein L11	-0,33	0,01
286140	RNF5P1	ring finger protein 5; ring finger protein 5 pseudogene 1	-0,33	0,00
22809	ATF5	activating transcription factor 5	-0,33	0,00
844	CASQ1	calsequestrin 1 (fast-twitch, skeletal muscle)	-0,33	0,00
79844	ZDHHC11	zinc finger, DHHC-type containing 11	-0,33	0,01

4888	NPY6R	neuropeptide Y receptor Y6 (pseudogene)	-0,33	0,03
657	BMPR1A	bone morphogenetic protein receptor, type IA; similar to ALK-3	-0,34	0,01
9587	MAD2L1BP	MAD2L1 binding protein	-0,34	0,00
537	ATP6AP1	ATPase, H+ transporting, lysosomal accessory protein 1	-0,34	0,01
10654	PMVK	phosphomevalonate kinase	-0,34	0,00
28955	DEXI	dexamethasone-induced transcript	-0,34	0,00
91380	SNORD107	small nucleolar RNA, C/D box 107	-0,34	0,00
6444	SGCD	sarcoglycan, delta (35kDa dystrophin-associated glycoprotein)	-0,34	0,05
9524	TECR	glycoprotein, synaptic 2	-0,34	0,01
64756	ATPAF1	ATP synthase mitochondrial F1 complex assembly factor 1	-0,34	0,01
5523	PPP2R3A	protein phosphatase 2 (formerly 2A), regulatory subunit B'', alpha	-0,34	0,01
1429	CRYZ	crystallin, zeta (quinone reductase)	-0,34	0,01
9249	DHRS3	dehydrogenase/reductase (SDR family) member 3	-0,34	0,00
8082	SSPN	sarcospan (Kras oncogene-associated gene)	-0,34	0,04
2009	EML1	echinoderm microtubule associated protein like 1	-0,34	0,00
9099	USP2	ubiquitin specific peptidase 2	-0,34	0,00
55245	UQCC	ubiquinol-cytochrome c reductase complex chaperone	-0,34	0,01
23433	RHOQ	ras homolog gene family, member Q; similar to small GTP binding protein TC10	-0,34	0,00
4782	NFIC	nuclear factor I/C (CCAAT-binding transcription factor)	-0,34	0,01
9497	SLC4A7	solute carrier family 4, sodium bicarbonate cotransporter, member 7	-0,34	0,03
57493	HEG1	HEG homolog 1 (zebrafish)	-0,34	0,00
284451	ODF3L2	outer dense fiber of sperm tails 3-like 2	-0,34	0,00
5351	PLOD1	procollagen-lysine 1, 2-oxoglutarate 5-dioxygenase 1	-0,35	0,01
84896	ATAD1	ATPase family, AAA domain containing 1	-0,35	0,01
55929	DMAP1	DNA methyltransferase 1 associated protein 1	-0,35	0,01
8854	ALDH1A2	aldehyde dehydrogenase 1 family, member A2	-0,35	0,03
6183	MRPS12	mitochondrial ribosomal protein S12	-0,35	0,00
84681	HINT2	histidine triad nucleotide binding protein 2	-0,35	0,02
11018	TMED1	transmembrane emp24 protein transport domain containing 1	-0,35	0,00
10422	UBAC1	UBA domain containing 1	-0,35	0,00

5

5

285440	CYP4V2	cytochrome P450, family 4, subfamily V, polypeptide 2	-0,35	0,00
4240	MFGE8	milk fat globule-EGF factor 8 protein	-0,35	0,00
219348	PLAC9	placenta-specific 9	-0,35	0,03
6453	ITSN1	intersectin 1 (SH3 domain protein)	-0,35	0,00
25842	ASF1A	DKFZP564O0823 protein	-0,35	0,01
151242	PPP1R1C	protein phosphatase 1, regulatory (inhibitor) subunit 1C	-0,35	0,01
81533	ITFG1	integrin alpha FG-GAP repeat containing 1	-0,35	0,01
51085	MLXIPL	MLX interacting protein-like	-0,35	0,00
30011	SH3KBP1	SH3-domain kinase binding protein 1	-0,35	0,01
85457	KIAA1737	KIAA1737	-0,35	0,04
90135	BTBD6	BTB (POZ) domain containing 6	-0,35	0,00
3373	HYAL1	hyaluronoglucosaminidase 1	-0,35	0,01
170302	ARX	aristaless related homeobox	-0,36	0,00
29083	GTPBP8	GTP-binding protein 8 (putative)	-0,36	0,01
54345	SOX18	SRY (sex determining region Y)-box 18	-0,36	0,05
55333	SYNJ2BP	synaptojanin 2 binding protein	-0,36	0,01
23767	FLRT3	fibronectin leucine rich transmembrane protein 3	-0,36	0,01
6253	RTN2	reticulon 2	-0,36	0,05
7423	VEGFB	vascular endothelial growth factor B	-0,36	0,00
2178	FANCE	Fanconi anemia, complementation group E	-0,36	0,00
5104	SERPINA5	serpin peptidase inhibitor, clade A (alpha-1 antiproteinase, antitrypsin), member 5	-0,36	0,01
92241	RCSD1	RCSD domain containing 1	-0,36	0,00
5774	PTPN3	protein tyrosine phosphatase, non-receptor type 3	-0,36	0,03
161247	FIT1	fat storage-inducing transmembrane protein 1	-0,36	0,01
7360	UGP2	UDP-glucose pyrophosphorylase 2	-0,36	0,01
51207	DUSP13	dual specificity phosphatase 13	-0,36	0,01
55625	ZDHHC7	zinc finger, DHHC-type containing 7	-0,36	0,00
23646	PLD3	phospholipase D family, member 3	-0,37	0,01
51660	BRP44L	brain protein 44-like	-0,37	0,02
81621	KAZALD1	Kazal-type serine peptidase inhibitor domain 1	-0,37	0,02

6391	SDHC	succinate dehydrogenase complex, subunit C, integral membrane protein, 15kDa	-0,37	0,00
6867	TACC1	transforming, acidic coiled-coil containing protein 1	-0,37	0,02
10572	SIVA	SIVA1, apoptosis-inducing factor	-0,37	0,03
55353	LAPTM4B	lysosomal protein transmembrane 4 beta	-0,37	0,00
2819	GPD1	glycerol-3-phosphate dehydrogenase 1 (soluble)	-0,37	0,05
4700	NDUFA6	NADH dehydrogenase (ubiquinone) 1 alpha subcomplex, 6, 14kDa	-0,37	0,01
8405	SPOP	speckle-type POZ protein	-0,37	0,00
23344	ESYT1	family with sequence similarity 62 (C2 domain containing), member A	-0,37	0,01
8996	NOL3	nucleolar protein 3 (apoptosis repressor with CARD domain)	-0,37	0,01
3270	HRC	histidine rich calcium binding protein	-0,37	0,00
27335	EIF3K	eukaryotic translation initiation factor 3, subunit K	-0,37	0,02
57446	NDRG3	NDRG family member 3	-0,38	0,05
84191	FAM96A	family with sequence similarity 96, member A	-0,38	0,02
114782	KIAA1881	phosphoinositide-3-kinase interacting protein 1	-0,38	0,02
57380	MRS2	MRS2 magnesium homeostasis factor homolog (S. cerevisiae)	-0,38	0,01
53632	PRKAG3	protein kinase, AMP-activated, gamma 3 non-catalytic subunit	-0,38	0,02
815	CAMK2A	calcium/calmodulin-dependent protein kinase II alpha	-0,38	0,02
8483	CILP	cartilage intermediate layer protein, nucleotide pyrophosphohydrolase	-0,38	0,05
284403	WDR62	WD repeat domain 62	-0,38	0,02
2542	SLC37A4	solute carrier family 37 (glucose-6-phosphate transporter), member 4	-0,38	0,01
8728	ADAM19	ADAM metallopeptidase domain 19 (meltrin beta)	-0,38	0,00
51537	MTP18	mitochondrial protein 18 kDa	-0,38	0,00
23240	KIAA0922	KIAA0922	-0,38	0,04
10867	TSPAN9	tetraspanin 9	-0,38	0,00
131474	CHCHD4	coiled-coil-helix-coiled-coil-helix domain containing 4	-0,38	0,00
4702	NDUFA8	NADH dehydrogenase (ubiquinone) 1 alpha subcomplex, 8, 19kDa	-0,39	0,01
339896	GADL1	glutamate decarboxylase-like 1	-0,39	0,02
4239	MFAP4	microfibrillar-associated protein 4	-0,39	0,05
9958	USP15	ubiquitin specific peptidase 15	-0,39	0,02
56910	STARD7	StAR-related lipid transfer (START) domain containing 7	-0,39	0,01

5

5

928	CD9	CD9 molecule	-0,39	0,00
27122	DKK3	dickkopf homolog 3 (Xenopus laevis)	-0,39	0,01
27231	ITGB1BP3	integrin beta 1 binding protein 3	-0,40	0,02
4128	MAOA	monoamine oxidase A	-0,40	0,05
51204	TACO1	coiled-coil domain containing 44	-0,40	0,00
57571	ATPGD1	ATP-grasp domain containing 1	-0,40	0,03
3743	KCNA7	potassium voltage-gated channel, shaker-related subfamily, member 7	-0,40	0,00
64801	ARV1	ARV1 homolog (S. cerevisiae)	-0,40	0,00
284119	PTRF	polymerase I and transcript release factor	-0,40	0,00
845	CASQ2	calsequestrin 2 (cardiac muscle)	-0,40	0,02
339456	TMEM52	transmembrane protein 52	-0,40	0,03
25849	PARM1	SIN3 homolog A, transcription regulator (yeast)	-0,40	0,00
26273	FBXO3	3-hydroxyisobutyryl-Coenzyme A hydrolase	-0,40	0,03
84281	MGC13057	chromosome 2 open reading frame 88	-0,40	0,00
3052	HCCS	holocytochrome c synthase (cytochrome c heme-lyase)	-0,41	0,00
441531	PGAM4	phosphoglycerate mutase family member 4	-0,41	0,01
5376	PMP22	peripheral myelin protein 22	-0,41	0,03
306	ANXA3	annexin A3	-0,41	0,00
148932	MOBKL2C	MOB1, Mps One Binder kinase activator-like 2C (yeast)	-0,41	0,02
3590	IL11RA	interleukin 11 receptor, alpha	-0,42	0,00
29903	CCDC106	coiled-coil domain containing 106	-0,42	0,00
4624	MYH6	myosin, heavy chain 6, cardiac muscle, alpha	-0,42	0,02
23095	KIF1B	kinesin family member 1B	-0,42	0,00
79191	IRX3	iroquois homeobox 3	-0,42	0,04
113457	TUBA3D	tubulin, alpha 3d; tubulin, alpha 3c	-0,42	0,00
94274	PPP1R14A	protein phosphatase 1, regulatory (inhibitor) subunit 14A	-0,42	0,00
130827	TMEM182	transmembrane protein 182	-0,43	0,05
4208	MEF2C	myocyte enhancer factor 2C	-0,43	0,03
29	ABR	active BCR-related gene	-0,43	0,00
9922	IQSEC1	IQ motif and Sec7 domain 1	-0,43	0,00

80206	FHOD3	formin homology 2 domain containing 3	-0,43	0,01
8028	MLLT10	myeloid/lymphoid or mixed-lineage leukemia (trithorax homolog, Drosophila); translocated to, 10	-0,43	0,00
4094	MAF	v-maf musculoaponeurotic fibrosarcoma oncogene homolog (avian)	-0,43	0,00
11155	LDB3	LIM domain binding 3	-0,43	0,01
5588	PRKCQ	protein kinase C, theta	-0,43	0,05
786	CACNG1	calcium channel, voltage-dependent, gamma subunit 1	-0,43	0,00
9719	ADAMTSL2	similar to ADAMTS-like 2; ADAMTS-like 2	-0,43	0,00
2199	FBLN2	fibulin 2	-0,43	0,03
116138	KLHDC3	kelch domain containing 3	-0,44	0,00
26873	OPLAH	HMG-box transcription factor 1	-0,44	0,01
256691	MAMDC2	MAM domain containing 2	-0,44	0,03
2875	GPT	glutamic-pyruvate transaminase (alanine aminotransferase)	-0,44	0,01
253512	SLC25A30	solute carrier family 25, member 30	-0,44	0,00
29796	UCRC	ubiquinol-cytochrome c reductase complex (7.2 kD)	-0,44	0,00
55700	MAP7D1	MAP7 domain containing 1	-0,44	0,00
83543	AIF1L	allograft inflammatory factor 1-like	-0,44	0,03
64328	XPO4	exportin 4	-0,44	0,03
29904	EEF2K	eukaryotic elongation factor-2 kinase	-0,45	0,01
57801	HES4	hairy and enhancer of split 4 (Drosophila)	-0,45	0,00
5287	PIK3C2B	phosphoinositide-3-kinase, class 2, beta polypeptide	-0,45	0,01
284612	SYPL2	synaptophysin-like 2	-0,45	0,01
5961	PRPH2	peripherin 2 (retinal degeneration, slow)	-0,45	0,03
9499	MYOT	myotilin	-0,45	0,00
8195	MKKS	McKusick-Kaufman syndrome	-0,46	0,00
23052	ENDOD1	endonuclease domain containing 1	-0,46	0,00
80772	GLTPD1	glycolipid transfer protein domain containing 1	-0,46	0,00
10039	PARP3	poly (ADP-ribose) polymerase family, member 3	-0,46	0,00
142685	ASB15	ankyrin repeat and SOCS box-containing 15	-0,47	0,01
51805	COQ3	coenzyme Q3 homolog, methyltransferase (S. cerevisiae)	-0,47	0,01

5

5

84908	FAM136A	family with sequence similarity 136, member A	-0,47	0,00
64981	MRPL34	mitochondrial ribosomal protein L34	-0,47	0,00
54536	EXOC6	exocyst complex component 6	-0,48	0,01
5150	PDE7A	phosphodiesterase 7A	-0,48	0,00
7871	SLMAP	sarcolemma associated protein	-0,48	0,02
595	CCND1	cyclin D1	-0,48	0,00
91977	MYOZ3	myozenin 3	-0,48	0,00
7283	TUBG1	tubulin, gamma 1; similar to Tubulin, gamma 1	-0,48	0,00
23112	TNRC6B	trinucleotide repeat containing 6B	-0,48	0,00
6790	AURKA	aurora kinase A; aurora kinase A pseudogene 1	-0,48	0,00
10994	ILVBL	ilvB (bacterial acetolactate synthase)-like	-0,48	0,00
11138	TBC1D8	TBC1 domain family, member 8 (with GRAM domain)	-0,49	0,00
245806	VGLL2	vestigial like 2 (Drosophila)	-0,49	0,02
145957	NRG4	neuregulin 4	-0,49	0,00
79140	CCDC28B	coiled-coil domain containing 28B	-0,49	0,00
6821	SUOX	sulfite oxidase	-0,49	0,02
23632	CA14	carbonic anhydrase XIV	-0,49	0,00
3727	JUND	jun D proto-oncogene	-0,50	0,00
84812	PLCD4	phospholipase C, delta 4	-0,50	0,00
84814	PPAPDC3	phosphatidic acid phosphatase type 2 domain containing 3	-0,50	0,02
1737	DLAT	dihydrolipoamide S-acetyltransferase	-0,50	0,00
22906	TRAK1	trafficking protein, kinesin binding 1	-0,50	0,00
55234	SMU1	smu-1 suppressor of mec-8 and unc-52 homolog (C. elegans)	-0,50	0,00
178	AGL	amylo-1, 6-glucosidase, 4-alpha-glucanotransferase	-0,50	0,01
6913	TBX15	T-box 15	-0,50	0,00
1634	DCN	decorin	-0,51	0,02
3417	IDH1	isocitrate dehydrogenase 1 (NADP+), soluble	-0,51	0,01
147808	ZNF784	zinc finger protein 784	-0,51	0,00
55334	SLC39A9	solute carrier family 39 (zinc transporter), member 9	-0,51	0,03
3622	ING2	inhibitor of growth family, member 2	-0,51	0,00

ID	Symbol	Description	Value	p
27244	SESN1	sestrin 1	-0,51	0,05
7123	CLEC3B	C-type lectin domain family 3, member B	-0,52	0,00
124222	PAQR4	progestin and adipoQ receptor family member IV	-0,52	0,00
114881	OSBPL7	oxysterol binding protein-like 7	-0,52	0,03
127495	LRRC39	leucine rich repeat containing 39	-0,52	0,02
3422	IDI1	isopentenyl-diphosphate delta isomerase 1	-0,53	0,00
51621	KLF13	Kruppel-like factor 13	-0,53	0,00
84870	RSPO3	R-spondin 3 homolog (Xenopus laevis)	-0,53	0,02
113655	MFSD3	tubulin, alpha 3d; tubulin, alpha 3c	-0,53	0,00
79365	BHLHB3	basic helix-loop-helix family, member e41	-0,53	0,00
51676	ASB2	ankyrin repeat and SOCS box-containing 2	-0,53	0,00
1628	DBP	D site of albumin promoter (albumin D-box) binding protein	-0,53	0,01
136371	ASB10	ankyrin repeat and SOCS box-containing 10	-0,54	0,00
79594	MUL1	mitochondrial E3 ubiquitin ligase 1	-0,54	0,00
54873	PALMD	palmdelphin	-0,54	0,01
5648	MASP1	mannan-binding lectin serine peptidase 1 (C4/C2 activating component of Ra-reactive factor)	-0,55	0,00
1573	CYP2J2	cytochrome P450, family 2, subfamily J, polypeptide 2	-0,55	0,00
7277	TUBA4A	tubulin, alpha 4a	-0,55	0,00
6512	SLC1A7	solute carrier family 1 (glutamate transporter), member 7	-0,55	0,00
80303	EFHD1	EF-hand domain family, member D1	-0,55	0,01
25780	RASGRP3	beta-site APP-cleaving enzyme 2	-0,55	0,01
286101	ZNF252	zinc finger protein 252	-0,56	0,00
3177	SLC29A2	solute carrier family 29 (nucleoside transporters), member 2	-0,56	0,04
1649	DDIT3	DNA-damage-inducible transcript 3	-0,56	0,00
6275	S100A4	S100 calcium binding protein A4	-0,57	0,02
150572	SMYD1	SET and MYND domain containing 1	-0,57	0,00
165186	FAM179A	family with sequence similarity 179, member A	-0,57	0,02
23066	CAND2	cullin-associated and neddylation-dissociated 2 (putative)	-0,57	0,00
126755	LRRC38	leucine rich repeat containing 38	-0,57	0,01

5

5

4330	MN1	meningioma (disrupted in balanced translocation) 1	-0,58	0,03
51449	PCYOX1	prenylcysteine oxidase 1	-0,59	0,01
57644	MYH7B	myosin, heavy chain 7B, cardiac muscle, beta	-0,59	0,00
1396	CRIP1	cysteine-rich protein 1 (intestinal)	-0,59	0,00
7422	VEGFA	vascular endothelial growth factor A	-0,60	0,00
57142	RTN4	reticulon 4	-0,60	0,01
79933	SYNPO2L	synaptopodin 2-like	-0,60	0,01
79929	MAP6D1	MAP6 domain containing 1	-0,60	0,00
137735	ABRA	actin-binding Rho activating protein	-0,60	0,05
5959	RDH5	retinol dehydrogenase 5 (11-cis/9-cis)	-0,61	0,00
51318	MRPL35	mitochondrial ribosomal protein L35	-0,61	0,00
6525	SMTN	smoothelin	-0,62	0,00
284	ANGPT1	angiopoietin 1	-0,63	0,01
221662	RBM24	RNA binding motif protein 24	-0,63	0,03
361	AQP4	aquaporin 4	-0,63	0,04
85366	MYLK2	myosin light chain kinase 2	-0,63	0,02
57467	HHATL	hedgehog acyltransferase-like	-0,64	0,00
54463	FAM134B	family with sequence similarity 134, member B	-0,64	0,03
26027	ACOT11	WD repeat domain 21A	-0,64	0,00
43	ACHE	acetylcholinesterase (Yt blood group)	-0,66	0,00
1490	CTGF	connective tissue growth factor	-0,66	0,02
51285	RASL12	RAS-like, family 12	-0,67	0,00
64682	ANAPC1	anaphase promoting complex subunit 1; similar to anaphase promoting complex subunit 1	-0,68	0,00
122416	ANKRD9	ankyrin repeat domain 9	-0,68	0,00
53354	PANK1	pantothenate kinase 1	-0,68	0,00
160760	PPTC7	PTC7 protein phosphatase homolog (S. cerevisiae)	-0,71	0,00
9935	MAFB	v-maf musculoaponeurotic fibrosarcoma oncogene homolog B (avian)	-0,71	0,00
91663	MYADM	myeloid-associated differentiation marker	-0,71	0,00
93058	COQ10A	coenzyme Q10 homolog A (S. cerevisiae)	-0,71	0,00
3306	HSPA2	heat shock 70kDa protein 2	-0,72	0,00

4060	LUM	lumican	-0,72	0,00
53342	IL17D	interleukin 17D	-0,75	0,02
286	ANK1	ankyrin 1, erythrocytic	-0,75	0,00
64793	CCDC21	coiled-coil domain containing 21	-0,77	0,00
14	AAMP	angio-associated, migratory cell protein	-0,78	0,00
284358	FLJ36070	MEF2 activating motif and SAP domain containing transcriptional regulator	-0,78	0,01
340156	MYLK4	myosin light chain kinase family, member 4	-0,80	0,00
23439	ATP1B4	ATPase, (Na+)/K+ transporting, beta 4 polypeptide	-0,80	0,01
5506	PPP1R3A	protein phosphatase 1, regulatory (inhibitor) subunit 3A	-0,85	0,00
84988	PPP1R16A	protein phosphatase 1, regulatory (inhibitor) subunit 16A	-0,86	0,00
79156	PLEKHF1	pleckstrin homology domain containing, family F (with FYVE domain) member 1	-0,91	0,00
10140	TOB1	transducer of ERBB2, 1	-1,00	0,00
5507	PPP1R3C	protein phosphatase 1, regulatory (inhibitor) subunit 3C	-1,01	0,00
123722	FSD2	fibronectin type III and SPRY domain containing 2	-1,05	0,00
10891	PPARGC1A	peroxisome proliferator-activated receptor gamma, coactivator 1 alpha	-1,10	0,00
6876	TAGLN	transgelin	-1,10	0,00
50486	G0S2	G0/G1switch 2	-1,14	0,01
388228	SBK1	SH3-binding domain kinase 1	-1,17	0,00
9123	SLC16A3	solute carrier family 16, member 3 (monocarboxylic acid transporter 4)	-1,32	0,00
59	ACTA2	actin, alpha 2, smooth muscle, aorta	-1,50	0,00
7037	TFRC	transferrin receptor (p90, CD71)	-1,53	0,00
114789	SLC25A25	solute carrier family 25 (mitochondrial carrier; phosphate carrier), member 25	-1,64	0,00

5

5

Chapter 6

Food cues do not modulate the neuroendocrine response to a prolonged fast in healthy men

Marieke Snel[1*], Marjolein A. Wijngaarden[2*], Maurice B. Bizino[1], Jeroen van der Grond[3], Wouter M. Teeuwisse[3], Mark A. van Buchem[3], Ingrid M. Jazet[1] and Hanno Pijl[2]
* These authors contributed equally to this work

[1] Department of Internal Medicine, Leiden University Medical Center, Leiden, The Netherlands
[2] Department of Endocrinology and Metabolism, Leiden University Medical Center, Leiden, The Netherlands
[3] Department of Radiology, Leiden University Medical Center, Leiden, The Netherlands

6

6

Abstract

Introduction

Dietary restriction benefits health and increases lifespan in several species. Food odorants restrain the beneficial effects of dietary restriction in *Drosophila melanogaster*. We hypothesized that the presence of visual and odorous food stimuli during a prolonged fast modifies the neuroendocrine and metabolic response to fasting in humans.

Subjects & Methods

In this randomized, cross-over intervention study, healthy young men (n=12) fasted twice for 60 hours; once in the presence and once in the absence of food-related visual and odorous stimuli. At baseline and on the last morning of each intervention an oral glucose tolerance test (OGTT) was performed. During the OGTT blood was sampled and a functional MRI scan was made.

Results

The main effects of prolonged fasting were: 1) decreased plasma thyroid stimulating hormone (TSH) and triiodothyronine (T3) levels 2) down-regulation of the pituitary-gonadal axis; 3) reduced plasma glucose and insulin concentrations, but increased glucose and insulin responses to glucose ingestion; 4) altered hypothalamic blood oxygenation level dependent (BOLD) signal in response to the glucose load (particularly during the first 20 minutes after ingestion); 5) increased resting energy expenditure. Exposure to food cues did not affect these parameters.

Conclusion

This study shows that 60 hours of fasting in young men 1) decreases the hypothalamic BOLD signal in response to glucose ingestion; 2) induces glucose intolerance; 3) increases resting energy expenditure and, 4) down-regulates the pituitary-thyroid- and pituitary-gonadal axes. Exposure to visual and odorous food cues did not alter these metabolic and neuroendocrine adaptations to nutrient deprivation.

6

Introduction

Dietary restriction extends life span and prevents prevalent age-related diseases like cancer and diabetes in a variety of species, including non-human primates [1]. The benefits appear to come about at least in part through metabolic and neuroendocrine adaptations to nutrient deprivation [2]. Circumstantial evidence suggests that dietary restriction may have similar effects on health and longevity in humans, probably at least in part via established endocrine and metabolic adaptations to nutrient deprivation [1].

It has recently been shown that food odorants (from live yeast) restrain the beneficial effects of dietary restriction on longevity in *Drosophila melanogaster* [3]. Moreover, mutation of a gene leading to severe olfactory defects (Orb83b) alters metabolism, enhances stress resistance and extends life span in fully fed *Drosophila* [3], corroborating other evidence that aging and longevity are regulated by olfactory neurons in *Caenorhabditis Elegans* [4].

The vomeronasal organ (VNO) is an evolutionary conserved part of the (mammalian) olfactory system, which primarily responds to nonvolatile cues to relay environmental information to the hypothalamus (in mammals), allowing subsequent adaptation of reproductive and ingestive behavior and neuro-endocrine secretion [5].The VNO primarily transmits pheromonal signals, mediating social and sexual behaviors and neuro-endocrine changes pertaining to reproduction. Limited evidence indicates that (non-pheromonal) odorous stimuli perceived by the main olfactory epithelium (MOE) can also engage hypothalamic neurons in humans [6]. The hypothalamus controls systemic glucose and lipid flux in response to circulating metabolic and hormonal cues reflecting bodily energy reserves [7]. Visual food cues also impact on hypothalamic neuronal activity in healthy humans [8], suggesting that this type of stimulus may add to the putative effects of odors on neuroendocrine and metabolic features in the current experimental context.

Here we hypothesized that visual and odorous food stimuli impact on neuroendocrine and metabolic responses to a prolonged fast in humans. Specifically, we predict that exposure to attractive visual and odorous food cues during fasting blunts the hypothalamic and metabolic adaptations that normally occur in response to nutrient dep-

6

rivation. Although we realize that fasting is not an ideal model of chronic (mild) restriction of calories, we use (prolonged) fasting as a *proxy*, since randomized offering of food cues to people who restrict their calories for a long time is virtually impossible. Moreover, we reasoned that if odorous cues counteract the benefits of mild restriction, they may impact the corollaries of more severe restriction to an even greater extent. We quantify neuronal activity in the hypothalamus by functional magnetic resonance imaging (fMRI); this technique has previously been used to determine hypothalamic activity in response to glucose ingestion in humans [9-11]. We chose to use total fasting instead of (prolonged) calorie restriction as a model of nutrient deprivation to maximize the endocrine effects of short term deprivation, since longer term experiments of this kind are not feasible in humans, particularly with respect to modulation of exposure to food cues. Visual food stimuli were offered in addition to odorous cues to maximize the potential impact of exposure.

6

Subjects and Methods

Subjects

This study was executed in accordance with the principles of the revised Declaration of Helsinki and commenced after approval of the Medical Ethics Committee of the Leiden University Medical Centre. This trial was registered in at Clinicaltrials.gov (NCT01243879). All volunteers gave written informed consent before participation. We studied 12 healthy Caucasian males who were recruited via local advertisements. All participants were between 18 and 30 years (mean 22 years), had a body mass index (BMI) ranging from 20-25 kg/m^2 (mean 22.5 kg/m^2) and had fasting serum glucose levels below 6.1 mmol/l. Subjects who used medication, smoked, suffered from anosmia, had MRI contraindications or had recently donated blood were excluded from participation.

Study design

In this randomized, controlled, cross-over intervention study, participants were exposed to two sequential interventions that consisted of 60 hours of fasting in the presence or absence of food-related stimuli. Interventions occurred in random order with a wash-out period of at least 2 weeks. In the week before the first intervention, after an overnight fast, the baseline functional magnetic resonance imaging (fMRI) scan and oral glucose tolerance test (OGTT) were performed.

On a separate day the next week, subjects were admitted to our clinical research centre at 08:00 am after an overnight fast (12 hours) for a subsequent period of 48 hours of fasting. After arrival, anthropometric measures were taken, body composition was determined and substrate oxidation was measured by indirect calorimetry. During both interventions, volunteers were allowed to drink water *ad libitum*, but were not permitted to leave the research center. During the intervention without food-related cues, participants were not allowed to talk about food or to watch food-related matters on television.

During the other intervention, subjects were exposed to visual and odorous food stimuli food from 10.00 am to 12.30 pm (eggs with bacon, grilled sandwich and coffee), from 1.00 to 3.30 pm (apple pie and banana cake), from 5.00 to 8.30 pm (French fries with meat croquettes, pizza salami and garlic bread) and from 9.00 to 10.00 pm (coffee). All food items were freshly prepared and presented to the participants. On

the last morning, food stimuli were given from 6.00 to 7.00 am (bacon, grilled sandwich and coffee).

After each 60 hour fast (with or without exposure to visual and odorous food stimuli), an OGTT and fMRI were performed simultaneously. At 7.00 am an intravenous catheter was inserted. Subjects drank 75g of glucose dissolved in 300ml of water. Blood samples were drawn at t=-15, 0, 15, 30, 45, 60, 75, 90, 105 and 120 min. During the OGTT, hypothalamic neuronal activity was measured by fMRI from time -8 till +28 minutes.

Anthropomorphic Measurements, body composition, blood pressure, heart rate
Height, weight, body mass index (BMI), hip and waist circumference were measured according to WHO recommendations. Blood pressure was measured automatically (Omron 705IT, Kyoto, Japan) at the left arm with the subject in supine position after 5 minutes of rest. Heart rate was measured by palpation of a radial artery during one minute (in rest).

Indirect Calorimetry
Subjects were placed under the ventilated hood after 12 and 60 hours of fasting (Oxycon Beta, Mijnhardt Jaegher, Breda, The Netherlands). After voiding, the patient had to lie still with eyes closed, while staying awake, for 30 minutes. Substrate oxidation was calculated from CO_2 and O_2 concentrations in the exhaled air as previously described [12]. If a calculated substrate oxidation value was below zero, we used 0 instead for our statistical analysis.

MRI
fMRI scans were made using a 3.0 Tesla scanner (Philips Achieva; Philips Healthcare, Best, The Netherlands). A 14mm thick midsaggital brain slice was imaged for a total time of 38.2 minutes by T2*-weighted echo-planar imaging (repetition time 120ms, echo time 30ms, flip angle 30^0, scan matrix 256x231, FOV 208x208x14mm, 900 dynamics). We used a multishot EPI sequence with an EPI-factor of 33, with 3 signal averages (nsa). No parallel imaging was used. To diminish rotations during the scanning procedure, each participant's head was fixated with cushions inside the coil

MRI analysis

fMRI data were analyzed using FSL software (FMRIB's Software Library, www.fmrib.ox.ac.uk/fsl) [13;14]. First, imaginary and real images were calculated from the 900 magnitude and corresponding phase images that were acquired. Next, for each participant separately all magnitude images were registered (aligned) to a dynamic image that was acquired shortly after drinking had finished and that showed no motion artifacts (MCFLIRT) [15]. The resulting transformation matrix was then used to register the real and imaginary images (FLIRT). After complex averaging of every 4 images, the real and imaginary data were converted back to magnitude and phase images, resulting in 225 magnitude images to be analyzed. A region of interest was manually drawn in the hypothalamic area to calculate (with the "fslmeants" command) the average hypothalamic signal for all 225 time points. We used the anterior commissure, the mammillary bodies and the optic chiasm as border "points" of the hypothalamic region of interest. The fourth border point was estimated on the virtual square resulting from the three defined points. After drawing the regions of interest, an average was created for each minute that scanning was performed. The signal of each time point was normalized to the averaged pre-drink signal, rendering the relative signal change. The investigator was not blind to the occasion when analyzing the fMRI data, but the only subjective (i.e. not automated) analytical procedure was the definition of the hypothalamic region. Moreover, all analyses were performed twice to minimize observer bias.

Blood chemistry

Serum glucose was measured using a Modular P800 chemistry analyzer of Roche Diagnostics (Mannheim, Germany) with a total coefficient of variation (CV) of 1.7%. Insulin was measured with an immunometric assay on an automated Immulite 2500 (Siemens, Breda, The Netherlands) with an intra-assay CV 6-7.5%. Serum cholesterol, high density lipoprotein (HDL) and triglycerides (TG) were measured with a fully automated P-800 module (Roche, Almere, The Netherlands). For both TG and total cholesterol (TC) the CV was less than 2%. For HDL the CV was less than 3%. Low density lipoprotein (LDL) cholesterol was calculated according to the Friedewald equation. Prolactin, luteinizing hormone (LH) and follicle-stimulating hormone (FSH) were measured using an electrochemoluminescence immunoassay (ECLIA) on a Modular E170 analyzer of Roche Diagnostics. Total CVs were less than 3.5%. Serum growth hormone (GH) was measured with a sensitive immuno-fluorometric assay

(Wallac, Turku, Finland), specific for the 22-kDA GH protein, calibrated against World Health Organization International Reference Preparation (WHO IRP) 80/505. The detection limit is 0.03 mU/liter; the interassay CV between 2% and 9% for concentrations from 0.25–40 mU/liter. Serum insulin-like growth factor 1 (IGF-1) was measured using an immunometric technique on an Immulite 2500 system (Diagnostic Products Corporation, Los Angeles, CA). The intra-assay CVs were 5.0 and 7.5% at mean plasma levels of 8 and 75 nmol/liter, respectively.

Insulin-like growth factor binding protein 3 (IGFBP-3) was measured using an immunometric technique on an Immulite 2500 system (Diagnostic Products Corporation, Los Angeles, USA). The lower limit of detection was 0.02 mg/l and inter-assay variation was 4.4 and 4.8% at 0.91 and 8.83 mg/l.

Serum free T4 (FT4) and thyroid stimulating hormone (TSH) were measured using a chemoluminescence immunoassay with a Modular Analytics E-170 system (Roche, Almere, The Netherlands). The intra-assay CVs were respectively 1.6-2.2 % and 1.3-5.0 %. Serum triiodothyronine (T3) was measured with a fluorescence polarization Immunoassay on an AxSym system (Abbott, Abbott Park, IL, USA). The CV was 2.5-9.0 %.

Dehydroepiandrosterone (DHEA) was measured by radioimmunoassay (RIA) (DSL, a Beckman Coulter Company). The detection limit was 0.012 µg/liter (0.04 nmol/l); the intra-assay CV was between 5.2% and 10.8%, the interassay CV between 5.9% and 11.7%.

Testosterone was determined by a direct RIA of Siemens Healthcare Diagnostics, total CV was approximately 15%.

Sex hormone-binding globulin (SHBG) was measured on an automated Immulite 2500 (Siemens, Breda, The Netherlands) with a total CV of 8%.

Cortisol was measured using a chemoluminescence immunoassay on a Modular Analytics E-170 system (Roche, Almere, The Netherlands). Total CV was less than 3.5 % for levels between 0.19 and 1.08 µmol/L.

Statistics

The differences between values before and after interventions were statistically evaluated by two-sided paired Student's t-tests. The impact of food cues on the response to nutrient deprivation was evaluated by subtracting values obtained after intervention from those obtained before, yielding 'delta' values. The difference between deltas observed during fasting with vs. without stimuli was subsequently evaluated by two-

6

sided paired Student's t-test. BOLD signals were averaged per minute and subsequently evaluated statistically by repeated measures ANOVA and post hoc tested with pairwise comparisons. All statistics were performed with SPSS for Windows version 16.0 (SPSS Inc., Chicago, IL, United States of America).

6

Results

Anthropometric Measurements, heart rate & blood pressure

Body weight, BMI, hip circumference and lean body mass, were diminished to a similar extent by the prolonged fast with and without exposure to food-related stimuli (Table 1). Heart rate diminished significantly during fasting without stimuli, whereas heart rate increased when food-related stimuli were given during the fast (delta heart rate -7.3 ± 3.9 after fasting without stimuli versus 1.4 ± 3.8 after fasting with stimuli, p=0.041). The prolonged fast did not significantly alter blood pressure (Table 1).

Table 1 Anthropomorphic and Cardiovascular Measurements‡

	Before starvation without stimuli	After starvation without stimuli	Before starvation with stimuli	After starvation with stimuli
Age	22.3 ± 0.8			
Length (cm)	183 ± 2			
Body weight (kg)	75.8 ± 2.3	73.0 ± 2.2 *	75.8 ± 2.1	72.8 ± 2.1 *
BMI (kg/m^2)§	22.5 ± 0.5	21.7 ± 0.5 *	22.5 ± 0.5	21.6 ± 0.5 *
Heart Rate (bpm)	76 ± 4	69 ± 3	66 ± 3	67 ± 4
Delta Heart Rate (bpm)		-7,3 ± 3,9		1,4 ± 3,8 **
Systolic Blood pressure (mmHg)	139 ± 4	143 ± 3	138 ± 4	141 ± 6
Diastolic Blood pressure (mmHg)	78 ± 2	76 ± 2	77 ± 2	73 ± 2

‡ data are depicted as mean ± SEM (standard error of the mean)
§ BMI: body mass index
* is significantly (p<0.05) different before and after the starvation intervention
** is significantly (p<0.05) different between the two starvation paradigms
There are no significant differences between the different (with and without stimuli) starvation paradigms.

Lipids and hormones in plasma

Plasma levels of cholesterol, triglycerides and the cholesterol/HDL ratio significantly increased, whereas HDL-cholesterol decreased significantly and equally after 60 hours of food abstinence with or without stimuli. LDL-cholesterol only increased significantly after fasting without stimuli. Plasma TSH and T3 levels decreased, whereas T4 levels remained unchanged in response to the prolonged fast (Table 4). Plasma levels of LH, FSH and testosterone decreased significantly, whereas SHBG levels increased (Table 4).

Table 2 Results of OGTT: measurements of glucose, insulin and C-peptide at baseline and after the interventions[‡]

	Baseline[#]	Starvation without stimuli after intervention	Starvation with stimuli after intervention
Glucose (mmol/l)	5.20 ± 0.09	3.69 ± 0.13*	3.67 ± 0.10*
Insulin (mU/l)	4.33 ± 0.56	2.33 ± 0.19*	2.08 ± 0.08*
AUC glucose	1068 ±44	1481± 51**	1455 ± 41**
AUC insulin	3959 ± 312	8472 ± 1376**	8042 ± 1202**
Time to peak glucose	51 ± 8	101 ± 8*	104 ± 7*
Time to peak insulin	75 ± 9	113 ± 6*	120 ± 6*

‡ data are depicted as mean ± SEM (standard error of the mean)
# as measured at screening after an overnight fast
* is significantly (p<0.025) different from baseline
** is significantly (p<0.01) different from baseline
There are no significant differences between the different (with and without stimuli) starvation paradigms.

Prolactin, cortisol and IGFBP-3 levels remained unaltered. The concentrations of 2 hormones were altered significantly only in response to fasting without stimuli: DHEA levels increased, whereas IGF-1 levels decreased in this experimental context. However, the difference in response between fasting with and without food cues did not reach statistical significance for either hormone.

Oral glucose tolerance test (OGTT)

Plasma glucose and insulin concentrations reduced considerably upon prolonged fasting (Table 2). In contrast, the fast significantly increased the areas under the curves of plasma glucose and insulin concentrations in response to glucose ingestion (Figure 1). The times to peak of plasma glucose and insulin concentrations were delayed by nutrient deprivation. Exposure to odorous food cues during the prolonged fast did not affect any of these metabolic adaptations.

fMRI

The hypothalamic blood oxygenation level dependent (BOLD) signal, expressed as percentage of the averaged pre-drink values, was reduced in response to glucose ingestion compared to baseline (at several time points to a significant extent, particularly during the first 20 minutes after ingestion), irrespective of exposure to food cues during the prolonged fast (Figure 2). The prolonged fast *with stimuli* induced significant differences compared to baseline at minutes 4 (p<0.001), 9 (p=0.033), 16
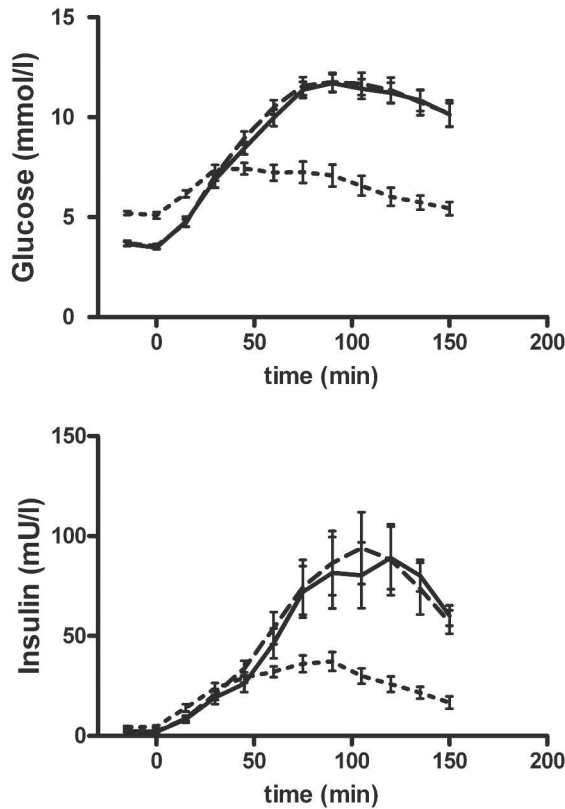
Figure 1: Plasma glucose and insulin concentrations in response to an oral glucose load at baseline and after the interventions
The dotted line represents baseline levels, the thick dotted line represents levels after the prolonged fast without stimuli and the continuous line represents levels after the prolonged fast with stimuli.

(p=0.025), 20 (p=0.025) and 27 (p=0.031). The prolonged fast *without stimuli* induced significant differences when compared to baseline at minutes 4 (p=0.012), with trends at minutes 7 (p=0.053), 20 (p=0.060), 25 (p=0.056), 26 (p=0.055). Repeated analysis confirmed these results (data not shown).

Indirect Calorimetry
Prolonged fasting significantly decreased glucose oxidation and increased lipid oxidation. There were no significant differences between the fasting paradigms (Table 3). Prolonged fasting increased resting energy expenditure significantly and consistently, irrespective of the exposure to food cues.
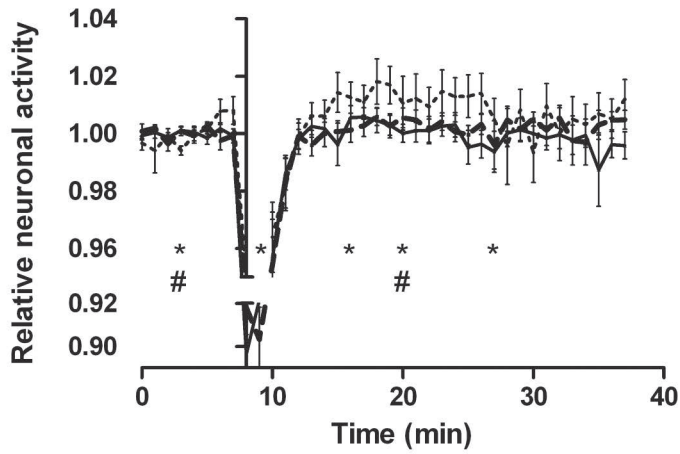
Figure 2: Hypothalamic neuronal activity in response to glucose intake at time 0 minutes as measured by functional MRI

Relative neuronal hypothalamic activity measured before and after the OGTT (started at t=8min), % change to pre-drink average is depicted.

* The prolonged fast with stimuli (continuous line) showed significant differences when compared to baseline (dotted line) at minutes 4 (p=0.000), 9 (p=0.033), 16 (p=0.025), 20 (p=0.025) and 27 (p=0.031).

The prolonged fast without stimuli (thick dotted line) showed significant differences when compared to baseline (dotted line) at minutes 4 (p=0.012), with trends at minutes 7 (p=0.053), 20 (p=0.060), 25 (p=0.056) and 26 (p=0.055)

6

Table 3 Substrate oxidation rates at baseline and after 3 days of starvation with or without the presence of food-related stimuli‡

	Before starvation without stimuli	After starvation without stimuli	Before starvation with stimuli	After starvation with stimuli
Glucose Oxidation (μmol/kg$_{FFM}$/min)	12.3 ± 1.5	7.9 ± 2.3$^{\alpha}$	12.6 ± 2.6	4.0 ± 1.0*
Lipid Oxidation (μmol/kg$_{FFM}$/min)	1.4 ± 0.1	2.3 ± 0.3*	1.5 ± 0.2	2.7 ± 0.3*
Resting Energy Expenditure (kcal/day)	1631 ± 51	1829 ± 71*	1696 ± 51	1895 ± 103*
Resting Energy Expenditure (kcal/day/LBM)	25.6 ± 0.7	30.5 ± 0.9*	27.2 ± 0.7	31.9 ± 1.3*

‡ data are depicted as mean ± SEM (standard error of the mean)
$^{\alpha}$ p=0.076
* is significantly (p<0.05) different before and after the starvation intervention
There are no significant differences between the different (with and without stimuli) starvation paradigms.

6

Table 4 Plasma metabolites and hormones at baseline and after the interventions‡

	Before starvation without stimuli	After starvation without stimuli	Before starvation with stimuli	After starvation with stimuli
Total cholesterol (mmo/l)	4.22 ± 0.18	4.42 ± 0.20 *	4.25 ± 0.18	4.39 ± 0.19
Triglycerides (mmol/l)	0.94 ± 0.08	1.33 ± 0.11 *	0.98 ± 0.13	1.36 ± 0.11 *
HDL (mmol/l)	1.42 ± 0.08	1.25 ± 0.07 *	1.43 ± 0.06	1.25 ± 0.06 *
Cholesterol/HDL	3.06 ± 0.19	3.63 ± 0.19 *	3.05 ± 0.22	3.58 ± 0.23 *
LDL (mmol/l)	2.38 ± 0.15	2.58 ± 0.19 *	2.38 ± 0.21	2.54 ± 0.21
FT4 (nmol/l)	16.53 ± 0.60	16.60 ± 0.70	16.67 ± 0.37	17.18 ± 0.60
T3 (nmol/l)	1.82 ± 0.08	1.14 ± 0.08 *	1.91 ± 0.06	1.28 ± 0.04 *
TSH (mU/l)	2.92 ± 0.54	1.26 ± 0.19 *	2.47 ± 0.37	1.25 ± 0.18 *
Prolactin (μg/l)	13.4 ± 1.25	14.18 ± 2.79	10.93 ± 1.66	11.23 ± 1.59
DHEA (nmol/l)	10.20 ± 0.78	12.30 ± 1.26 *	11.99 ± 1.56	12.88 ± 1.31
hGH (mU/l)	4.63 ± 3.25	11.74 ± 5.19	2.11 ± 1.23	7.97 ± 2.38 [α]
IGF-1 (nmol/l)	27.30 ± 1.46	23.01 ± 1.40 *	25.05 ± 2.99	23.79 ± 1.59
IGFBP-3 (mg/l)	4.32 ± 0.18	4.33 ± 0.31	6.72 ± 2.74	4.18 ± 0.28
Cortisol (μmol/l)	0.51 ± 0.03	0.55 ± 0.04	0.53 ± 0.04	0.49 ± 0.05
FSH (U/l)	4.0 ± 0.6	3.2 ± 0.5*	4.1 ± 0.6	3.3 ± 0.5*
LH (U/l)	5.0 ± 0.3	3.3 ± 0.4*	5.1 ± 0.2	3.2 ± 0.4*
SHBG (nmol/l)	25.3 ± 1.9	28.3 ± 2.1*	24.7 ± 1.8	28.0 ± 1.7*
Testosterone (nmol/l)	28 ± 2.5	14.4 ± 1.8*	27 ± 1.6	14.7 ± 1.3*

‡ data are depicted as mean ± SEM (standard error of the mean)
* is significantly (p<0.05) different before and after the starvation intervention
[α] p= 0.06
There are no significant differences between the different (with and without stimuli) starvation paradigms.

6

Discussion

This study shows that 60 hours of food deprivation in healthy young men 1) alters the hypothalamic BOLD signal in response to glucose ingestion; 2) induces profound glucose intolerance; 3) down-regulates the pituitary-thyroid and pituitary-gonadal axes; and 4) increases resting metabolic rate. Exposure to (attractive) visual and odorous food cues does not alter any of these metabolic and neuroendocrine adaptations to nutrient deprivation.

This is the first study to show that prolonged fasting alters the BOLD signal produced by the hypothalamus in response to an oral glucose load in healthy humans. Since BOLD signals reflect neuronal activity [16], the data suggest that a prolonged fast renders the hypothalamic neurons relatively insensitive to glucose ingestion. It is conceivable that alterations of hypothalamic neuronal activity are an integral part of the systemic adaptations required for survival during nutrient deprivation. The hypothalamus plays a critical role in the control of (postprandial) metabolism; it integrates metabolic and hormonal cues reflecting the bodily energy status to produce neuroendocrine output, adapting energy metabolism accordingly [17]. For example, neuropeptide Y (NPY, a well-known orexigenic neuropeptide) gene expression is strongly up-regulated in the arcuate nucleus and paraventricular nucleus of fasting rhesus macaque monkeys and food-restricted type I diabetic rats [18;19]. Hypothalamic NPY induces hepatic insulin resistance via activation of sympathetic neural efferents [20]. Other hypothalamic neuronal circuits are also sensitive to nutritional cues and contribute to proper (postprandial) metabolic control [21]. Therefore, the neuronal changes in response to nutrient deprivation we observed here may be involved in the physiology of the glucose intolerance of our fasting volunteers. Insulin resistance is an appropriate metabolic adaptation to nutrient deprivation, as it renders incidentally consumed glucose available for combustion by the brain (which is largely dependent on glucose as fuel). Since nutrients tend to modulate hypothalamic neural circuits so as to reinforce insulin action [22], resistance to the neuronal effects of nutrient ingestion may be advantageous in terms of brain energetics and survival during prolonged periods of food deprivation.

The greatest effect of the oral glucose tolerance test on plasma values of glucose and insulin are seen at 50 and 75 minutes after glucose ingestion respectively,

6

whereas fMRI signals respond within 10-20 minutes (table 2, figure 1). These observations suggest that neither plasma glucose nor insulin is involved in the neuronal response to glucose ingestion. This inference is supported by previous work suggesting that neuronal signals emanating from the gut rather than plasma metabolite concentrations are critical for the hypothalamic response to nutrient ingestion [23].

Although we have used fMRI to quantify hypothalamic neuronal activity in similar experimental settings before [11], it seems important to note that the use of this imaging technique to measure neuronal activity in response to a single (non-iterative) stimulus is relatively uncommon and bears some difficulties. Perhaps the most important pitfall in our analysis is the rather subjective determination of the region of interest (designating the hypothalamus in the current study): small differences may significantly impact the average signal. To preclude observer bias as much as possible, the same author (M.A.W.), performed all analyses of BOLD signal changes twice, yielding similar results.

The fall of circulating triiodothyronine and TSH levels in the face of relatively stable free T4 concentrations are typical physiological adaptations of the pituitary-thyroid axis to short term fasting in humans [24;25]. These changes, which may serve to dampen basal energy expenditure, partly result from an adaptive mechanism driven by diminished activity of leptin sensitive hypothalamic TRH neurons [25]. However, despite these apparent effects of nutrient deprivation on thyroid axis activity, 60 hours of fasting paradoxically *increased* resting energy expenditure by ~11% in our volunteers. We are not the first to report this counterintuitive observation: a few previous studies similarly showed that the resting metabolic rate (RMR) of healthy humans is increased by 6 and 4% after 36 or 48 hours of food deprivation respectively [24;26]. The increase in RMR during short-term fasting might be due to the energy costs of a temporary increase in gluconeogenesis and ketogenesis [24]. Activation of the sympathetic nervous system may modify RMR during prolonged fasting [27]. In apparent contrast, RMR is clearly reduced after longer term calorie restriction and weight loss in obese humans [28], but this is probably due to the significant loss of lean body mass in this context [29].

Plasma levels of FSH, LH and testosterone significantly decreased upon fasting, while SHBG concentrations increased, which confirms the findings of other studies [30]. Long

term dietary restriction over the course of years also down-regulates the pituitary-gonadal axis in members of the Calorie Restriction Society [31]. These endocrine adaptations probably serve to postpone reproduction until food is available again. Reduction of plasma leptin levels may be mechanistically involved, since leptin administration during a prolonged fast prevents changes in testosterone levels (but not LH and SHBG) in healthy men [25].

We also show that fasting increases circulating dehydroepiandrosterone (DHEA) levels (significantly in the group that was not exposed to food-related stimuli). DHEA and its sulfate ester DHEAS are markers of human aging, since these adrenal steroids reach peak levels in the second decade of life and then gradually decline [32]. Moreover, high plasma DHEA concentrations correlate with longevity and survival in men but not in women [33]. DHEA may have beneficial effects on inflammation, cell growth, oxidative stress, carcinogenesis and atherosclerosis, possibly via inhibition of glucose-6-phosphate dehydrogenase [34]. However, longer term restriction of calories has been reported to leave plasma DHEA(S) concentrations unaffected in humans [31] and DHEAS supplements fail to extend lifespan or prevent chronic disease in rodents [35]. Therefore, the biological significance of the rise of plasma DHEA level we observed is uncertain. We did not find an effect of the prolonged-fast on cortisol levels, which may have been caused by the relatively high levels of cortisol at baseline, perhaps induced by stress due to the insertion of the intravenous catheter.

Exposure to odorous and visual food cues did not modify any of the above mentioned metabolic and neuroendocrine adaptations to a prolonged fast. It may be that olfactory cues do not impact on neuroregulatory mechanisms in humans. The olfactory system in higher mammals, including humans, comprises the olfactory bulb, the orbitofrontal cortex and the hypothalamus among other tertiary relay stations. A small number of *in vivo* fMRI studies show that odorous stimuli can alter hypothalamic neuronal activity in humans [6]. In our study, the presence of olfactory stimuli during fasting did not alter hypothalamic neuronal activity in response to a subsequent oral glucose load (during which no visual or odorous cues were offered). Although intuitively unlikely, the exposure time (9.5h/day in total) we used may have been too short or the intensity of the odors may have been too weak to bring about significant effects. Furthermore, the impact of fasting on the regulation of metabolism may be too strong to allow significant effects of modulatory processes of lesser power. Indeed, the evidence in lower organisms indicates that olfactory cues restrain the beneficial corol-

6

laries of calorie restriction, not total starvation. Accordingly, *Drosophila* species were calorie restricted, not starved, in the study by Libert *et al.* [3] In yeast (*Saccharomyces cerevisiae*), severe calorie restriction engages regulatory pathways to extend life span fundamentally different from those activated by more modest restriction [36;37]. In analogy, in humans (obese humans, we are unaware of studies in lean humans), modest restriction of calories does not affect insulin action in the short term [38], whereas total fasting considerably hampers insulin action in a similar timeframe [39], suggesting that the degree of dietary restriction differentially affects regulatory mechanisms in humans as well. Thus, in contrast to calorie restriction, fasting may be too strong a stimulus for metabolic adaptation to allow olfactory cues to modulate the changes.

In conclusion, prolonged fasting changes the hypothalamic neuronal response to glucose ingestion in healthy normal weight humans, which may guide postprandial endocrine and metabolic adaptations to nutrient deprivation that are meant to shunt any incidentally consumed carbohydrates towards the brain. Indeed, 60 hours of total nutrient deprivation elicits profound glucose intolerance, most likely because it hampers insulin action. Prolonged fasting also down-regulates the pituitary-gonadal and -thyroid axes, probably to appropriately adapt fecundity and energy expenditure to nutrient scarcity. Food-related olfactory cues do not modulate these neuroendocrine and metabolic adaptations to a prolonged fast in humans.

Acknowledgements

6

References

1. Fontana L, Partridge L, Longo VD. Extending healthy life span—from yeast to humans. *Science* 2010; 328(5976): 321-326.

2. Bishop NA, Guarente L. Genetic links between diet and lifespan: shared mechanisms from yeast to humans. *Nat Rev Genet* 2007; 8(11): 835-844.

3. Libert S, Zwiener J, Chu X, Vanvoorhies W, Roman G, Pletcher SD. Regulation of Drosophila life span by olfaction and food-derived odors. *Science* 2007; 315(5815): 1133-1137.

4. Alcedo J, Kenyon C. Regulation of C. elegans longevity by specific gustatory and olfactory neurons. *Neuron* 2004; 41(1): 45-55.

5. Keverne EB. The vomeronasal organ. *Science* 1999; 286(5440): 716-720.

6. Wang J, Eslinger PJ, Smith MB, Yang QX. Functional magnetic resonance imaging study of human olfaction and normal aging. *J Gerontol A Biol Sci Med Sci* 2005; 60(4): 510-514.

7. Lam CK, Chari M, Lam TK. CNS regulation of glucose homeostasis. *Physiology (Bethesda)* 2009; 24:159-70.: 159-170.

8. Schur EA, Kleinhans NM, Goldberg J, Buchwald D, Schwartz MW, Maravilla K. Activation in brain energy regulation and reward centers by food cues varies with choice of visual stimulus. *Int J Obes (Lond)* 2009; 33(6): 653-661.

9. Matsuda M, Liu Y, Mahankali S, Pu Y, Mahankali A, Wang J, DeFronzo RA, Fox PT, Gao JH. Altered hypothalamic function in response to glucose ingestion in obese humans. *Diabetes* 1999; 48(9): 1801-1806.

10. Liu Y, Gao JH, Liu HL, Fox PT. The temporal response of the brain after eating revealed by functional MRI. *Nature* 2000; 405(6790): 1058-1062.

11. Vidarsdottir S, Smeets PA, Eichelsheim DL, van Osch MJ, Viergever MA, Romijn JA, van der GJ, Pijl H. Glucose ingestion fails to inhibit hypothalamic neuronal activity in patients with type 2 diabetes. *Diabetes* 2007; 56(10): 2547-2550.

12. Simonson DC, DeFronzo RA. Indirect calorimetry: methodological and interpretative problems. *Am J Physiol* 1990; 258(3 Pt 1): E399-E412.

13. Smith SM, Jenkinson M, Woolrich MW, Beckmann CF, Behrens TE, Johansen-Berg H, Bannister PR, De LM, Drobnjak I, Flitney DE, Niazy RK, Saunders J, Vickers J, Zhang Y, De SN et al. Advances in functional and structural MR image analysis and implementation as FSL. *Neuroimage* 2004; 23 Suppl 1:S208-19.: S208-S219.

6

14. Woolrich MW, Jbabdi S, Patenaude B, Chappell M, Makni S, Behrens T, Beckmann C, Jenkinson M, Smith SM. Bayesian analysis of neuroimaging data in FSL. *Neuroimage* 2009; 45(1 Suppl): S173-S186.

15. Jenkinson M, Bannister P, Brady M, Smith S. Improved optimization for the robust and accurate linear registration and motion correction of brain images. *Neuroimage* 2002; 17(2): 825-841.

16. Ogawa S, Lee TM, Kay AR, Tank DW. Brain magnetic resonance imaging with contrast dependent on blood oxygenation. *Proc Natl Acad Sci U S A* 1990; 87(24): 9868-9872.

17. Schwartz MW, Woods SC, Porte D, Jr., Seeley RJ, Baskin DG. Central nervous system control of food intake. *Nature* 2000; 404(6778): 661-671.

18. Grove KL, Chen P, Koegler FH, Schiffmaker A, Susan SM, Cameron JL. Fasting activates neuropeptide Y neurons in the arcuate nucleus and the paraventricular nucleus in the rhesus macaque. *Brain Res Mol Brain Res* 2003; 113(1-2): 133-138.

19. McKibbin PE, McCarthy HD, Shaw P, Williams G. Insulin deficiency is a specific stimulus to hypothalamic neuropeptide Y: a comparison of the effects of insulin replacement and food restriction in streptozocin-diabetic rats. *Peptides* 1992; 13(4): 721-727.

20. van den Hoek AM, van HC, Schroder-van der Elst JP, Ouwens DM, Havekes LM, Romijn JA, Kalsbeek A, Pijl H. Intracerebroventricular administration of neuropeptide Y induces hepatic insulin resistance via sympathetic innervation. *Diabetes* 2008; 57(9): 2304-2310.

21. Hillebrand JJ, de WD, Adan RA. Neuropeptides, food intake and body weight regulation: a hypothalamic focus. *Peptides* 2002; 23(12): 2283-2306.

22. Heijboer AC, Pijl H, van den Hoek AM, Havekes LM, Romijn JA, Corssmit EP. Gut-brain axis: regulation of glucose metabolism. *J Neuroendocrinol* 2006; 18(12): 883-894.

23. Smeets PA, Vidarsdottir S, de GC, Stafleu A, van Osch MJ, Viergever MA, Pijl H, van der GJ. Oral glucose intake inhibits hypothalamic neuronal activity more effectively than glucose infusion. *Am J Physiol Endocrinol Metab* 2007; 293(3): E754-E758.

24. Webber J, Macdonald IA. The cardiovascular, metabolic and hormonal changes accompanying acute starvation in men and women. *Br J Nutr* 1994; 71(3): 437-447.

6

25. Chan JL, Heist K, DePaoli AM, Veldhuis JD, Mantzoros CS. The role of falling leptin levels in the neuroendocrine and metabolic adaptation to short-term starvation in healthy men. *J Clin Invest* 2003; 111(9): 1409-1421.

26. Mansell PI, Macdonald IA. The effect of starvation on insulin-induced glucose disposal and thermogenesis in humans. *Metabolism* 1990; 39(5): 502-510.

27. Chan JL, Mietus JE, Raciti PM, Goldberger AL, Mantzoros CS. Short-term fasting-induced autonomic activation and changes in catecholamine levels are not mediated by changes in leptin levels in healthy humans. *Clin Endocrinol (Oxf)* 2007; 66(1): 49-57.

28. Leibel RL, Rosenbaum M, Hirsch J. Changes in energy expenditure resulting from altered body weight. *N Engl J Med* 1995; 332(10): 621-628.

29. Speakman JR, Westerterp KR. Associations between energy demands, physical activity, and body composition in adult humans between 18 and 96 y of age. *Am J Clin Nutr* 2010; 92(4): 826-834.

30. Bergendahl M, Aloi JA, Iranmanesh A, Mulligan TM, Veldhuis JD. Fasting suppresses pulsatile luteinizing hormone (LH) secretion and enhances orderliness of LH release in young but not older men. *J Clin Endocrinol Metab* 1998; 83(6): 1967-1975.

31. Cangemi R, Friedmann AJ, Holloszy JO, Fontana L. Long-term effects of calorie restriction on serum sex hormone concentrations in men. *Aging Cell* 2010; %20.

32. Orentreich N, Brind JL, Rizer RL, Vogelman JH. Age changes and sex differences in serum dehydroepiandrosterone sulfate concentrations throughout adulthood. *J Clin Endocrinol Metab* 1984; 59(3): 551-555.

33. Mazat L, Lafont S, Berr C, Debuire B, Tessier JF, Dartigues JF, Baulieu EE. Prospective measurements of dehydroepiandrosterone sulfate in a cohort of elderly subjects: relationship to gender, subjective health, smoking habits, and 10-year mortality. *Proc Natl Acad Sci U S A* 2001; 98(14): 8145-8150.

34. Schwartz AG, Pashko LL. Dehydroepiandrosterone, glucose-6-phosphate dehydrogenase, and longevity. *Ageing Res Rev* 2004; 3(2): 171-187.

35. Pugh TD, Oberley TD, Weindruch R. Dietary intervention at middle age: caloric restriction but not dehydroepiandrosterone sulfate increases lifespan and lifetime cancer incidence in mice. *Cancer Res* 1999; 59(7): 1642-1648.

36. Lin SJ, Defossez PA, Guarente L. Requirement of NAD and SIR2 for life-span extension by calorie restriction in Saccharomyces cerevisiae. *Science* 2000; 289(5487): 2126-2128.

6

37. Kaeberlein M, Powers RW, III, Steffen KK, Westman EA, Hu D, Dang N, Kerr EO, Kirkland KT, Fields S, Kennedy BK. Regulation of yeast replicative life span by TOR and Sch9 in response to nutrients. *Science* 2005; 310(5751): 1193-1196.

38. Jazet IM, Pijl H, Frolich M, Romijn JA, Meinders AE. Two days of a very low calorie diet reduces endogenous glucose production in obese type 2 diabetic patients despite the withdrawal of blood glucose-lowering therapies including insulin. *Metabolism* 2005; 54(6): 705-712.

39. DeFronzo RA, Soman V, Sherwin RS, Hendler R, Felig P. Insulin binding to monocytes and insulin action in human obesity, starvation, and refeeding. *J Clin Invest* 1978; 62(1): 204-213.

6

Chapter 7

Discussion

7

The prevalence of obesity has been increasing now for several decades [1]. Obesity is associated with an increased morbidity and an increased risk for type 2 diabetes mellitus, cardiovascular disease and cancer. To date, there is no effective non-invasive treatment for obesity. Lifestyle interventions often fail in the long run. Therefore, a better understanding of the (patho)physiological alterations that occur in patients with obesity will be useful for the development of adequate therapies. Besides, this could lead to a decrease in the stigmatization of obesity. Finally, a better understanding of this disease could lead to an improved political recognition of this problem that cannot simply be solved on an individual level.

Seemingly paradoxical, studying the physiology of fasting might contribute to a better understanding of obesity pathology. Fasting has profound effects on metabolism. The plasma levels of several hormones decrease, lipid oxidation increases, liver glycogen stores get depleted and insulin resistance develops [2-4]. In skeletal muscle, energy-sensing factors react to maintain homeostasis. A better understanding of the function of these energy-sensing factors, and the possible differences between lean and obese subjects, might lead to new targets for the treatment of obesity. With respect to energy sensing, we mainly focused on the AMP-activated kinase (AMPK). This enzyme is activated by upstream liver kinase B1 (LKB1) in response to the increased AMP/ATP ratio caused by energy depletion [5].

In this thesis, we compared the skeletal muscle, neuroendocrine, autonomic nervous system and metabolic adaptations to a 48 hour fast in obese compared to lean subjects. Besides, we investigated the time course of adaptations to a 24 hour fast in healthy young men. Finally, we performed an experimental study to determine whether the presence of odors would affect the hormonal and neuronal adaptations to a 60 hour fast.

7

COMPARING THE RESPONSE TO A 48 HOUR FAST BETWEEN LEAN AND OBESE SUBJECTS

Skeletal muscle

In **chapter two**, we hypothesized that the whole-body and skeletal muscle metabolic adaptations to a 48 hour fast would be different between lean and obese individuals. More specifically, we hypothesized that AMPK phosphorylation would be increased after 48 hours of fasting and that the increase would be attenuated in obese subjects. In contrast to our expectations we found that AMPK was slightly but significantly reduced after the 48 hour fast, but only in lean individuals. As expected from previous studies, we did demonstrate that the response of insulin, leptin, growth hormone and substrate oxidation to the fast is attenuated in obese subjects. Indeed, obese subjects are characterized by metabolic inflexibility [6]. We also found that the expression of mitochondrial respiratory-chain protein subunits was significantly reduced in obese individuals. This might have a causal link with the reduced metabolic flexibility in obese individuals. Future studies are necessary to determine the precise role of AMPK and the molecular pathways of the mitochondrial protein downregulation in the metabolic inflexibility that exists in obese subjects.

Heart rate variability

In **chapter three**, we describe the effects of a 48 hour fast on heart rate variability (HRV) parameters in lean and obese subjects. Heart rate variability is under control of the autonomic nervous system [7] and has been shown to be decreased in obesity, mainly due to an increase in sympathetic nervous system (SNS) activity [8]. Fasting has previously shown to increase SNS activity [9;10].

Contrasting our expectations, we did not observe any differences in HRV between lean and obese subjects at baseline. This may be due to our study design; we performed HRV measurements in the postprandial state (75 minutes after a standardized breakfast), which might have affected HRV, since meal ingestion increases the sympathetic tone [11;12]. We demonstrated that fasting decreased both vagal tone as well as the sympathetic tone in the lean subjects. In obese subjects, the fast induced a slightly smaller decrease in vagal tone and in fact increased the sympathetic tone. However, the differences between groups did not reach statistical significance. Finally

7

we show that the 8 week weight-loss intervention increased the postprandial sympathetic tone in the obese subjects. Taken together, our results suggest that the response to fasting might be attenuated in obese subjects but since statistical analysis of the difference of this response between groups did not reach significance our study may have been underpowered. Finally we showed that weight-loss increased the sympathetic response to meal ingestion. Future studies are necessary to investigate how long this adaptation is maintained and what the physiological meaning is.

Neuronal; functional magnetic resonance imaging

The effects of a 48 hour fast on three different "functional connectivity" brain networks, supposedly involved in the control of energy metabolism and mapped by functional magnetic resonance imaging (fMRI), were studied in 12 lean and 12 obese individuals. The results of this study are described in **chapter four**. fMRI scans were made at baseline (after an overnight fast) and after 48 hours of fasting. Functional connectivity (FC) is used to study how different brain regions interact. It can be either 'positive' or 'negative' [13;14]. FC is considered positive when brain regions show a similar response (increase or decrease) simultaneously. FC is considered negative when brain regions show an opposite neuronal response at the same time (one region increases activity whereas the other decreases neuronal activity or vice versa). We studied FC networks of the amygdala, the posterior cingulate cortex (PCC, default-mode network) and most importantly the hypothalamus. At baseline, lean individuals demonstrated increased amygdala functional connectivity with the ventromedial prefrontal cortex (vmPFC) and the superior temporal gyrus. Mainly the vmPFC is of interest, since previous studies suggest that this region might be involved in reward sensation [15]. Notably, the response to fasting in amygdala connectivity was not significantly different between groups.

PCC connectivity (default-mode network) with the brainstem was stronger in lean subjects, whereas PCC connections with the bilateral frontal opercular cortices, extending into the insula, were stronger in obese individuals at baseline possibly reflecting alterations in satiety/gustation [16;17]. PCC connectivity in response to fasting was not significantly different between groups.

Our most important findings were in hypothalamic connectivity. Connectivity between hypothalamus and left insula decreased to a greater extent in response to fasting in the obese subjects. This effect is probably the result of a (non-significant) stronger

7

connectivity with the left insula in the obese subjects at baseline. Furthermore, we found that the connectivity between the hypothalamus and the dACC turned from negative to positive in lean subjects, whereas it turned from positive to negative in the obese subjects upon fasting. Since the hypothalamus, insula and dACC are all part of the so-called 'salience' network [18] which has been proposed to perceive both internal and external cues to adapt behavior and/or physiology accordingly [19]. This possibly difference in the salience network's response to fasting may indicate a different neuronal perception of calorie-imbalance between lean and obese subjects. However, before strong conclusions are drawn, the physiological and behavioral ramifications need to be established.

In **chapter five**, we investigated the effects of 24 hours of fasting on skeletal muscle in healthy young individuals on three different time points. We found that the well-known shift from glucose towards lipid oxidation and the downregulation of insulin levels coincided with a decreased activation state of PKB/Akt and mTOR pathways in skeletal muscle. We had expected that AMPK, as an important energy sensor, would be activated upon fasting. However, AMPK activity was not affected at any of the studied time points. We cannot rule out that AMPK is activated at an earlier moment after meal termination (at the beginning of the fast). Future studies are therefore necessary to identify if and exactly when AMPK is activated upon fasting/ meal termination. On our skeletal muscle biopsies, transcriptome analysis identified 23 genes that were significantly affected by fasting at both 10 and 24 hours of fasting. Some of these genes had already previously been shown to be up (ANGPLT4, CITED2, PDK4, PFKFB3, TXNIP and UCP3) or down-regulated (SLC25A25) in response to fasting and are probably implicated in the shift from glucose to lipid oxidation. With respect to several other genes, results have to be confirmed in other studies and their precise role has to be elucidated since only few previous data is available.

THE EFFECTS OF ODORS ON METABOLIC, HORMONAL AND NEURONAL ADAPTATIONS TO A 60 HOUR FAST

In **chapter six** we translated a study performed in *Drosophila Melanogaster* to humans. Libert et al. showed that the caloric restriction induced increase in life span was attenuated when fruit flies were exposed to food odors during caloric restriction [20]. Food odors have been shown to impact on hypothalamic function in humans. We

hypothesized that the human adaptations to a short-term fast would be affected by the presence of food odors during fasting. We were mainly interested whether the hypothalamic response, measured by fMRI, to glucose ingestion would be affected. To study this hypothesis, we exposed 12 healthy young men to a 60 hour fast on two occasions in random order. During one fasting intervention, the volunteers were refrained from visual and odorous food cues. During the second fasting intervention volunteers were exposed to visual and odorous food stimuli at regular time points.

In contrast with our expectations, we found that the hypothalamic signal was similar between the fasting conditions. The well-known downregulation of pituitary-hypothalamus and pituitary-gonadal axes upon fasting was also similar in both conditions. Finally, the development of insulin resistance (another well-known effect of fasting) was not affected by the presence of food cues. In summary, the presence of odors during a short-term fast did neither affect the hypothalamic signal nor the hormonal and metabolic adaptations that occur in response to fasting.

OVERALL CONCLUSIONS

In this thesis we examined the hormonal; metabolic; molecular and neuronal effects of fasting in both lean and obese individuals. As expected, fasting induced a shift from glucose towards lipid oxidation. As expected, both the hormonal response as well as the metabolic shift from glucose towards lipid oxidation was impaired in obese individuals. With respect to the molecular pathways we investigated, our most striking finding was that – at baseline - the mitochondrial protein content in skeletal muscle of obese subjects was significantly reduced when compared to that of lean individuals.

The shift towards fat oxidation coincided with a time-dependent decrease in hormonal levels of insulin as well as a decreased activation state of PKB/Akt and mTOR pathways in skeletal muscle of lean young men. Interestingly, AMPK – an important energy-sensing kinase - was not affected by 24 hours of fasting. However, we found a trend ($p=0.08$) for a decreased AMPK activity and its downstream target ACC upon 48 hours of fasting in the lean subjects but not in obese subjects. Since this finding did not reach significance, it needs to be confirmed and further investigated in future studies.

We also assessed the neuronal response to fasting by performing fMRI scanning. We demonstrated that the neuronal response to fasting was significantly different in

7

lean compared to obese individuals in terms of functional connectivity between the hypothalamus and respectively the dACC and insula. Since these regions are part of the saliency network, these differences may reflect distinct perception of calorie-imbalance between lean and obese subjects. The physiological and behavioral implications of this finding need to be established.

Then, the effects of fasting on sympathetic tone (estimated by heart rate variability) were studied. Our data suggests that fasting decreases sympathetic tone in lean subjects, whereas it increases sympathetic activity in obese individuals. However, the group interaction statistic test did not reach significance. We also showed that weight-loss in the obese individuals significantly increased HRV parameters that reflect the postprandial sympathetic tone.

Finally, we studied the effects of fasting in the presence and absence of food-odors since this has been shown to reduce the fasting-induced increase in life span in fruit flies. However, we show that fasting physiology (hormonal, metabolic and neuronal responses) was not affected by the presence of food-related odors in a group of healthy young volunteers.

FUTURE PLANS

Our main plan for the future, directly related to the work described in this thesis, is to study the effects of weight-loss in obese subjects on gene expression as well as on energy-sensing pathways in skeletal muscle. The study design was already described in **chapter three**. Of course it would be interesting to investigate gene expression in this study as well. Besides, we think it would be very interesting to perform a study similar to **chapter five** but with biopsies performed at time points closer to meal termination. We think it is possible that we missed AMPK activation in our studies due to sampling error, we still think it is likely that AMPK is activated during fasting. By studying at earlier time points during fasting we would hope to find exactly when AMPK is activated during fasting.

7

References

1. World Health Organization. Obesity and Overweight, Fact Sheet No 311. 2011.

2. Cahill GF, Jr. Fuel metabolism in starvation. *Annu Rev Nutr* 2006; 26:1-22.: 1-22.

3. Heemstra KA, Soeters MR, Fliers E, Serlie MJ, Burggraaf J, van Doorn MB, van der Klaauw AA, Romijn JA, Smit JW, Corssmit EP, Visser TJ. Type 2 iodothyronine deiodinase in skeletal muscle: effects of hypothyroidism and fasting. *J Clin Endocrinol Metab* 2009; 94(6): 2144-2150.

4. Bergendahl M, Aloi JA, Iranmanesh A, Mulligan TM, Veldhuis JD. Fasting suppresses pulsatile luteinizing hormone (LH) secretion and enhances orderliness of LH release in young but not older men. *J Clin Endocrinol Metab* 1998; 83(6): 1967-1975.

5. Hawley SA, Boudeau J, Reid JL, Mustard KJ, Udd L, Makela TP, Alessi DR, Hardie DG. Complexes between the LKB1 tumor suppressor, STRAD alpha/beta and MO25 alpha/beta are upstream kinases in the AMP-activated protein kinase cascade. *J Biol* 2003; 2(4): 28.

6. Kelley DE, Goodpaster B, Wing RR, Simoneau JA. Skeletal muscle fatty acid metabolism in association with insulin resistance, obesity, and weight loss. *Am J Physiol* 1999; 277(6 Pt 1): E1130-E1141.

7. Dampney RA. Functional organization of central pathways regulating the cardiovascular system. *Physiol Rev* 1994; 74(2): 323-364.

8. Muscelli E, Emdin M, Natali A, Pratali L, Camastra S, Gastaldelli A, Baldi S, Carpeggiani C, Ferrannini E. Autonomic and hemodynamic responses to insulin in lean and obese humans. *J Clin Endocrinol Metab* 1998; 83(6): 2084-2090.

9. Chan JL, Mietus JE, Raciti PM, Goldberger AL, Mantzoros CS. Short-term fasting-induced autonomic activation and changes in catecholamine levels are not mediated by changes in leptin levels in healthy humans. *Clin Endocrinol (Oxf)* 2007; 66(1): 49-57.

10. Webber J, Macdonald IA. The cardiovascular, metabolic and hormonal changes accompanying acute starvation in men and women. *Br J Nutr* 1994; 71(3): 437-447.

11. Lu CL, Zou X, Orr WC, Chen JD. Postprandial changes of sympathovagal balance measured by heart rate variability. *Dig Dis Sci* 1999; 44(4): 857-861.

7

12. Tentolouris N, Tsigos C, Perea D, Koukou E, Kyriaki D, Kitsou E, Daskas S, Daifotis Z, Makrilakis K, Raptis SA, Katsilambros N. Differential effects of high-fat and high-carbohydrate isoenergetic meals on cardiac autonomic nervous system activity in lean and obese women. *Metabolism* 2003; 52(11): 1426-1432.

13. Raichle ME, MacLeod AM, Snyder AZ, Powers WJ, Gusnard DA, Shulman GL. A default mode of brain function. *Proc Natl Acad Sci U S A* 2001; 98(2): 676-682.

14. Greicius MD, Krasnow B, Reiss AL, Menon V. Functional connectivity in the resting brain: a network analysis of the default mode hypothesis. *Proc Natl Acad Sci U S A* 2003; 100(1): 253-258.

15. Stoeckel LE, Weller RE, Cook EW, III, Twieg DB, Knowlton RC, Cox JE. Widespread reward-system activation in obese women in response to pictures of high-calorie foods. *Neuroimage* 2008; 41(2): 636-647.

16. Berthoud HR. The vagus nerve, food intake and obesity. *Regul Pept* 2008; 149(1-3): 15-25.

17. Scott TR, Yaxley S, Sienkiewicz ZJ, Rolls ET. Gustatory responses in the frontal opercular cortex of the alert cynomolgus monkey. *J Neurophysiol* 1986; 56(3): 876-890.

18. Seeley WW, Menon V, Schatzberg AF, Keller J, Glover GH, Kenna H, Reiss AL, Greicius MD. Dissociable intrinsic connectivity networks for salience processing and executive control. *J Neurosci* 2007; 27(9): 2349-2356.

19. Menon V, Uddin LQ. Saliency, switching, attention and control: a network model of insula function. *Brain Struct Funct* 2010; 214(5-6): 655-667.

20. Libert S, Zwiener J, Chu X, Vanvoorhies W, Roman G, Pletcher SD. Regulation of Drosophila life span by olfaction and food-derived odors. *Science* 2007; 315(5815): 1133-1137.

7

Chapter 8

Nederlandse Samenvatting

Vasten

Vasten heeft een enorm effect op het metabolisme. De spiegels van insuline en ook glucose dalen flink tijdens slechts een paar dagen vasten. Normaal gesproken komt energie vooral beschikbaar uit de verbranding van koolhydraten. Tijdens vasten verandert dit en is het juist de vetverbranding die zorgt voor de beschikbare energie. De wisseling van koolhydraat naar vetverbranding is echter niet onmiddellijk slecht voor de hersenen ook al zijn deze gewoon vooral glucose gebruiken als energie. Bij vetverbranding ontstaan namelijk ketonzuren welke ook door de hersenen gebruikt kunnen worden om energie te krijgen. Glucose wordt in de lever opgeslagen als glycogeen om tussen de maaltijden door de glucosespiegel in het bloed op peil te kunnen houden. Na 2 tot 3 dagen vasten zijn deze voorraden echter op. Dan wordt glucose gemaakt in de nieren en ook in de lever uit lactaat, pyruvaat, glycerol en uit bepaalde aminozuren zoals alanine (gluconeogese). Tijdens het vasten worden verschillende hormonale regelkringen (schildklier, reproductieve hormonen) platgelegd wat waarschijnlijk de voortplanting voorkomt in tijden van voedselschaarste. Op een meer moleculair niveau ondergaan (eiwit)-signaaltransductieroutes tijdens vasten een aanpassing. Vooral in het adenosine monophosphate-activated kinase (AMP-activated kinase, AMPK) waren wij geïnteresseerd en wilden wij de rol tijdens vasten bestuderen. Dit enzym wordt tijdens energietekort in de cel geactiveerd. De activiteit van dit enzym is er via allerlei cellulaire routes op gericht de energie balans weer te herstellen. Het is ook belangrijk voor de wisseling naar vetverbranding.

Overgewicht en obesitas

Overgewicht en obesitas worden gedefinieerd aan de hand van de body mass index (gewicht / lengte (m) in het kwadraat). Overgewicht wordt gedefinieerd als een BMI tussen 25 en 30 kg/m^2; obesitas als een BMI ≥ 30 kg/m^2. In 2008 waren er wereldwijd 1.5 miljard mensen met overgewicht en 500 miljoen mensen met obesitas. Helaas neemt de prevalentie van overgewicht en obesitas steeds verder toe zonder dat er, afgezien van bariatrische chirurgie, een langdurig effectieve behandeling bestaat. Politieke erkenning van dit veelvoorkomende probleem is nog niet optimaal. Wellicht dat een beter begrip van de ziekte kan lijden tot een verbetering hiervan.
Obesitas heeft een ongunstig effect op de gezondheid; het is een risicofactor voor hart- en vaatziekten, diabetes, spieraandoeningen en bepaalde vormen van kanker

8

(bijvoorbeeld borst en darmkanker). Aangezien AMPK zo belangrijk is tijdens verstoringen van de energiebalans, werd in dit proefschrift de rol van AMPK in overgewicht/obesitas onderzocht. De activiteit van AMPK kan het beste in cellen worden bestudeerd, hiervoor kan bijvoorbeeld spierweefsel worden gebruikt. Tot dusver zijn er niet veel veranderingen in de activitieit van AMPK gevonden in patiënten met obesitas of "ouderdoms"suikerziekte (type 2 diabetes mellitus).

Ook de hersenen zijn erg belangrijk voor het handhaven van de energiebalans. Dierstudies toonden aan dat met name de hypothalamus, een hersenstructuur die ook veel hormonale assen (schildklier, voortplanting) aanstuurt, een essentieel hersengebied is dat de voedselinname kan reguleren. De hypothalamus krijgt informatie over de voedingsstatus via de bloedbaan. In reactie op deze informatie kan de hypothalamus hormonen en ook neurotransmitters aanmaken of de hoeveelheid van deze hormonen aanpassen om een verstoring in de energiebalans te kunnen herstellen.

Gebruikte technieken

In dit proefschrift zijn meerdere technieken gebruikt in de verschillende onderzoeken. Er is bijvoorbeeld gebruikt gemaakt van functionele magnetische resonantie beeldvorming (fMRI; functional magnetic resonance imaging). Door het aanleggen van een magnetisch veld door een MRI scanner en het gebruik van radiogolven kunnen waterstofkernen geactiveerd worden. Deze activatie kan vervolgens omgezet worden tot beelden. fMRI maakt gebruik van een toegenomen signaal in de hersenen bij toegenomen activiteit in een bepaald hersengebied. Dit signaal is afhankelijk van de oxygenatie (zuurstofgehalte) van het bloed dat toeneemt bij toegenomen hersenactiviteit. Deze techniek werd in ons onderzoek gebruikt om de hersenactiviteit van de hypothalamus en andere hersengebieden te bestuderen.

Daarnaast is gebruik gemaakt van de zogenaamde hart ritme variabiliteit (HRV; heart rate variability). HRV kan gebruikt worden om een schatting te maten van de activiteit van verschillende onderdelen van het zenuwstelsel.

De activiteit van AMPK werd gemeten in spierweefsel van de proefpersonen dat werd afgenomen door middel van een spierbiopt (onder lokale verdoving). Verder vonden er bloedafnames plaats om onder andere hormoonspiegels te bepalen.

8

Doel van dit proefschrift

Het overkoepelende doel van dit proefschrift was om te onderzoeken welke aanpassingen het lichaam doet in reactie op vasten gedurende langere tijd en hoe deze aanpassingen verschillen tussen proefpersonen met en zonder obesitas. Verschillende parameters werden bestudeed. Eerdere studies lieten al zien welke effecten vasten heeft op bloedspiegels van hormonen en op de mate van koolhydraat versus vetverbranding. Onze interesse lag vooral bij de moleculaire veranderingen in het skeletspierweefsel, de veranderingen in hersenactiviteit en de aanpassingen van het zenuwstelsel. Ten eerste werd gehoopt bij te dragen tot een beter begrip van de aanpassingen die het lichaam maakt in reactie op vasten. Ten tweede werd gehoopt eventuele verschillen in deze aanpassingen aan te kunnen tonen tussen proefpersonen met of zonder obesitas om uiteindelijk nieuwe behandelvormen te kunnen vinden voor de behandeling van obesitas. Dit alles werd bestudeed in verschillende onderzoeken waarvan de resultaten in onderstaande hoofdstukken worden beschreven.

Indeling proefschrift

In **Hoofdstuk 2** was de hypothese dat vrijwilligers met en zonder overgewicht verschillend zouden reageren op 48 uur vasten. We hebben de effecten van het vasten vergeleken tussen de groepen op de volgende parameters: fMRI ('hersenactiviteit'), HRV ('zenuwstelsel'), hormonen, verbranding van vet of koolhydraat en moleculaire parameters in de skeletspier. Onze hypothese was dat AMPK geactiveerd zou raken na 48 uur vasten en dat deze activatie in mindere mate aanwezig zou zijn in de proefpersonen met obesitas.

Echter, wij toonden aan dat de activiteit van AMPK juist licht afnam na 48 uur vasten, maar alleen in de slanke individuen. Toch zou het kunnen dat vasten lijdt tot een activatie van AMPK, maar dan wellicht op een veel eerder tijdstip dan pas na 48 uur. Het was helaas niet mogelijk om dit in dit proefschrift verder te onderzoeken.

Verder laten we in deze studie zien, dat de reactie van verschillende hormoonspiegels (insuline, leptine, groeihormoon) en ook de wisseling van koolhydraat naar vetverbranding minder flexibel verloopt in de proefpersonen met overgewicht. Deze bevindingen bevestigen eerder onderzoek van andere onderzoeksgroepen. Verder toonden we aan dat de genetische expressie (het genetisch tot uiting komen) van

8

zogenaamde ´mitochondrial respiratory-chain protein subunits´ significant lager was in individuen met obesitas. Dit is een nieuwe bevinding waarvan de relevantie ver-duidelijkt moet worden door toekomstige onderzoek.

Hoofdstuk 3 toont de effecten die we vonden met betrekking tot de grootte van vari-atie van het hartritme (HRV) tussen personen met en zonder obesitas; na een maaltijd en na 48 uur vasten. HRV wordt grotendeels bepaald door het autonome zenuwstelsel. Eerdere studies toonden aan dat deze HRV verlaagd is in personen met obesitas, met name door een toegenomen activiteit van het sympathisch zenuw-stelsel (SZS). In een eerdere studie werd aangetoond dat vasten de activiteit van het SZS doet toenemen.

In tegenstelling tot onze verwachting, vonden we in onze studie geen verschil op baseline tussen de slanke personen en de personen met obesitas. Het zou kunnen dat dit een direct gevolg is van onze studieopzet; onze HRV metingen werden steeds ná een maaltijd verricht. Dit kan onze resultaten hebben kunnen beïnvloed omdat een maaltijd zelf al de bijdrage van het SZS aan het zenuwstelsel zou kunnen ver-groten.

In deze studie tonen we aan dat vasten zowel de vagale tonus (nervus vagus; parasympathisch zenuwstelsel dat actief is in rusttoestand) als de SZS (sympatisch zenuwstelsel dat actief is tijdens activiteit) tonus doet afnemen in slanke proefperso-nen. In de proefpersonen met obesitas werd een kleinere afname in de vagale tonus gezien en nam de SZS tonus juist toe. Echter, toetsing van het verschil in de reactie tussen personen met en zonder obesitas was niet significant. Verder tonen we in deze studie aan dat 8 weken leven op een laag calorisch dieet – leidend tot een gemiddelde afname van het gewicht met 13kg in de groep proefpersonen met overgewicht – leidt tot een toename van de bijdrage van het SZS aan het zenuws-telsel (wederom na een maaltijd gemeten).

Samenvattend laten we in deze studie zien dat 48 uur vasten de vagale en SZS tonus doet afnemen in slanke proefpersonen en dat de SZS tonus toenam in obese proef-personen. Na een laag calorisch dieet nam de SZS bijdrage toe waardoor deze een reactie vertoonden die meer lijkt op die van slanke proefpersonen. De slanke proef-personen lieten na een maaltijd namelijk ook een relatief hogere SZS bijdrage zien dan de obese proefpersonen. Het zou dus kunnen zijn dat de verschillen die er bestaan tussen slanke en obese proefpersonen minder worden nadat obese proef-personen zijn afgevallen.

8

Hoofdstuk 4 beschrijft de effecten van vasten in slanke en obese proefpersonen op connectiveits-netwerken in de hersenen, gemeten middels fMRI. In deze studie bekeken we de effecten van vasten in 12 slanke proefpersonen en 12 proefpersonen met overgewicht. We maakten MRI scans 's ochtends, nuchter, en na 48 uur vasten. We gebruikten zogenaamde 'functional connectivity' (FC) analyses om onze resultaten te bestuderen. FC wordt gebruikt om de interactie tussen verschillende hersengebieden in kaart te brengen. Deze FC kan zowel positief als negatief zijn; positief houdt een gelijke beweging in (toename of juist afname van activiteit) tussen de hersengebieden. Negatief houdt een tegengestelde beweging in. In dit onderzoek keken we naar FC met geselecteerde hersenregio's; de hypothalamus, de amygdala en het veel bestudeerde zogenaamde default-mode network (uitgaande van de posterieure cingulate cortex, PCC) om te kijken welke verschillen er zijn tussen slanke en obese proefpersonen.

Ons belangrijkste resultaat was dat de FC van de hypothalamus met bepaalde andere hersengebeiden (linker insula, dorsal anterieure cingulated cortex) verschillend reageerde op het vasten tussen de proefpersonen met en zonder overgewicht. Er werd een grotere afname gezien van de FC tussen de hypothalamus en de linker insula in de slanke proefpersonen, wat met name veroorzaakt werd door een hogere connectiviteit tussen deze gebieden in de proefpersonen met overgewicht op baseline. Verder zagen we dat de FC tussen de hypothalamus en de dACC veranderde van negatief naar positief in de slank proefpersonen en van positief naar negatief veranderde in de proefpersonen met overgewicht. Onze resultaten suggereren dus dat er verschillen bestaan in de FC tussen slanke proefpersonen en die met overgewicht. Meer studies zijn noodzakelijk om dit verder aan te tonen.

Hoofdstuk 5 beschrijft de effecten van 24 uur vasten in gezonde jonge mannen op drie verschillende tijdstippen. We hebben in deze studie gekeken naar andere tijdstippen ten opzichte van **hoofdstuk 2**. We bestudeerden de effecten op hormonen, op koolhydraat versus vetverbranding, en op moleculaire parameters in skeletspierweefsel. In deze studie werden meer biopten – en op andere tijdstippen – afgenomen dan in hoofdstuk 2. We toonden aan dat de bekende wisseling van koolhydraat naar vetverbranding en de daling van het insuline tegelijk optrad met een afgenomen activiteit van PKB/Akt en mTOR signaaltransuctieroutes in de skeletspier. We hadden verwacht dat AMPK, als belangrijke energie sensor,geactiveerd zou raken tijdens het vasten. In deze studie was AMPK echter totaal niet aangedaan door het vasten. We

weten wederom niet zeker of AMPK niet geactiveerd was op een eerder tijdstip; dat wil zeggen korter na de maaltijd die gegeven werd voordat het vasten begon. Toekomstige studies zijn derhalve nodig om te bestuderen of en zo ja wanneer AMPK geactiveerd raakt tijdens vasten.

Daarnaast laten we in deze studie de resultaten zien van een zogenaamde transcriptoom analyse. Hierin werd gekeken naar genen die geactiveerd werden in reactie op het vasten. Ook deze resultaten moeten in toekomstige studies bevestigd worden en de relevantie van deze veranderingen moet eveneens nog bestudeerd worden; misschien kan dat het beste in diermodellen.

In **Hoofdstuk 6** laten we de resultaten zien van een studie waarin onderzoek bij fruitvliegjes werd geëxtrapoleerd naar mensen. Fruitvliegjes leven langer als ze weinig te eten krijgen. In fruitvliegjes was aangetoond dat de aanwezigheid van geuren van voedsel (in vergelijking tot de afwezigheid hiervan) de levensverlenging die ontstaat door vasten teniet kan doen. Wij keken naar de effecten van deze geuren tijdens vasten op hormoonspiegels en het fMRI signaal van de hypothalamus. Onze hypothese was dat de aanwezigheid van geuren (en zichtbaar voedsel) tijdens vasten de effecten die vasten heeft op hormonen en de neuronale activiteit in de hypothalamus (geschat middels fMRI) teniet zou doen. Om dit te onderzoeken lieten we 12 jonge mannen tweemaal gedurende 60 uur vasten; éénmaal in de aanwezigheid, éénmaal in de afwezigheid van geuren en visuele voedsel prikkels. We vonden geen verschil tussen deze condities.

Conclusie en plannen voor de toekomst

In dit proefschrift beschrijven we de resultaten van verschillende onderzoeken die er op gericht waren de hormonale, metabole, moleculaire en neuronale effecten in zowel slanke als overgewichtige proefpersonen te bestuderen.

Zoals verwacht, tonen we opnieuw de bekende effecten van vasten aan; de stofwisseling wisselt van glucose naar vetverbranding. We tonen aan dat deze wisseling gepaard ging met een afname van bepaalde hormonen (met name insuline) en dat in de skeletspier bepaalde signaaltransductieroutes (PKB/Akt en mTOR) gelijktijdig omlaag werden bijgesteld.

Wat de signaaltransductieroutes betreft, bekeken in biopten van de skeletspier, waren we met name geïnteresseerd in AMPK – een belangrijk enzym dat geactiveerd raakt

8

tijdens energiegebrek. Echter, in de meeste van onze studies lijkt dit geen belangrijke rol te spelen tijdens het vasten. We kunnen alleen niet uitsluiten dat we een eventueel effect gemist hebben door op niet de juiste tijdstippen biopten te hebben afgenomen. Zoals verwacht, zijn de metabole en hormonale reactie in de proefpersonen met overgewicht enigszins verstoord geraakt. Een nieuwe bevinding in onze onderzoeken was dat de hoeveelheid eiwit afkomstig van mitochondriën, celorgaantjes die betrokken zijn bij het metabolisme, significant lager was in de skeletspieren van de proefpersonen met overgewicht.

Wat betreft de neuronale respons op vasten vonden we enkele verschillen tussen de proefpersonen met en zonder overgewicht. Meer studies zijn nodig om aan te tonen of deze effecten inderdaad betrokken zijn bij eventuele veranderingen in de verzadigings-/beloningsmechanismen van de hersenen.

Onze resultaten suggereren dat vasten het zenuwstelsel verschillend beïnvloedt tussen de verschillende groepen proefpersonen (slank versus obees), alleen dit haalde net geen significantie – meer onderzoek is dus noodzakelijk. Tot slot laten we zien dat de aanwezigheid van voedelstimuli (geuren en beelden) geen effect had op de metabole,neuronale en hormonale veranderingen die optreden tijdens vasten.

Ons voornaamste plan voor de toekomst, direct gerelateerd aan dit proefschrift, is om de effecten van gewichtsverlies te bestuderen in proefpersonen met overgewicht. We zullen dan kijken naar de hormonale veranderingen maar ook naar de veranderingen in de moleculaire signaaltransductieroutes in de skeletspier. De opzet van dit onderzoek staat in hoofdstuk 4 beschreven. Verder denken we dat het met name interessant zou zijn om een studie zoals beschreven in hoofdstuk 2 te herhalen maar met afname van biopten op een eerder tijdstip na de inname van de maaltijd om te zien of AMPK niet toch betrokken is op een vroeger moment tijdens vasten.

8

List of Publications

Regulation of skeletal muscle energy/nutrient-sensing pathways during metabolic adaptation to fasting in healthy humans
Wijngaarden MA*, Bakker LEH*, van der Zon GC, 't Hoen PAC, Willems van Dijk K, Jazet IM, Pijl H, Guigas B. * authors contributed equally.
American Journal of Physiology – Endocrinology and Metabolism 2014;307(10):E885-95.

Resting-state functional connectivity of brain regions involved in cognitive control, motivation, and reward is enhanced in obese females
Lips MA*, **Wijngaarden MA***, van der Grond J, van Buchem MA, de Groot GH, Rombouts SARB, Pijl H, Veer IM. * authors contributed equally.
American Journal of Clinical Nutrition 2014

Effects of prolonged fasting on AMPK signaling, gene expression and mitochondrial respiratory-chain content in skeletal muscle from lean and obese individuals
Wijngaarden MA, van der Zon GC, Willems van Dijk KW, Pijl H, Guigas B.
American Journal of Physiology – Endocrinology and Metabolism 2013;304(9):E1012-21.

Therapy resistant diabetes mellitus and lipodystrophy: leptin therapy leads to improvement.
Jazet IM, Jonker JT, **Wijngaarden MA**, Lamb H, Smelt AH
Nederlands Tijdschrift voor de Geneeskunde 2013;157(4):A5482.

Obesity is associated with an altered autonomic nervous system response to nutrient restriction
Wijngaarden MA, Pijl H, Willems van Dijk K, Klaassen ES, Burggraaf J.
Clinical Endocrinology 2013;79(5):648-51.

Food cues do not modulate the neuroendocrine response to a prolonged fast in healthy men
Snel M*, **Wijngaarden MA***, Bizino MB, van der Grond J, Teeuwisse WM, van Buchem MA, Jazet IM, Pijl H. * authors contributed equally.
Neuroendocrinology 2012;96(4):285-93.

Effects of low doses of casein hydrolysate on post-challenge glucose and insulin levels
Jonker JT, **Wijngaarden MA**, Kloek J, Groeneveld Y, Gerhardt C, Brand R, Kies AK, Romijn JA, Smit JW.
European Journal of Internal Medicine 2011;22(3):245-8.

Phosphopeptide screen uncovers novel phosphorylation sites of Nedd4-2 that potentiate its inhibition of the epithelial Na+ channel
Hallows KR, Bhalla V, Oyster NM, **Wijngaarden MA**, Lee JK, Li H, Chandran S, Xia X, Huang Z, Chalkley RJ, Burlingame AL, Pearce D.
Journal of Biological Chemistry 2010;285(28):21671-8.

AMP-activated kinase inhibits the epithelial Na+ channel through functional regulation of the ubiquitin ligase Nedd4-2
Bhalla V, Oyster NM, Fitch AC, **Wijngaarden MA**, Neumann D, Schlattner U, Pearce D, Hallows KR.
Journal of Biological Chemistry 2006;281(36):26159-69.

Curriculum Vitae

Marjolein Wijngaarden werd op 17 januari 1983 te Amsterdam geboren. Ze is de dochter van Elly Waterman en Rinke Wijngaarden en heeft één zus, Iris. Na afronding van het gymnasium, begon zij in 2001 aan haar studie Geneeskunde te Leiden. Ze deed wetenschappelijke stages bij dr. Onno Meijer op de afdeling Medische Farmacologie (Universiteit Leiden) en bij dr. David Pearce en Vivek Bhalla op de afdeling nefrologie (University of California San Francisco). Na het behalen van haar artsexamen, startte ze op 1 september 2008 haar promotietraject onder begeleiding van Prof. Dr. Hanno Pijl op de afdeling endocrinologie van het Leids Universitair Medisch Centrum. Per 1 januari 2012 is zij gestart met de opleiding tot internist. Ze woont samen met Stijn Crobach en zij hebben een dochter, Vera.

Dankwoord / Acknowledgements

Veel proefpersonen hebben zich ingezet voor mijn onderzoek door deel te nemen aan de verschillende projecten. Ik ben hen zeer veel dank verschuldigd voor de deelname en het vertrouwen.

Ook wil ik diegenen noemen die mij als student begeleiden tijdens het doen van wetenschappelijk onderzoek. Siem van der Laan, Onno Meijer hartelijk bedankt voor jullie enthousiasme. Thank you Vivek Bhalla and David Pearce for your inspiring supervision and teaching qualities.

Graag wil ik hierbij de begeleiders van mijn promotieonderzoek in het LUMC hartelijk bedanken. Hanno Pijl, dankjewel voor alle begeleiding en de vernieuwende ideeën – vaak onconventioneel – die je hebt. I would like to thank Bruno Guigas for his inspiring and enthousiasmic view on science and bench-side teaching. Daarnaast gaat mijn dank uit naar Ko Willems van Dijk, Serge Rombouts en Jeroen van der Grond voor hun betrokkenheid bij mijn onderzoeken.

Mirjam, ik ben heel blij dat we zoveel samen hebben gewerkt. Je bent een ontzettend harde werker en ook zo attent en humoristisch. Sacha, je bent me heel dierbaar. Je oordeelt nooit en daardoor is het niet moeilijk close met jou te worden.

Veel dank aan mijn leuke collega's en andere medewerkers van het LUMC. Ook de partners van mijn ouders, mijn lieve familie en schoonfamilie wil ik hier graag bedanken. Lieve en leuke ouders, heel erg bedankt voor alles wat jullie mij meegeven. Iris, lieve en creatieve zus, dankjewel voor het omslagontwerp.

Lieve Stijn, dankjewel voor al jouw liefde. Samen met jou door het leven gaan maakt me gelukkig.